THE COMPRESSIVE FAILURE OF GRAPHITE/EPOXY PLATES WITH CIRCULAR HOLES

by

James F. Knauss

Thesis submitted to the Graduate Faculty of the

Virginia Polytechnic Institute and State University

in partial fulfillment of the requirements for the degree of

MASTER OF SCIENCE

in

Engineering Mechanics

APPROVED:

E. G. Henneke, II, Chairman

C. T. Herakovich

J. H. Starnes, Jr.
NASA-Langley Research Center

December, 1977

Blacksburg, Virginia

ACKNOWLEDGMENTS

The author wishes to

-- acknowledge that the work reported in this text was funded by NASA Grant NGR 47-004-129.

-- thank , , for his guidance and technical assistance in the undertaking of this investigation.

-- thank of NASA Langley Research Center for his supervision and coordination during the fabrication, machining, instrumentation and testing of the specimens contained in this report and for having significantly contributed to the author's knowledge of stability dominated phenomena.

-- acknowledge and of the NASA-VPI&SU Program in Composite Materials Research and Education who made this research possible.

-- thank for his assistance in the mechanical testing of all specimens.

-- acknowledge the superior efforts of in the preparation of all computerized graphics contained in this manuscript.

-- thank for her diligence in typing the text.

TABLE OF CONTENTS

LIST OF TABLES

LIST OF FIGURES

Chapter 1

INTRODUCTION

1.1 Background

With the development of advanced fiber-reinforced materials as viable structural components, the characterization of these materials in various loading and geometric configurations has become a primary concern to the designer. The ability of composite materials to be tailored to a specific use, therein optimizing strength while reducing weight, makes them uniquely suited to aerospace applications. The materials system under consideration here is currently in use as control surface components on wide bodied commercial transports.

Incorporation of composites into aerospace vehicles requires that holes be drilled into the laminate to facilitate bolting or riveting to the primary structure or to provide access to the interior of the wing. These holes introduce stress concentrations which significantly reduce the failure stress of the panel, but the extent of this reduction is not completely understood. Considerable literature is available, both analytical and experimental, which addresses the problem of tensile loads on orthotropic plates with circular holes. Although not completely characterized at this point in time, the case of tension has been more thoroughly studied than that of compression.

The scope of the present investigation, therefore, is to characterize the compressive behavior of fiber-reinforced composite plates containing a circular cutout in terms of geometry (thickness, width, hole diameter), and material properties (bending/extensional

stiffness). In this way a data base will be established for use by designers in determining the ultimate strength of such a structure.

1.2 Review of Literature

The influence of holes on the behavior of plates has long been a subject of interest among researchers. Significant contributors include Kirsch [1] who is credited with the determination of the stress concentration factor (SCF_σ) in isotropic materials and Howland [2] for utilizing the solution of the bi-harmonic Airy's stress function in polar coordinates to determine the stresses in a perforated strip in the neighborhood of a hole including finite width effect (i.e., the slight increase in SCF_σ as the diameter of the hole approaches one half the plate width).

One of the first investigations into the compressive behavior of plates with holes was performed by Levy, Woolley, and Kroll [3] who considered both reinforced and unreinforced holes in isotropic square plates. The authors approach the problem of computing a buckling load from an energy standpoint using Gaussian quadrature techniques to perform numerical integration. Results of this analysis indicate that the buckling stress of square plates is reduced only a small amount by the presence of unreinforced holes. Kumai [4] utilizes the same numerical integration scheme as Levy et al and provides an energy solution which incorporates refined displacement functions. Analysis and experiment show good comparison in their prediction of increased buckling deflection with hole diameter for a perforated square plate with clamped

boundary conditions on the loaded edges. Results for both the fundamental and secondary buckling modes are reported. Schlack [5] presents a similar development concentrating on the determination of critical edge displacement and the proper expression for transverse deflection in the Ritz energy method. He briefly compares experimental results to those obtained analytically.

In proceeding from isotropic to orthotropic materials one finds that the subject of plates with holes in compression is non-existent in the literature to date. Therefore, the best approach is to understand the developments in orthotropic plates in tension to perhaps gain some insight into the compressive case. Greszczuk [6] has developed theoretical solutions for stress concentrations and failure stresses in orthotropic and anisotropic material. He extends previous solutions by Green and Zerna [7] to composite materials and includes various material lay-up and loading configurations. The failure criterion employed by Greszczuk is based on the Hencky-Von Mises distortion energy method and reports both the magnitude of the failure stress and its location around the hole. Results show little influence of maximum stress concentration on the magnitude or location of failure stress. Experimental photoelastic results compare favorably with this theory.

Tang [8] is one of the most recent researchers concerned with the tensile case. His development is an asymptotically expanded elasticity solution for the stresses around a cutout. Excellent agreement with other investigators in the stress state at a free edge is reported along with fair agreement for the influence of the hole.

There are several three-dimensional finite element codes available which deal with laminated plates containing a hole. Rybicki and Hopper [9] base their formulation on minimization of complementary energy using equilibrium finite elements. The stress state in the neighborhood of the hole is presented in graphical form for the linear orthotropic response of four and six ply laminates and is compared to the two-dimensional results of their previous work. Rybicki and Schmueser [10] address five areas which could influence the behavior of a pierced plate: the effect of stacking sequence, lay-up angle, temperature change during fabrication, laminate thickness and three-dimensional versus two-dimensional analytical results. Some interesting approaches are used in the report. Undoubtedly to increase the number of plies the code can handle, the (0_2), (90_2) and $(\pm\theta/\mp\theta)$ laminae are modelled as a single material with effective modulus properties. Rybicki and Schmueser found that laminated plate theory gives nonzero stresses σ_r and $\tau_{r\theta}$ on the boundary of the hole. In order to satisfy boundary conditions they then impose the negative of these stresses on the boundary of the hole in order to determine what effect this has on interlaminar stresses and the sign of σ_z.

A series of publications, Nuismer and Whitney [11], Whitney and Nuismer [12], Whitney and Kim [13], and Whitney [14] approach the problem of notched composite plates from a linear elastic fracture mechanics point of view. Basically, Nuismer and Whitney [11,12] attempt to explain the decrease in laminate failure stress with increasing hole

diameter by two failure criteria, point stress and average stress. Both papers model a circular hole by a crack of length equal to the hole diameter and consider the statistical nature of composite laminate failure using a two-parameter Weibull distribution. The two material systems examined are T300-5208 graphite/epoxy and Scotchply 1002. Identical treatment of T300-934 graphite/epoxy is the subject of Whitney and Kim [13]. The applicability of fracture mechanics to the compression failure regime, however, has not been established at this point.

For the purpose of understanding the tensile failure of composite plates with circular inclusions, Levy, Armen and Whiteside [15] is the first of a series of articles which investigate the effect of different material parameters on the type of failure observed experimentally. A finite element code is developed to study elastic and plastic interlaminar shear deformation by modeling the composite with alternating orthotropic (fiber-bearing) and isotropic elements through the thickness. A displacement formulation is used and graphical results are presented comparing linear and non-linear material behavior and showing the effects of varying the geometry such as the radius-to-thickness ratio.

A similar code is used in Daniel, Rowlands, and Whiteside [16] for the linear elastic case and compared with photoelastic results. The important conclusions from this work are that the magnitude of the tensile strain near the hole becomes larger than the strain at the hole boundary at high loads just prior to failure. Also, the strain levels

around the hole at failure are reported to be much higher than the failure strain for an unnotched specimen. This is possible due to the nonlinearity and nonuniformity of strain distribution and the steep gradient near the hole which confines the high strains to a small volume of material.

Having characterized the basic behavior, the same investigators study the effect of geometry and loading, and material and stacking sequence in Rowlands, Daniel and Whiteside [17], and Daniel, Rowlands and Whiteside [18], respectively. The results indicate that failure occurred off the axis perpendicular to load application where interlaminar shear and normal stress are maximum and where circumferential normal and shear strain increase nonlinearly with increased load. The strength reduction factor (ratio of unnotched failure stress to notched failure stress) was found to be conservatively estimated by the stress concentration factor in all cases.

The compressive failure case differs from the tensile case in that failure is either strength or stability critical or a combination of both. It is the primary objective of the present investigation to determine the mechanism by which each type of failure occurs and to characterize these in an effort to establish design criteria for the engineer.

Chapter 2

THEORY OF THIN LAMINATED PLATES

A preliminary consideration to any physical testing program should be the response of the system as dictated by theory. In addition, before the behavior of a plate with a hole can be characterized, the behavior of a homogeneous laminate must be completely understood. The manner in which laminated plate theory identifies the orthotropic bending stiffness as the dominant material property in plate buckling is presented in this section.

The theorem of stationary potential energy states that the sum of the potential energies of bending, V, applied transverse load, Q and inplane loads, U, must equal a stationary value for equilibrium to exist. Mathematically,

$$V+U+Q = \text{stationary value} \tag{2.1}$$

where

$$V = \frac{1}{2}\iiint_{\text{Volume}} \{\sigma_x\varepsilon_x+\sigma_y\varepsilon_y+\tau_{xy}\gamma_{xy}\}dV$$

(assuming transverse normal and shearing strains, ε_z, γ_{xz}, γ_{yz} are negligible),

$$U = \frac{1}{2}\iint_{\text{Area}} \{N_x(\frac{\partial w}{\partial x})^2+N_y(\frac{\partial w}{\partial y})^2+2N_{xy}\frac{\partial w}{\partial x}\frac{\partial w}{\partial y}\}dA$$

and

$$Q = -\iint_{Area} q\, w\, d\, A,$$

for a transverse load, q.

The volume integral for the potential energy of bending may be simplified by piecewise integration over the thickness for each layer by utilizing the lamina constitutive relations

$$\begin{Bmatrix} \sigma_x \\ \sigma_y \\ \tau_{xy} \end{Bmatrix}^k = [\bar{Q}]^k \begin{Bmatrix} \varepsilon_x \\ \varepsilon_y \\ \gamma_{xy} \end{Bmatrix}^k ,$$

where $[\bar{Q}]^k$ are the transformed reduced stiffnesses of the kth layer. Then

$$V = \frac{1}{2}\iint_{Area} \left[\sum_{k=1}^{N} \int_{h_{k-1}}^{h_k} \{[\bar{Q}_{11}^k\varepsilon_x+\bar{Q}_{12}^k\varepsilon_y+\bar{Q}_{16}^k\gamma_{xy}]\varepsilon_x \right.$$

$$\left. +[\bar{Q}_{12}^k\varepsilon_x+\bar{Q}_{22}^k\varepsilon_y+\bar{Q}_{26}^k\gamma_{xy}]\varepsilon_y+[\bar{Q}_{61}^k\varepsilon_x+\bar{Q}_{62}^k\varepsilon_y+\bar{Q}_{66}^k\gamma_{xy}]\gamma_{xy}\}dz \right] dA.$$

Substituting the strain-displacement relations in terms of midplane displacements

$$\varepsilon_x = \frac{\partial u^\circ}{\partial x} - z\,\frac{\partial^2 w}{\partial x^2}$$

$$\varepsilon_y = \frac{\partial v^\circ}{\partial y} - z\,\frac{\partial^2 w}{\partial y^2}$$

$$\gamma_{xy} = \frac{\partial u^\circ}{\partial y} + \frac{\partial v^\circ}{\partial x} - 2z\,\frac{\partial^2 w}{\partial x \partial y} ,$$

where the superscript $^\circ$ denotes midplane quantities, into the express-

sion for V and defining

$$[A] = \sum_{k=1}^{N} \int_{h_{k-1}}^{h_k} [\bar{Q}]^k dz = \sum_{k=1}^{N} [\bar{Q}]^k (h_k - h_{k-1})$$

$$[B] = \sum_{k=1}^{N} \int_{h_{k-1}}^{h_k} [\bar{Q}]^k z dz = \frac{1}{2} \sum_{k=1}^{N} [\bar{Q}]^k (h_k^2 - h_{k-1}^2)$$

$$[D] = \sum_{k=1}^{N} \int_{h_{k-1}}^{h_k} [\bar{Q}]^k z^2 dz = \frac{1}{3} \sum_{k=1}^{N} [\bar{Q}]^k (h_k^3 - h_{k-1}^3),$$

allows V to be written in a form compatible with U and Q. Therefore the generalized theorem of stationary potential energy yields

$$\frac{1}{2} \iint \{A_{11} (\frac{\partial u^\circ}{\partial x})^2 + 2A_{12} \frac{\partial u^\circ}{\partial x} \frac{\partial v^\circ}{\partial y} + A_{22} (\frac{\partial v^\circ}{\partial y})^2$$

$$+ 2A_{16} (\frac{\partial u^\circ}{\partial x} \frac{\partial u^\circ}{\partial y} + \frac{\partial u^\circ}{\partial x} \frac{\partial v^\circ}{\partial x}) + 2A_{26} (\frac{\partial v^\circ}{\partial y} \frac{\partial u^\circ}{\partial y}$$

$$+ \frac{\partial v^\circ}{\partial y} \frac{\partial v^\circ}{\partial x}) + A_{66} (\frac{\partial u^\circ}{\partial y} + \frac{\partial v^\circ}{\partial x})^2 + 2D_{12} \frac{\partial^2 w}{\partial x^2} \frac{\partial^2 w}{\partial y^2}$$

$$+ D_{22} (\frac{\partial^2 w}{\partial y^2})^2 + 4D_{16} \frac{\partial^2 w}{\partial x^2} \frac{\partial^2 w}{\partial x \partial y} + 4D_{26} \frac{\partial^2 w}{\partial y^2} \frac{\partial^2 w}{\partial x \partial y}$$

$$+ 4D_{66} (\frac{\partial^2 w}{\partial x \partial y})^2 + N_x (\frac{\partial w}{\partial x})^2 + N_y (\frac{\partial w}{\partial y})^2$$

$$+ 2N_{xy} \frac{\partial w}{\partial x} \frac{\partial w}{\partial y} - 2 qw\} dA = \text{stationary value} \qquad (2.2)$$

for a midplane symmetric laminate (i.e. [B] = 0).

Equ. (2.2) shows no coupling between the inplane displacements, u and v, and the normal displacements, w; hence all terms containing only inplane components do not contribute to buckling and can be considered constant and absorbed into the stationary value. Further, the case of static, uniaxial load dictates that $N_y = N_{xy} = q \equiv 0$. The result of these observations is a specialized expression of the potential energy as reported by Ashton and Whitney [19],

$$\frac{1}{2}\int_0^b \int_0^b \{D_{11}w,_{xx}^2+2D_{12}w,_x^2w,_y^2+D_{22}w,_{yy}^2$$

$$+4D_{16}w,_x^2w,_{xy}+4D_{26}w,_y^2w,_{xy}+4D_{66}w,_{xy}^2$$

$$+N_xw,_x^2\}dy\,dx = \text{stationary value}, \qquad (2.3)$$

for a plate of aspect ratio a/b. In Equ. (2.3) the comma denotes partial differentiation.

Figure 2-1 depicts the physical and analytical boundary conditions used in this investigation. Specifically,

for x=0, x=10" $\qquad w=0;\ \frac{\partial w}{\partial x} = 0$

for $y=\frac{3"}{16}$, $y=4\ \frac{5"}{8}$ $\qquad w=0;$

$$M_y=-D_{12}\frac{\partial^2 w}{\partial x^2} - D_{22}\frac{\partial^2 w}{\partial y^2} - 2D_{26}\frac{\partial^2 w}{\partial x \partial y} = 0.$$

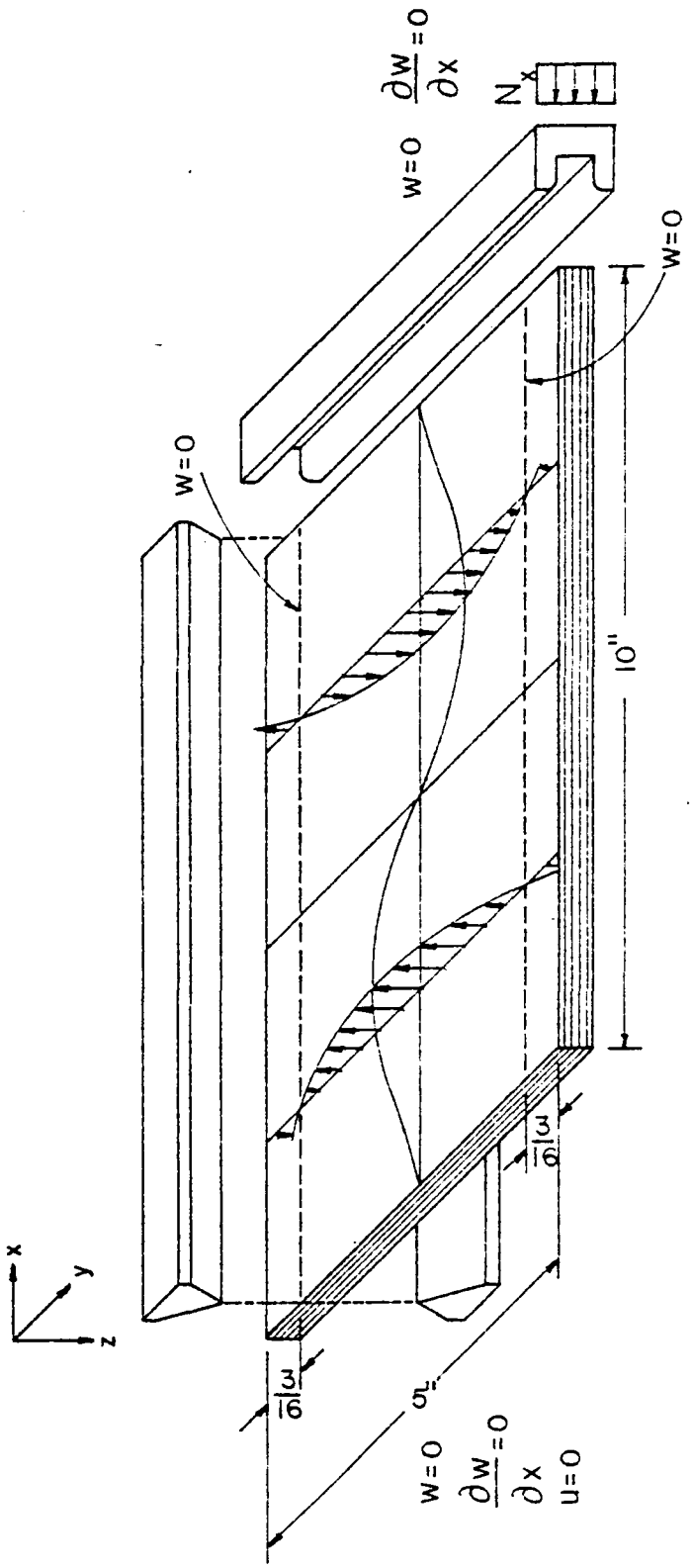

FIGURE 2-1. BUCKLED SHAPE OF LAMINATED PLATE AND APPLIED BOUNDARY CONDITIONS.

The remaining steps to the solution include assuming an expression for the transverse deflection in the form

$$w = \sum_{i=1}^{m} \sum_{j=1}^{n} a_{ij} \Phi_i(x) \, \Theta_j(y)$$

where $\Phi_i(x)$ and $\Theta_j(y)$ are functions which are chosen to satisfy natural boundary conditions. The coefficients a_{ij} are parameters which may be determined through minimizing the energy expressions by differentiating with respect to each a_{ij}. The purpose of this section is not the rigorous pursuit of an analytical solution, merely the determination of material property dependency which, from equ. (2.3), is the bending stiffness as previously stated. The effect of material property on the buckling behavior of a laminated plate was incorporated into the testing program by varying the laminate. The effect of this exercise will be reported in the following sections in terms of the ratio E_x/E_y. The predicted buckling load was determined using existing computer codes to be used primarily as a normalizing factor in the presentation of graphical results.

Chapter 3

EXPERIMENTAL PROGRAM

3.1 Introduction

An extensive experimental program was conducted to investigate the failure mechanisms of laminated composite plates containing circular holes. All panels were monotonically loaded in uniaxial compression to failure at a rate of 1112 N/sec (15.0 kip/min) or less in a 1.334 MN (300 kip) capacity Southwark-Emery testing machine. The specimens were mounted in hardened steel test fixtures which applied clamped boundary conditions on the loaded edges and simple support along the sides to prevent wide column Euler buckling, Figure 3-1. A gap of approximately 0.635 cm ($\frac{1}{4}$ in) was left between the side supports and the end grips to allow for compression of the panel without loading the fixture. Strain gages were applied to each panel as well as flat white paint on the front surface to facilitate a moire fringe grid of either 27.5 or 19.7 lines/cm (70.0 or 50.0 lines/in). Strain gage data were recorded during each test by the Beckman Automatic Data Acquisition System at NASA Langley Research Center.

Direct current differential transformers (DCDT) were used to measure crosshead displacement and to generate load-displacement curves. In the stability critical tests DCDT's were used to measure transverse deflection of the plates. This data was also recorded by the Beckman system.

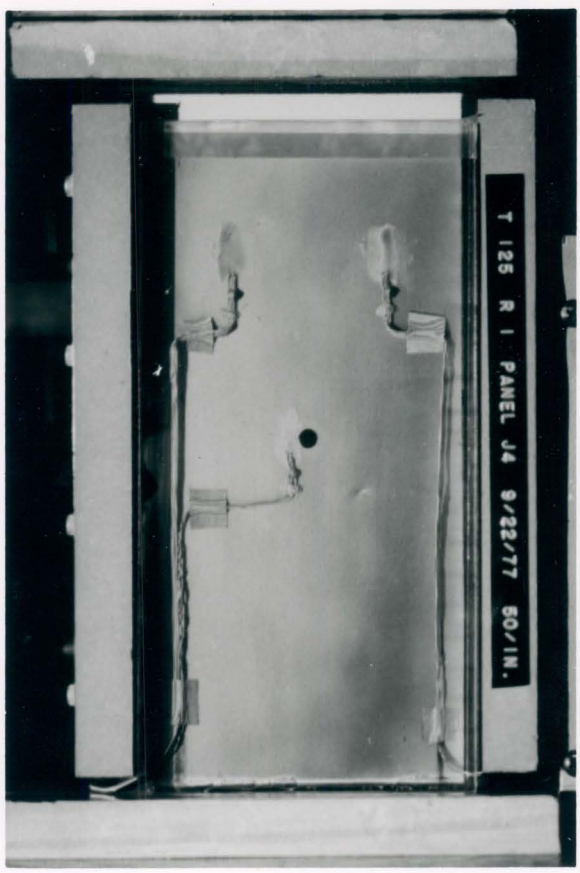

FIGURE 3-1. SPECIMEN IN GRIPS READY FOR TESTING.

3.2 Specimens

3.2.1 Fabrication

The constituents of the composite material system used for the testing program were Thornel 300 graphite fibers and Narmco 5208 epoxy resin. With the exception of panels prefixed "AK", all specimens were fabricated in-house by the Model Shop, NASA-Langley Research Center. Panels AK1 through AK9 were made by McDonnell Douglas Aircraft Company, Long Beach, California. In both cases the manufacturer's recommended cure cycle was used.

Initial lay-up was done with resin pre-impregnated tape of 7.62 cm (3.0 in) and 30.48 cm (12.0 in) widths and nominal ply thickness of 0.0203 cm (0.008 in). An entire laminate was layed up in 60.96 x 73.66 cm (24.0 x 29.0 in) sheets with a release agent and Mockburg bleeder material placed between every two plies. The material was placed in a vacuum bag and heated to 394°K (250°F) for 600 sec (10 min) in order to bleed off excess resin material (i.e., increase the fiber volume fraction) and reduce the ply thickness to 0.0140 - 0.0170 cm (0.0055 -0.0067 in). The bleeder material was then removed and the two ply laminae were stacked in the proper sequence.

Once stacked, the laminae were placed on a release coated flat aluminum caul plate and a dam of cork-like Corprene placed around the border to prevent additional resin loss during cure. Placed in a vacuum bag and then into the autoclave, the laminae underwent a temperature increase of 4.293 - 4.312 °K/sec (4. - 6.° F/min) up to 408. °K

(275. °F) and were allowed to dwell for 3600. sec (60. min). In a nitrogen atmosphere the pressure was raised to 586 - 689 kPa (85. - 100. psig) and the temperature increased to 453. °K (355. °F) for 7200. seconds (2.0 hours). The laminate was then cooled to 333. °K (140. °F) under pressure.

3.2.2 Geometry

In order to accurately characterize the role of plate geometry in panel failure, each dimension of the specimens was allowed to vary as well as the stiffness of the plate itself.

The bending stiffness was influenced by altering the stacking sequence. Two different 48 ply lay-ups were considered: quasi-isotropic $[(+45/-45/0/90/-45/+45/0/90)_3]_s$, and orthotropic $[+45/-45/0_2/+45/-45/0_2/+45/-45/0/90)_2]_s$. The objective of this exercise was to analyze a material which had a longitudinal/transverse modulus ratio, E_x/E_y, of 1.0 (quasi-isotropic), and that of a highly directional material whose ratio was other than unity (orthotropic, E_x/E_y = 2.015).

For composite materials, two different techniques exist for varying thickness: compressing the laminate to a predetermined thickness during fabrication or altering the number of plies. The latter method was chosen in order to preserve the average ply thickness and fiber volume fraction. An analytical study was undertaken to determine what laminate configuration would result in a laminate which was approximately half as thick, 24 plies, as the original and the same modulus ratio. The sequences selected were quasi-isotropic, ([+45/-45/0/90/-45/

+45/0/90/+45/-45/0/ 90]$_s$; E_x/E_y = 1.00) and orthotropic, ([+45/-45/0_2/ +45/-45/0_2/+45/-45/ 0/90]$_s$; E_x/E_y = 2.015). Since uniform laminate thickness, and therefore uniform ply thickness, is difficult to achieve in the fabrication of composites, a four point thickness distribution was taken and is reported in Tables 3-1 and 3-2 in terms of average thickness plus or minus a standard deviation.

The orthotropic stress concentration factor for an infinite plate is characteristic of the material and is not a function of hole size or plate geometry, Savin [23]. Therefore, any deviation from a given value for the material could be due, in this case, to the influence of plate width. To study this phenomenon, a series of holes were ultrasonically drilled into the plates varying from 0.1588 cm ($\frac{1}{16}$ in) to 3.81 cm ($1\frac{1}{2}$ in) diameter for the 48 ply specimens and from 0.1588 cm ($\frac{1}{16}$ in) to 2.54 cm (1.0 in) diameter for the 24 ply laminates for both configurations. The standard plate width was 12.7 cm (5.0 in) but several panels were wider to examine width effects. The hole sizes in these wider panels were selected to preserve a diameter-to-width ratio, $\frac{D}{W}$, of 0.167. The length was held constant for all panels.

3.2.3 Fiber Volume Fraction

The characteristics of a fiber reinforced material are not completely documented until the percentage of all constituents of the material are determined. To this end the fiber volume fraction of the T300-5208 graphite/epoxy specimen material was determined by two methods: matrix digestion and quantitative microscopy.

Table 3-1

48 Ply Quasi-Isotropic and Orthotropic Specimens

Panel No.	Thickness (cm)	Hole Diameter (cm)	Length (cm)	Width (cm)
	Orthotropic			
AK1	0.6248 ± 0.0023	-	24.92	12.70
K18	0.6284 ± 0.0030	0.1588	25.40	12.70
AK2	0.6300 ± 0.0117	0.3175	25.40	12.70
AK3	0.6289 ± 0.0061	0.6350	25.40	12.70
AK4	0.6214 ± 0.0091	0.9525	25.40	12.70
AK5	0.6185 ± 0.0058	1.2700	25.40	12.70
AK6	0.6231 ± 0.0069	1.5875	25.40	12.70
AK7	0.6200 ± 0.0047	1.9050	25.40	12.70
AK8	0.6226 ± 0.0028	2.2225	25.24	12.70
AK9	0.6233 ± 0.0020	2.5400	25.40	12.70
K14	0.6251 ± 0.0041	3.1750	25.40	12.70
K10	0.6284 ± 0.0025	3.8100	25.40	12.70
K11	0.6261 ± 0.0015	2.5400	25.40	15.24
K13	0.6248 ± 0.0030	3.1750	25.40	19.05
K12	0.6248 ± 0.0033	3.8100	25.40	22.86
K15	0.6262 ± 0.0023	-	25.40	12.70
	Isotropic			
J17	0.7132 ± 0.0036	-	25.40	12.70
J14	0.7216 ± 0.0071	-	25.40	12.70
J19	0.7158 ± 0.0062	0.1588	25.40	25.40
J3	0.7008 ± 0.0081	0.3175	25.40	12.70
J4	0.6934 ± 0.0071	0.6350	25.40	12.70
J5	0.6962 ± 0.0109	0.9525	25.40	12.70
J6	0.7021 ± 0.0051	1.2700	25.56	12.70
J7	0.6932 ± 0.0053	1.5875	25.40	12.70
J8	0.6988 ± 0.0025	1.9050	25.40	12.70
J9	0.6975 ± 0.0033	2.2225	25.40	12.70
J10	0.7033 ± 0.0018	2.5400	25.40	12.70
J11	0.7165 ± 0.0020	3.8100	25.40	12.70
J2	0.7046 ± 0.0081	2.5400	25.40	15.24
J1	0.7014 ± 0.0015	3.8100	25.40	22.86

Table 3-2

24 Ply Quasi-Isotropic and Orthotropic Specimens

Panel No.	Thickness (cm)	Hole Diameter (cm)	Length (cm)	Width (cm)
	Orthotropic			
K21	0.3726 ± 0.0010	0.1588	25.40	12.70
K22	0.3724 ± 0.0066	0.3175	25.40	12.70
K23	0.3680 ± 0.0005	0.4763	25.40	12.70
K24	0.3640 ± 0.0043	0.6350	25.40	12.70
K25	0.3607 ± 0.0122	0.7938	25.40	12.70
K26	0.3680 ± 0.0001	0.9525	25.40	12.70
K27	0.3685 ± 0.0025	1.1113	25.40	12.70
K28	0.3665 ± 0.0023	1.2700	25.40	12.70
K29	0.3604 ± 0.0043	1.5875	25.40	12.70
K30	0.3665 ± 0.0064	1.9050	25.40	12.70
K31	0.3495 ± 0.0051	2.5400	25.40	12.70
K32	0.3495 ± 0.0048	-	25.40	12.70
K33	0.3520 ± 0.0018	-	25.40	12.70
	Isotropic			
J28	0.3589 ± 0.0021	0.1588	25.40	12.70
J29	0.3541 ± 0.0053	0.3175	25.40	12.70
J27	0.3583 ± 0.0055	0.4763	25.40	12.70
J31	0.3452 ± 0.0065	0.6350	25.40	12.70
J25	0.3582 ± 0.0030	0.7938	25.40	12.70
J26	0.3626 ± 0.0034	0.9525	25.40	12.70
J32	0.3443 ± 0.0042	1.1113	25.40	12.70
J21	0.3634 ± 0.0029	1.2700	25.40	12.70
J24	0.3581 ± 0.0050	1.5875	25.40	12.70
J35	0.3412 ± 0.0022	1.9050	25.40	12.70
J22	0.3628 ± 0.0016	2.5400	25.40	12.70
J30	0.3372 ± 0.0056	3.8100	25.40	12.70
J37	0.3419 ± 0.0048	-	25.48	12.70

The matrix digestion technique was done in accordance with ASTM Standard D3171 [20]. Using the weights of the composite before the digestion and of the remaining fibers after matrix removal, the fiber volume fraction can be calculated from the relation

$$V_f = \frac{w_f}{\rho_f} / \frac{w_c}{\rho_c}$$

where V, w, ρ are the volume percent, weight and density respectively, and subscripts f and c denote fiber and composite. This procedure yielded a fiber volume fraction of 52.2%.

The quantitative microscopy method used a bench metallograph with a television screen attachment. A grid was superimposed on the screen and the point fraction statistical method of fiber distribution used to determine volume fraction, Figure 3-2. Whereas in matrix digestion one can use a composite of arbitrary layup, the section examined by microscopy must be perpendicular to the fiber direction in a unidirectional laminate since the respective areas of fiber-matrix-void are of importance. A unidirectional laminate was fabricated as outlined in Section 3.2.1 for this purpose.

The number of sample counts required depends on the confidence value desired, the error to be tolerated, and the statistical consistency of a representative sample. The procedure began by counting the number of grid intersections falling on fiber, matrix or void in twenty different areas of a cross-section. For a 95.0% confidence level and an error tolerance of 3.0%, the number of sample counts, n, required is

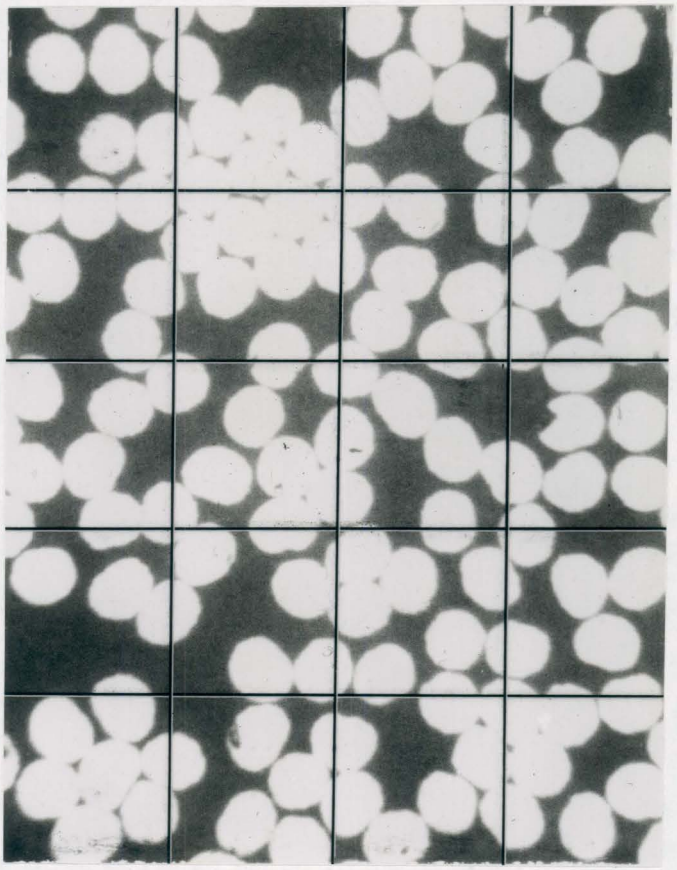

FIGURE 3-2. 1000X MAGNIFICATION OF T300-5208 GRAPHITE EPOXY SHOWING POINT FRACTION STATISTICAL METHOD OF FIBER VOLUME FRACTION DETERMINATION.

$$n = \left(\frac{1.96\ \sigma_x}{0.030\ \bar{x}}\right)^2$$

where $\bar{x}$ and σ_x are the mean and standard deviation respectively of the first twenty sample counts. For this case

$$n = \left(\frac{1.96(3.05)}{0.03(12.98)}\right)^2 = 235.7$$

means that 236 representative samples must be taken before the statistical nature of the point fraction technique will give a 95.0 percent confidence level that the volume fraction is within 3.0 percent of the correct value. For the panels fabricated at NASA-LaRC this method yielded three values:

$$V_f = 52.8 \pm 1.58\%$$
$$V_m = 39.5 \pm 1.19\%$$
$$V_v = 7.7 \pm 0.23\%$$

where V_f, V_m and V_v are the volume fraction of the fiber, matrix and void, respectively. The advantage of the quantitative microscopy procedure is that it yields the volume fraction of void in the material. To do this with matrix digestion requires that the volatiles be captured during digestion in order to measure the amount of matrix dissolved which significantly complicates the technique.

3.2.4 Strain Gage Patterns

Foil type strain gages were applied to each specimen to record the material response of the panel to the compressive load. Far field

strain was recorded by two pairs of back-to-back gages located equidistant from the horizonal centerline of the hole nad the top edge of the plate. The single value used for far field strain is the average of these four gages in every case.

Hole size was the critical factor in determining the number and location of strain gages to be used for each specimen. For hole diameters less than 0.635 cm ($\frac{1}{4}$ in) only one gage was used, located on the lateral centerline of the cutout and 0.0794 cm ($\frac{1}{32}$ in) from the edge of the hole. This gage was included to get an approximation of the strain concentration factor (SCF_ε). For hole diameters between 0.635 cm and 1.27 cm ($\frac{1}{4}$ in and $\frac{1}{2}$ in) a series of gages were placed along the lateral centerline at 0.1588 cm ($\frac{1}{16}$ in) increments beginning at 0.0794 cm ($\frac{1}{32}$ in) from the hole. Information concerning the strain gradient away from the hole as well as an approximation to the SCF_ε was obtained.

Placement of gages inside the hole was a physical impossibility below diameters of 1.27 cm ($\frac{1}{2}$ in). Between 1.27 cm ($\frac{1}{2}$ in) and 2.54 cm (1.0 in) circumferential strain was measured on the lateral centerline of the hole boundary. Perpendicular to the load direction both circumferential and through-the-thickness strains were measured on opposite sides of the hole, Figure 3-3. Thus, the SCF_ε could be measured exactly. Finally, for hole sizes greater than 2.54 cm (1.0 in), through-the-thickness and circumferential strain could be measured at several selected points around the hole in the quasi-isotropic panels. The placement of these gages was necessary because preliminary

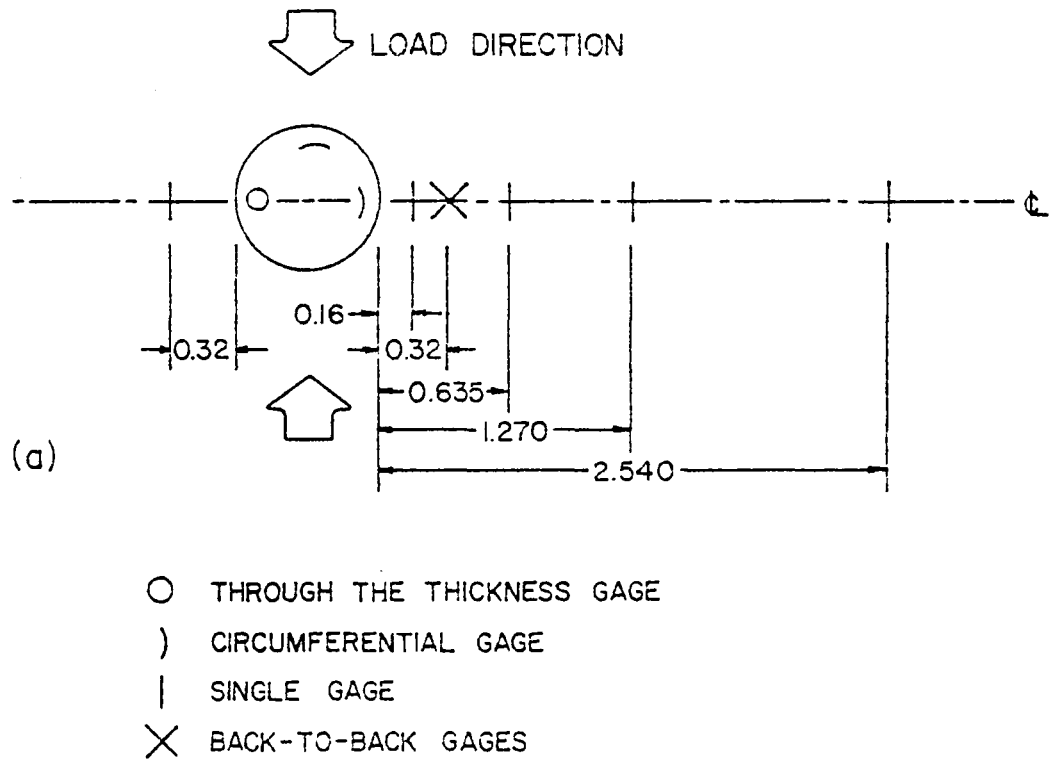

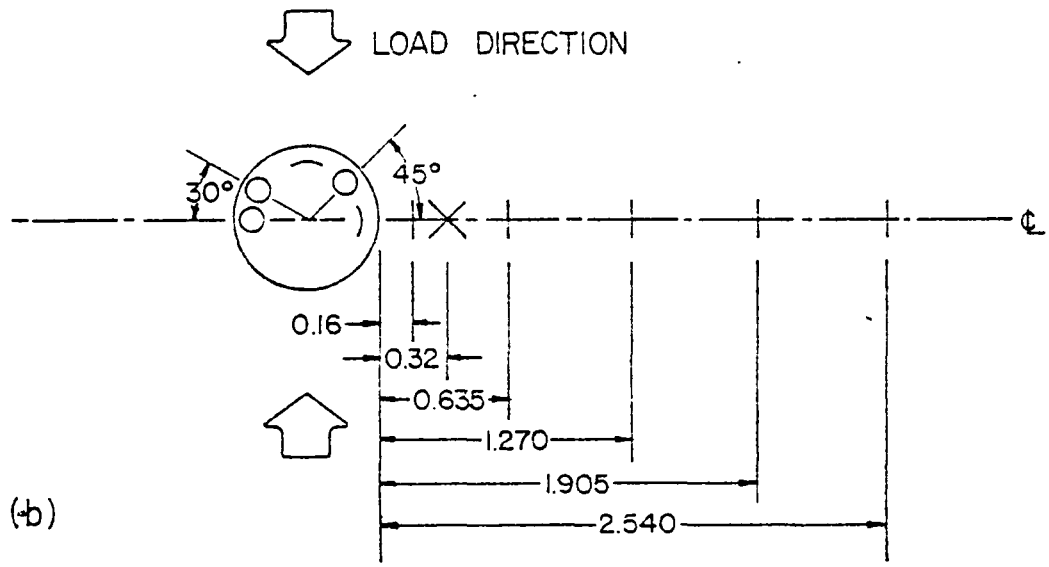

FIGURE 3-3. STRAIN GAGE LOCATIONS WITH RESPECT TO THE HOLE FOR (a) DIAMETERS BETWEEN 1.270 ≤ 2.540 cm AND (b) DIAMETERS GREATER THAN 2.540 cm. ALL DIMENSIONS IN CENTIMETERS.

tests suggested that the 48 ply laminates failed because of instabilities in regions of the hole boundary other than at the lateral or longitudinal centerlines, Figure 3-3b.

Chapter 4

RESULTS AND DISCUSSION

To preserve clarity, the individual results of the 24 ply and 48 ply specimens are presented independently. Thickness dominated phenomena are discussed separately for each series and general conclusions will be presented in the next chapter.

A total of twenty-six 48 ply and twenty-five 24 ply panels were tested. Throughout the remainder of this chapter, buckling will be defined as that point during load application at which the flat form of the plate ceases to be an equilibrium state and significant out-of-plane displacement begins, denoted experimentally by a reversal in the far field strain gages. For those cases where post-buckling strength is exhibited, the critical load is the intersection of the extensions of the primary and secondary linear portions of the load-displacement curves which denote the elastic and tangent moduli, respectively.

4.1 Forty-Eight Ply Specimens

4.1.1 Failure Strain and Mechanisms

Table 4-1 presents the cutout dimension, modulus, failure load and failure strain for the series of 48 ply specimens tested. For cutout diameters, D, of $0.0 < D \leq 0.3175$ cm ($0.0 < D \leq \frac{1}{8}$ in.) strain reversal occurred in the far field gages of the orthotropic laminates just prior to failure. The critical load of the laminate is reached just before failure strain of the material so that the increase in strain on the

Table 4-1

Strain and Load at Failure of 48 Ply Specimens

Panel Number	Diameter (cm)	$\frac{D}{T}$	Modulus, E_x ($\times 10^4$ MPa)	Failure Load, P_f ($\times 10^2$ kN (Kips))	Failure Strain, ε_f ($\times 10^{-3}$ $\frac{cm}{cm}$)
Orthotropic					
AK1	-	-	8.124	4.390 (98.70)	7.988
AK2	0.318	0.51	7.615	4.237 (95.25)	7.718
AK3	0.635	1.01	7.735	3.567 (80.20)	6.321
AK4	0.952	1.53	8.110	3.292 (74.00)	5.762
AK5	1.270	2.05	7.976	2.927 (65.80)	5.149
AK6	1.588	2.55	7.808	2.713 (61.00)	4.752
AK7	1.905	3.07	8.070	2.613 (58.75)	4.552
AK8	2.223	3.57	-	2.344 (52.70)	4.022
AK9	2.540	4.07	7.543	2.411 (54.20)	4.141
K10	3.810	6.06	7.432	2.202 (49.50)	3.673
K11	2.540	4.06	6.565	2.958 (66.50)	4.140
K12	3.810	6.10	5.023	3.214 (72.25)	2.761
K13	3.175	5.08	4.853	3.358 (75.50)	3.694
K14	3.175	5.08	6.592	2.302 (51.75)	3.887
K15	-	-	7.7035	4.315 (97.00)	8.129
Isotropic					
J1	3.810	5.43	4.702	3.314 (74.50)	3.843
J2	2.540	3.61	4.762	2.969 (66.75)	5.847
J3	0.318	0.45	4.853	3.670 (82.50)	9.380
J4	0.635	0.92	5.261	4.637 (67.25)	7.368
J5	0.953	1.37	4.764	4.878 (70.75)	7.759
J6	1.270	1.81	5.125	2.936 (66.00)	7.199
J7	1.588	2.29	5.158	4.482 (65.00)	7.115
J8	1.905	2.73	4.822	3.930 (57.00)	6.196
J9	2.223	3.19	4.877	2.469 (55.50)	5.932
J10	2.540	3.61	4.882	2.335 (52.50)	4.965
J11	3.810	5.32	4.192	3.344 (48.50)	5.583
J14	-	-	4.540	4.755 (106.90)	12.62

concave side that accompanied the onset of buckling was enough to fail the material. Figure 4-1a shows compressive strain 0.159 cm. ($\frac{1}{16}$ in.) from the hole and the corresponding far field strain. Failure strain occurs at approximately 0.010 cm/cm and 0.423 MN (95. kips) whereas buckling begins around 0.409 MN (92. kips). The load-displacement curve, Figure 4-1b, is essentially linear to failure exhibiting no post-buckling strength. The moiré fringe pattern for this specimen is shown in Figure 4-2; the dark rings connect points of equal out-of-plane deflection thereby outlining the buckled shape. Denoting the number of longitudinal halfwaves of the buckled shape by m and the number of lateral halfwaves by n, Figure 4-2 shows the buckled shape to be m=n=1. In contrast, buckling is apparent only in the control specimen of the quasi-isotropic series. The buckling load is 97.3 percent of the final failure load and bifurcation occurs in the m=2, n=1 mode at a far field strain of 0.0128 cm/cm.

Failure occurred at the point of maximum out-of-plane deflection in the quasi-isotropic case and at the ends of the side supports for orthotropic panels. The side support failure is explained by the fact that the gap between the end grips and the side supports, as previously mentioned, allows rigid body motion between the two fixtures at buckling. Severe displacement gradients can occur in this region allowing the ends of the supports to dig into the specimen and cause local strain concentrations which precipitate failure, Figure 4-3. For plates with small holes, the concentration due to this anomaly is greater than that due to the presence of the cutout.

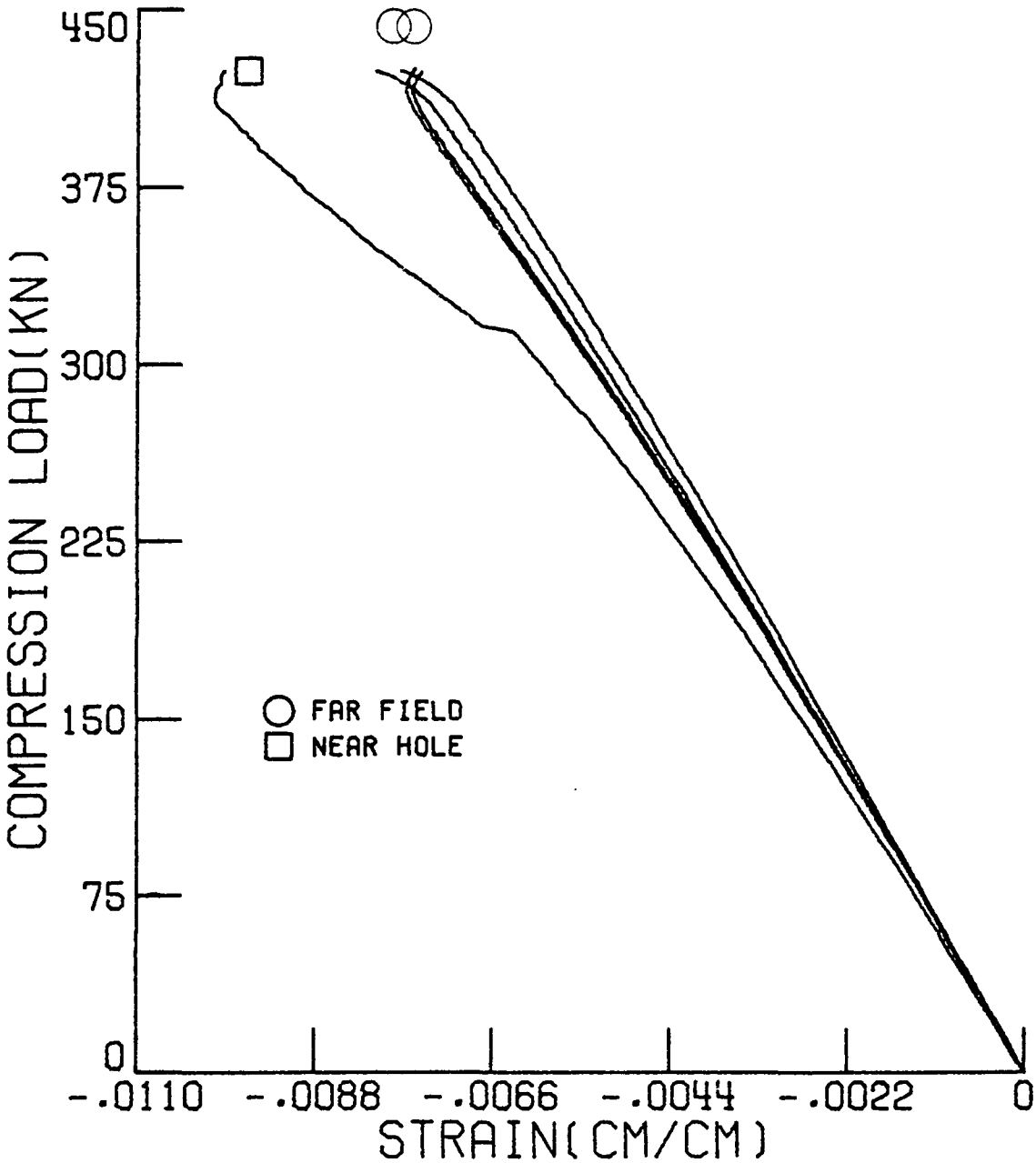

FIGURE 4-1a. STRAIN RESPONSE OF ORTHOTROPIC LAMINATE NEAR HOLE AND FAR FIELD.

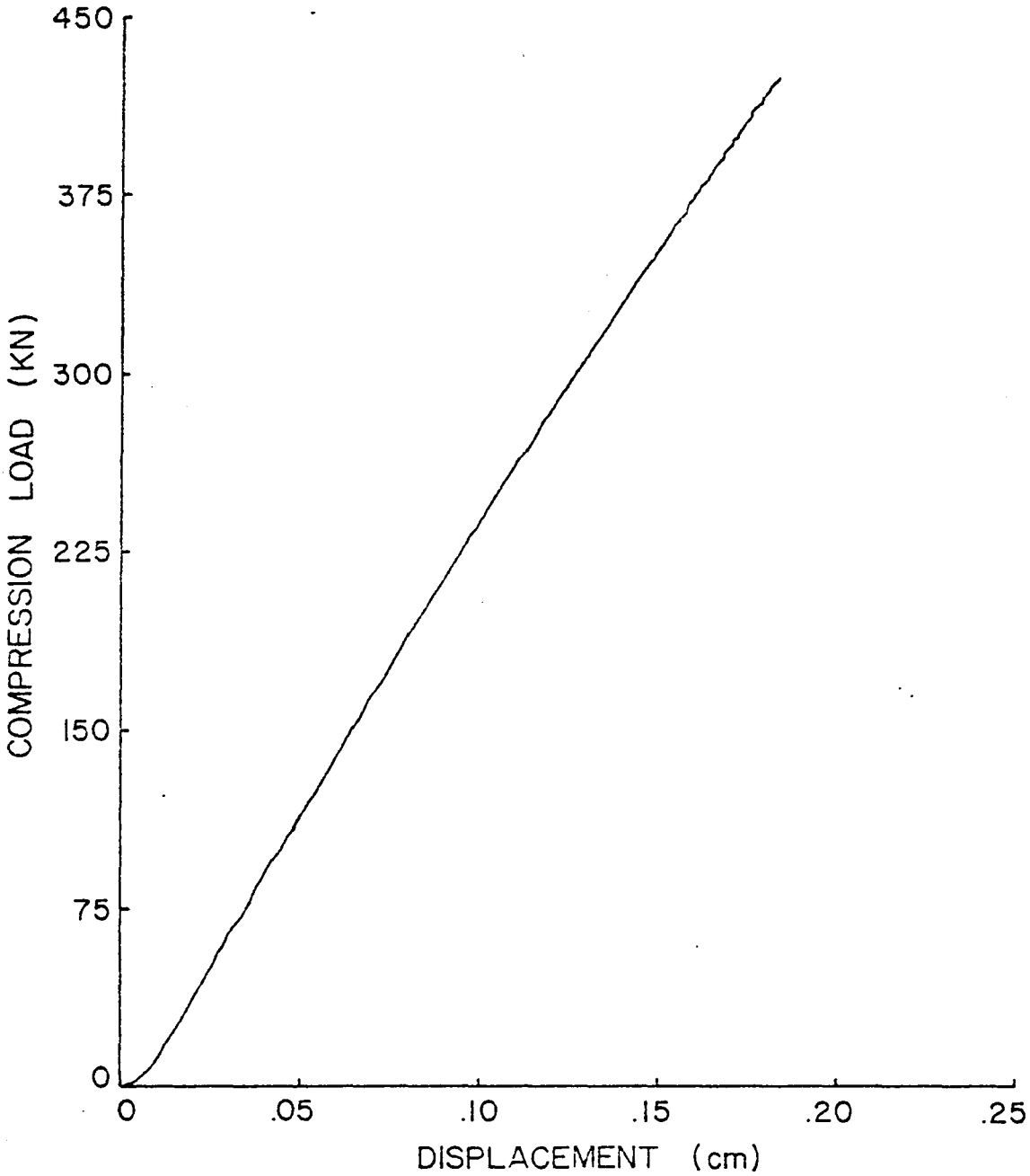

FIGURE 4-1b. LOAD-DISPLACEMENT CURVE FOR A 48 PLY ORTHOTROPIC LAMINATE WITH 0.3175 cm ($\frac{1}{8}$ in) CUTOUT.

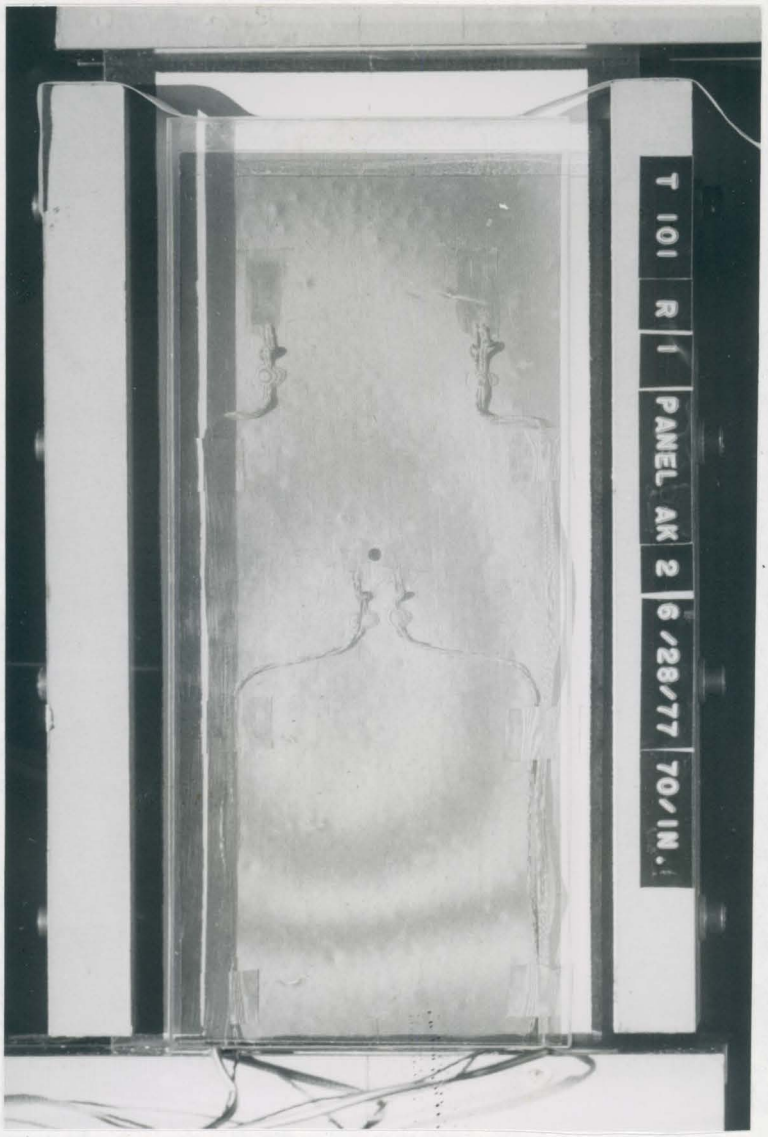

FIGURE 4-2. THE BUCKLED SHAPE OF 48 PLY ORTHOTROPIC PANEL WITH A 0.3175 cm ($\frac{1}{8}$ in) HOLE IS SHOWN BY MOIRÉ FRINGE PATTERN TO BE m=n=1.

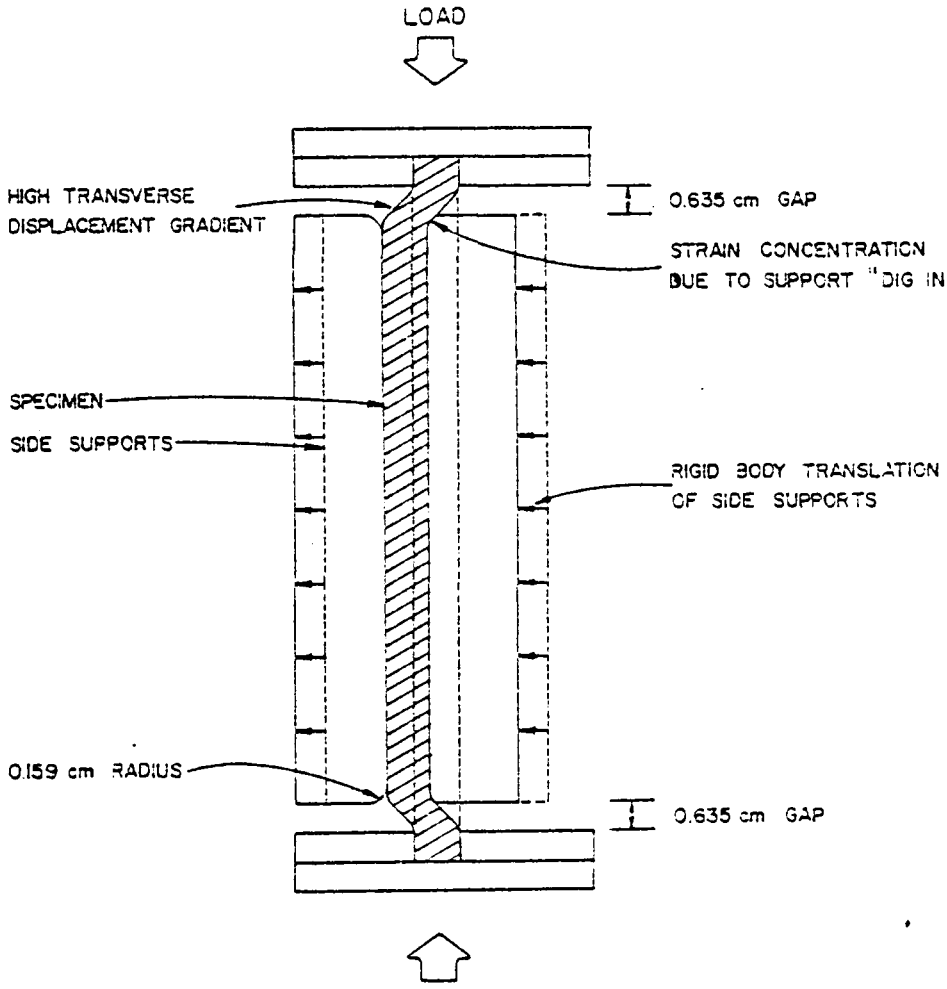

FIGURE 4-3. SIDE VIEW OF SPECIMEN AND FIXTURE SHOWING STRAIN CONCENTRATION ANOMALY.

The greater tendency of the orthotropic lay-up to buckle, even with strain concentrations introduced by a small hole, deserves discussion. The larger percentage of 0° fibers in the orthotropic lay-up imparts a larger longitudinal bending stiffness and a smaller transverse bending stiffness to these panels as shown below in units of Newton-meters

$$[D]_{ortho} = \begin{bmatrix} 2001.2 & 516.4 & 25.2 \\ 561.4 & 890.0 & 25.5 \\ 25.5 & 25.5 & 551.3 \end{bmatrix}$$

$$[D]_{iso} = \begin{bmatrix} 1488.7 & 516.4 & 3.9 \\ 516.4 & 1402.5 & 3.9 \\ 3.9 & 3.9 & 551.3 \end{bmatrix}$$

More important than the relationships between D_{11} and D_{22} is the increase in the D_{16} and D_{26} terms for the orthotropic case. The effect of increasing the twist coupling stiffness is to decrease the buckling load, [19], which explains the experimental results. The observed out-of-plane deflection magnitudes are shown in Figure 4-4 in terms of moiré fringe patterns. The greater the number of fringes the larger the out of plane displacement, therefore the deflection of the orthotropic panel is seen to be many times greater than that of the quasi-isotropic panel.

For hole sizes between 1.27 and 2.54 cm. ($\frac{1}{2}$ and 1.0 in.) strain gages were applied to the interior of the hole at the position of

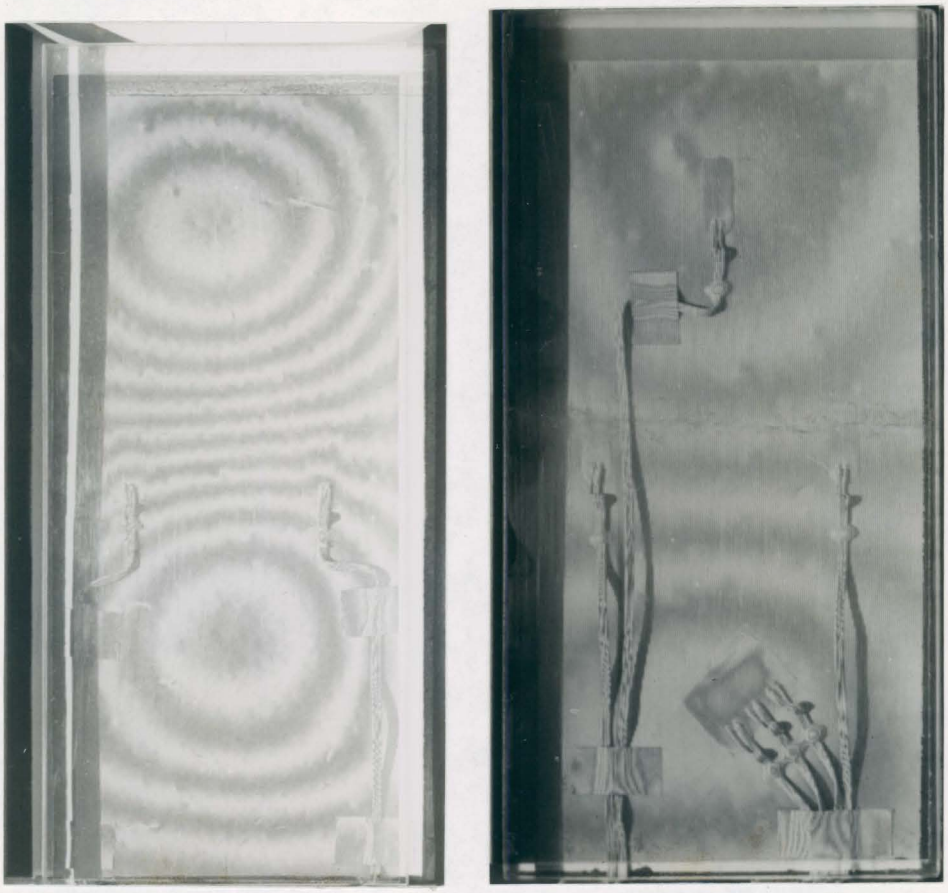

(a) (b)

FIGURE 4-4. MOIRÉ FRINGE RESPONSE OF EACH 48 PLY PANEL UNDER LOAD. a) THE ORTHOTROPIC PANEL HAS MANY MORE WELL DEFINED FRINGES DENOTING LARGER OUT-OF-PLANE DEFLECTION THAN b) THE QUASI-ISOTROPIC PANEL.

expected maximum strain. Both circumferential and through-the-thickness strains were measured. This facilitated the measurement of a true strain concentration factor by comparing hole boundary circumferential strain on an axis perpendicular to load application to far field strain.

As the diameter of the cutout increased, the amount of local material failure around the hole increased. For hole diameters greater than 1.27 cm. ($\frac{1}{2}$ in.) in the orthotropic lay-up, panel failure was preceded by local bending around the hole, Figure 4-5. The bending caused high out-of-plane deflection gradients to be established inducing delamination and load redistribution which can be seen as an instability in the through-the-thickness gage, Figure 4-6, for a 2.22 cm. ($\frac{7}{8}$ in.) diameter hole. This instability was less pronounced in the quasi-isotropic case, Figure 4-6. These figures also show the relative magnitudes of the through-the-thickness normal strain in the two laminates. In the quasi-isotropic specimens, the normal strain is higher, ofter exceeding the orthotropic response by 100 percent.

The delamination which caused the transverse strain instability might be explained by micro-mechanical consideration of fiber buckling or matrix failure. When the fibers buckle in different directions, which could be influenced by local imperfections, high interfiber strains are established in the matrix. As load is increased, the strength of the matrix is finally exceeded and matrix cracking or debonding occurs, Figure 4-7. This same effect is present in the quasi-isotropic lay-up, only to a lesser degree.

Finally, for hole sizes of 2.54 to 3.81 cm. (1.0 to $1\frac{1}{2}$ in.) strain

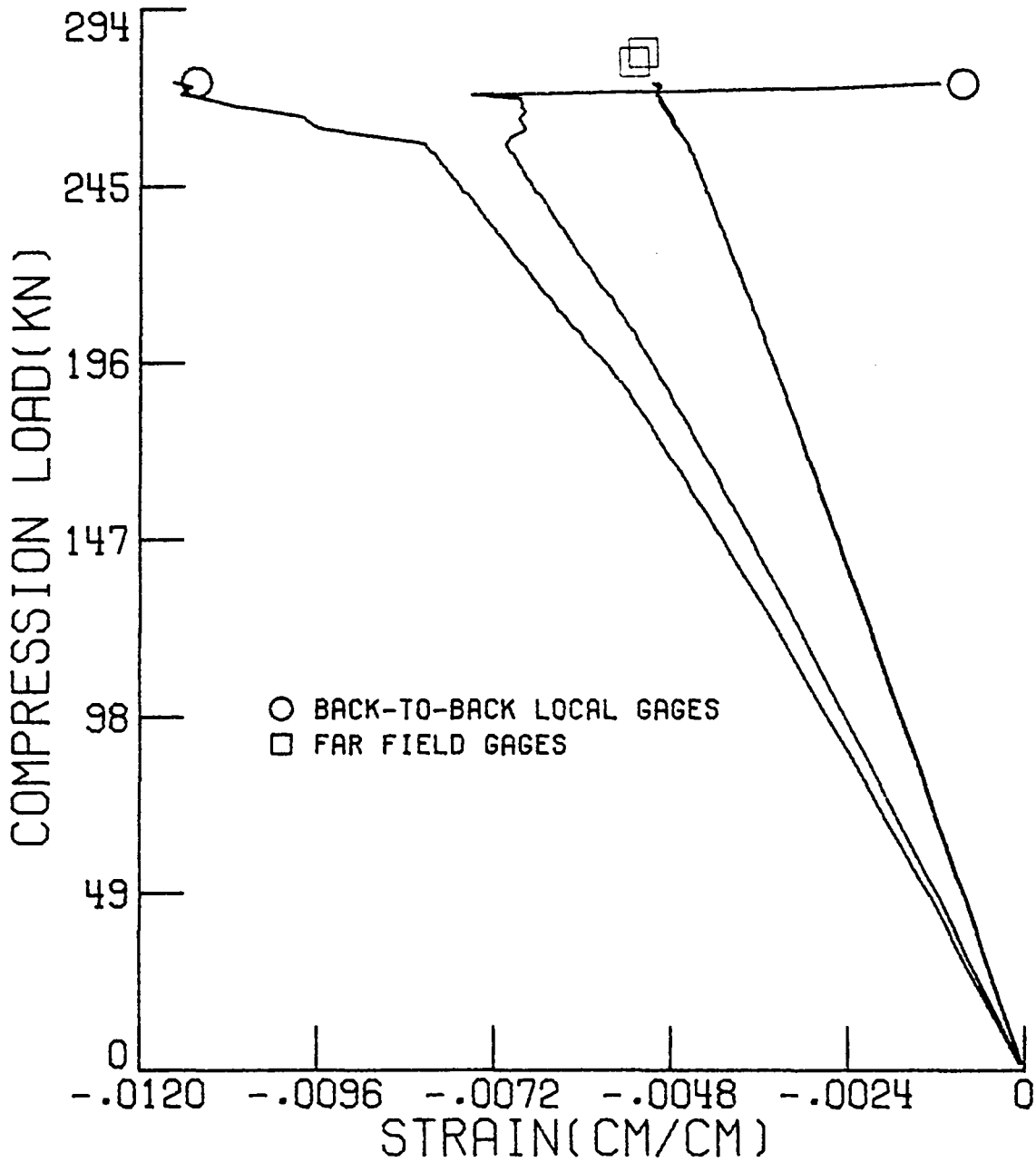

FIGURE 4-5. EVIDENCE OF LOCAL BENDING AROUND HOLE IN A 48 PLY ORTHOTROPIC PANEL WITH A 1.5875 cm ($\frac{5}{8}$ in) HOLE. LOCAL GAGES ARE 0.3175 cm ($\frac{1}{8}$ in) FROM HOLE BOUNDARY.

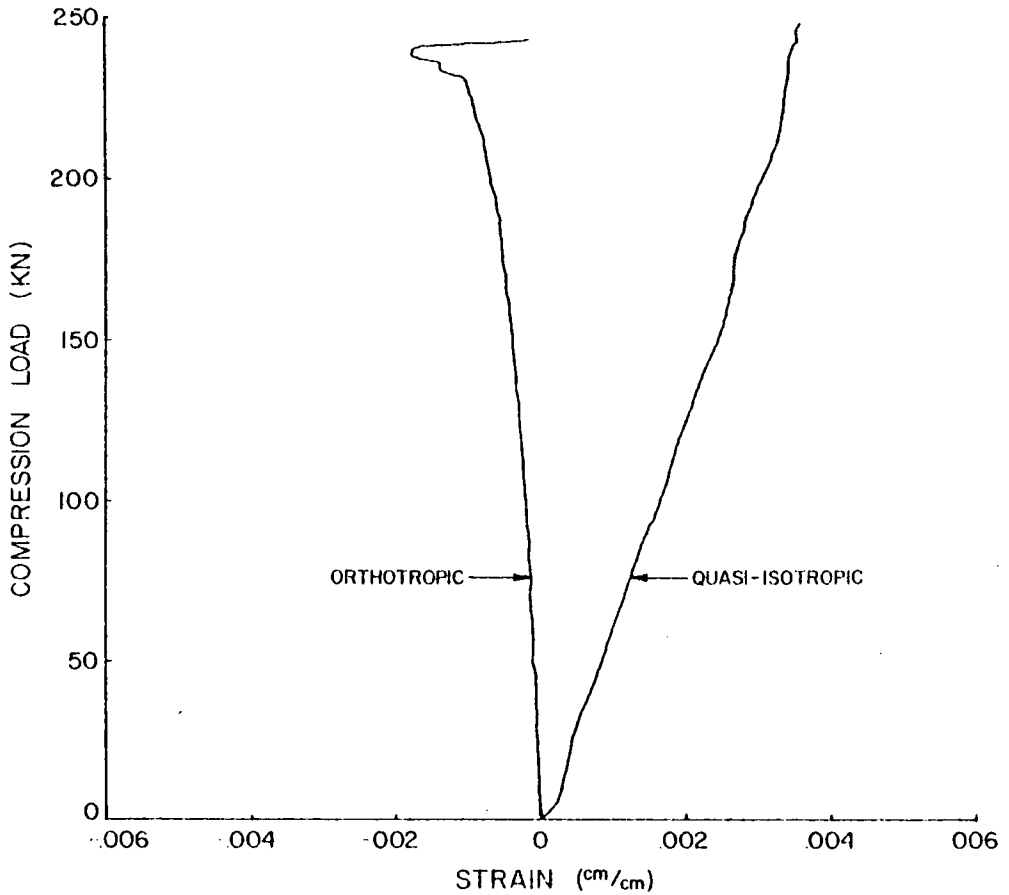

FIGURE 4-6. EFFECT OF LOCAL BENDING ON NORMAL STRAIN, ϵ_z.

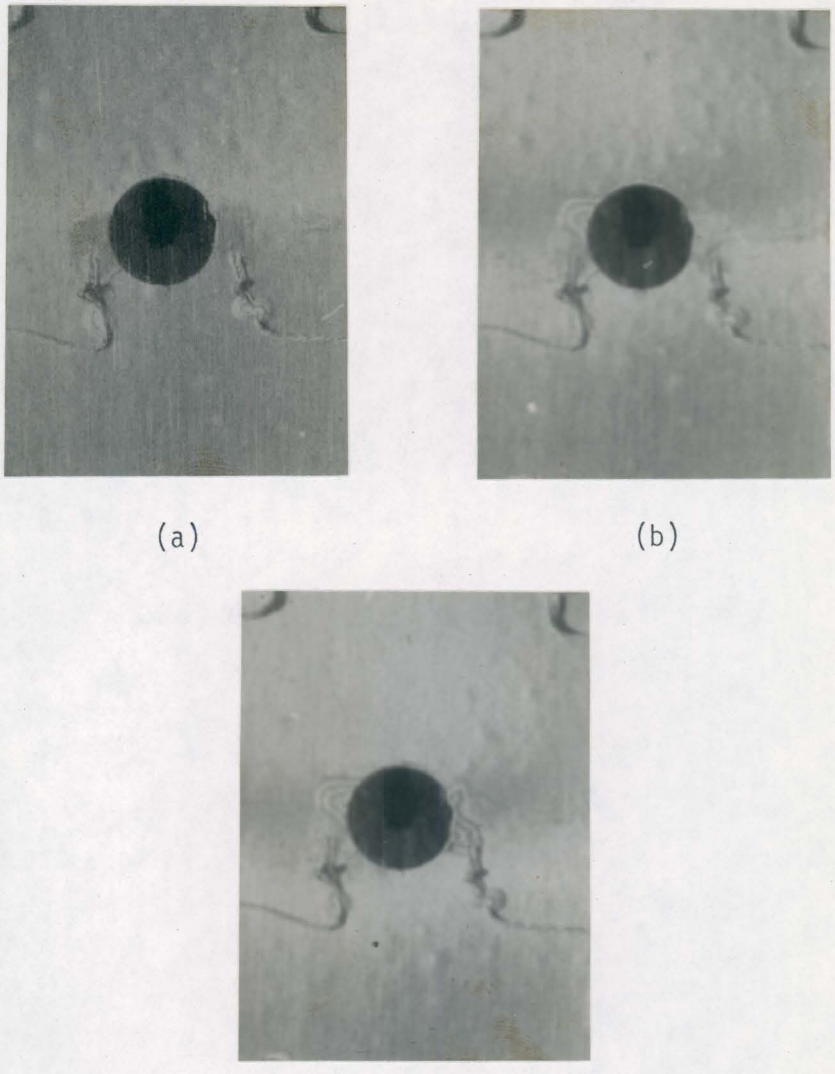

(a) (b)

(c)

FIGURE 4-7. PROGRESSION OF MATERIAL FAILURE AROUND HOLE. 48 PLY ORTHOTROPIC. a) ZERO LOAD. SHADED PORTIONS TO EACH SIDE OF HOLE ARE STRAIN GAGES. b) 257.1 kN (57.8 kip) LOAD. c) 261.1 kN (58.7 kip) LOAD.

gages were applied at additional locations around the hole to measure normal and circumferential strain. In every case the maximum compressive circumferential strain occurred on the lateral centerline of the hole. A difference was observed between the orthotropic and quasi-isotropic cases, however, in the position of maximum normal strain around the hole as discussed below. For orthotropic specimens, gages were placed on the lateral centerline and 30 degrees (clockwise) off-centerline. In addition to these locations, the quasi-isotropic panels had a gage oriented at 45° to the load axis (Figure 3-3b). Figure 4-8 shows typical results of the orthotropic tests. The strain at the 30 degree location varies between two and three times the strain on the lateral centerline. The trace is very erratic, beginning in tension and finally failing in compression. The quasi-isotropic case, Figure 4-9, shows relatively uniform strain levels at all gage locations and the failure response of the gages is less catastrophic. The commonly accepted value for ultimate strain of the Narmco 5208 resin system is 0.0036 cm/cm. The off-axis value of normal strain, ε_z, in the orthotropic panel does not approach this value, therefore the local out-of-plane deflection seen in Figure 4-7b,c must be due to an interaction between normal strain and other strain components such as interlaminar shear.

A three-dimensional finite element code was used to determine the interlaminar stress state in the orthotropic panel [21]. The finite element model grouped the laminate into a series of four-ply laminae through the half-thickness in order to match the limitation of six

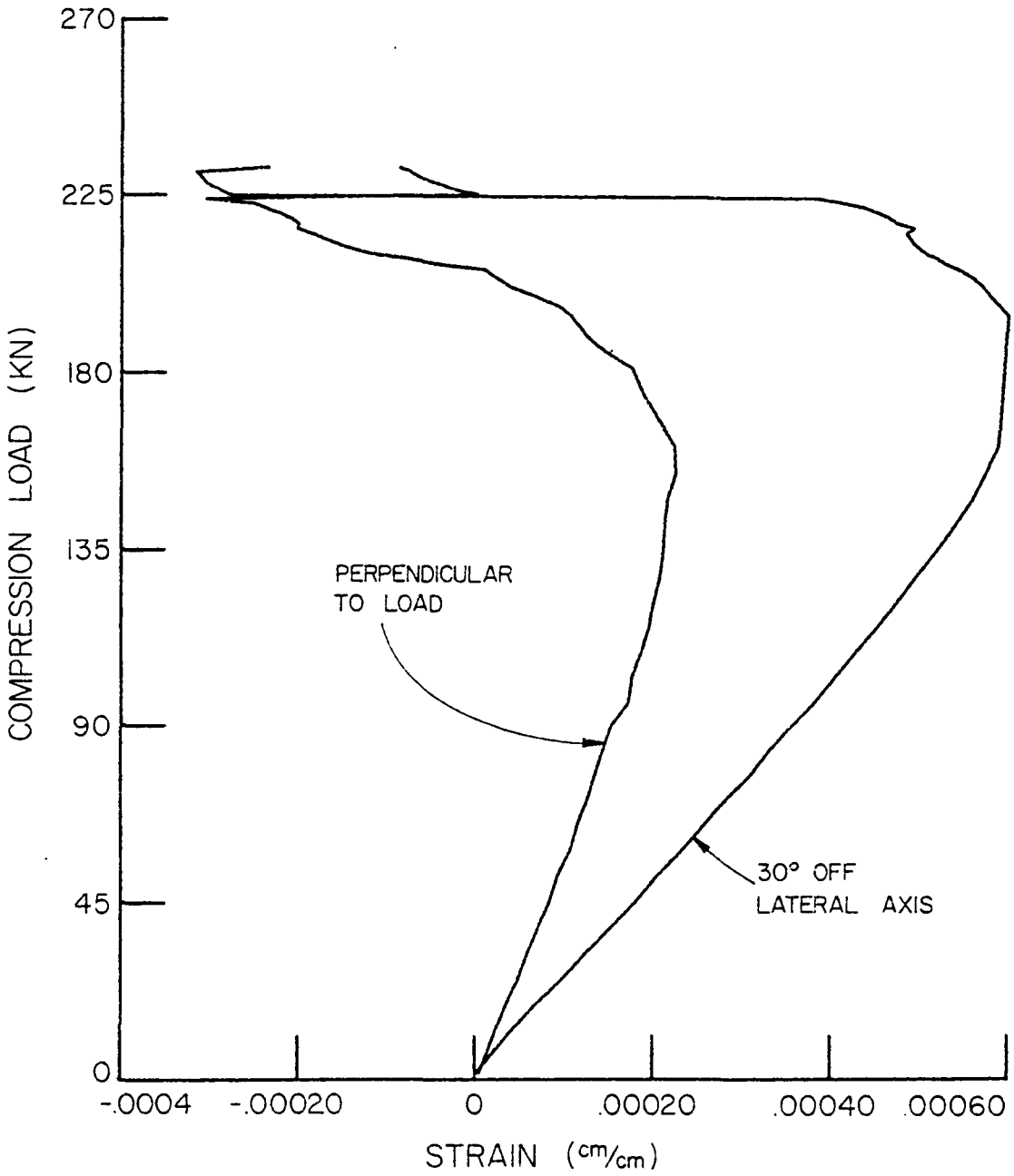

FIGURE 4-8. TRANSVERSE STRAIN ON LATERAL CENTERLINE OF HOLE BOUNDARY. ORTHOTROPIC PANEL, 3.175 cm ($1\frac{1}{4}$ in) CUTOUT.

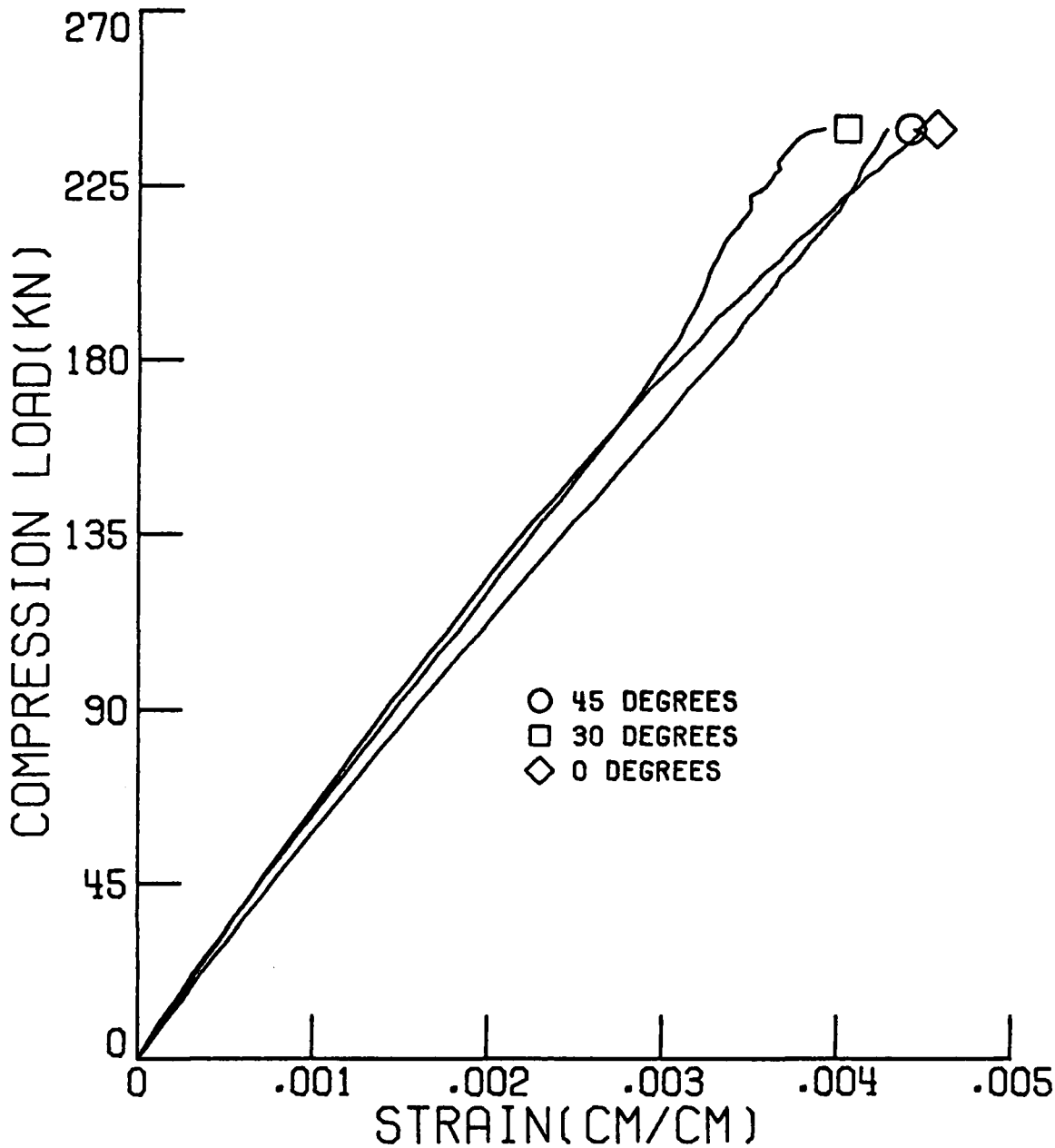

FIGURE 4-9. TRANSVERSE STRAIN ON HOLE BOUNDARY AT DIFFERENT LOCATIONS FROM LATERAL AXIS. QUASI-ISOTROPIC LAMINATE, 2.54 cm (1.0 in) DIAMETER CUTOUT.

elements in the z-direction established by the program. The effective modulus properties of the combined laminae were calculated by laminated plate theory and used as input to the code.

The linear elastic profile of the intralaminar shear stress, τ_{xy}, between the elements closest to the plate surface (i.e., the two outermost four-ply layers) is reported for both lay-ups in Figure 4-10. The magnitudes have been normalized with respect to the maximum τ_{xy} around the cutout. Such asymmetric behavior has also been reported by other authors for various orthotropic geometries [8,9,15,16,22]. Failure is most likely due to a complicated interaction of the various strain components around the hole. Although initial failure in the orthotropic specimens is seen to begin off-axis, Figure 4-7b,c, the final failure zone of the panel is seen to extend along the centerline of the cutout normal to the load axis, Figure 4-11.

During load application, a combination of high intralaminar shear stress, due to mismatch of the Poisson's ratio of the laminae, and high out-of-plane normal strain, possibly due to three-dimensional effects, is developed locally in a 45 degree arc clockwise from the axis normal to load application. The effect of this combination is to fail the matrix, causing local delamination. In effect, the single plate becomes two or more thinner plates locally with significantly reduced buckling loads. Local off-axis buckling occurs and the subsequent load redistribution which follows causes catastrophic failure perpendicular to the load axis because of the already high compressive circumferential strain in this area.

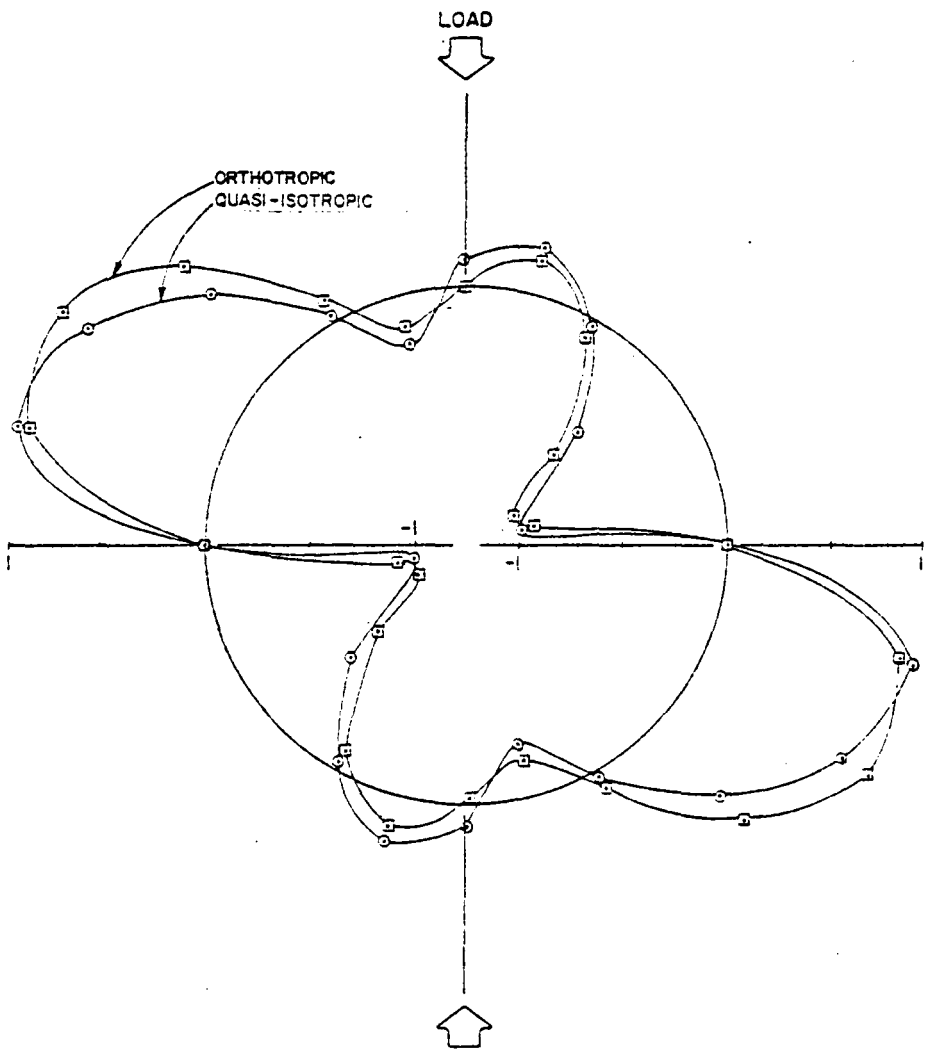

FIGURE 4-10. τ_{xy} BETWEEN TWO OUTER MOST FOUR-PLY LAYERS. FINITE ELEMENT SOLUTION.

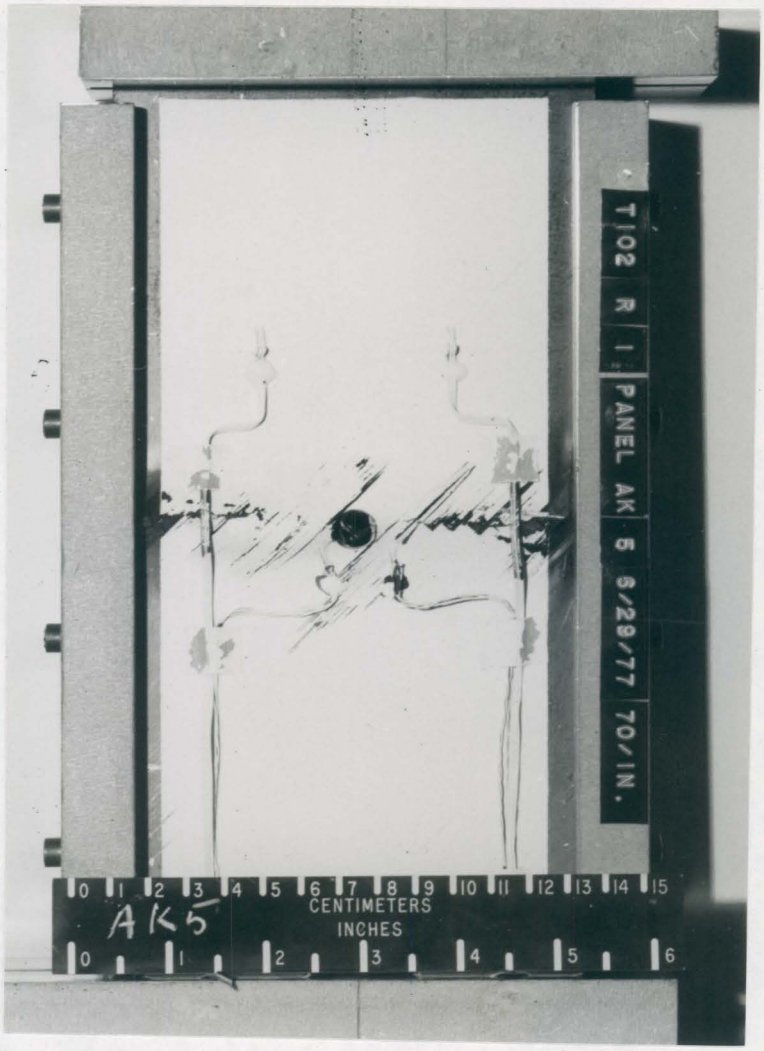

FIGURE 4-11. FAILED 48 PLY ORTHOTROPIC SPECIMEN.

In the quasi-isotropic laminate, the stress state is more confined. The maximum shear stress, Figure 4-10, is closer to the lateral axis along with high out-of-plane normal and circumferential strains in the same region. Figure 4-9 shows that the out-of-plane normal strain, ε_z, is at a constant high level around the cutout; Figure 4-12 compares the circumferential strain levels for similar specimens of each orientation. The matrix is well above its failure strain, 0.0036 cm/cm, and the circumferential strain is well above the analytical buckling strain of a plate without a hole. The ability of the composite to support such high strains locally is due to the nonuniform strain gradient away from the hole, confining the strains to a small volume of material [18].

In general, panel failure was not preceded by local material failure around the hole in the quasi-isotropic case; failure was sudden without visual or acoustic warning. The failure surface of a quasi-isotropic panel, Figure 4-13, appeared to be more the result of an explosive, crushing material failure than the sequential delamination and local buckling of the orthotropic panel.

4.1.2 Diameter to Thickness Ratio

The influence of hole size on the compressive behavior of a laminate was found to be more pronounced in the 48 ply specimens than in the 24 ply specimens. This was due to the fact that a majority of the 48 ply panels were strength failures as opposed to buckling failures.

Figure 4-14 shows how both the circumferential and far field failure strain is inversely proportional to the diameter dimension,

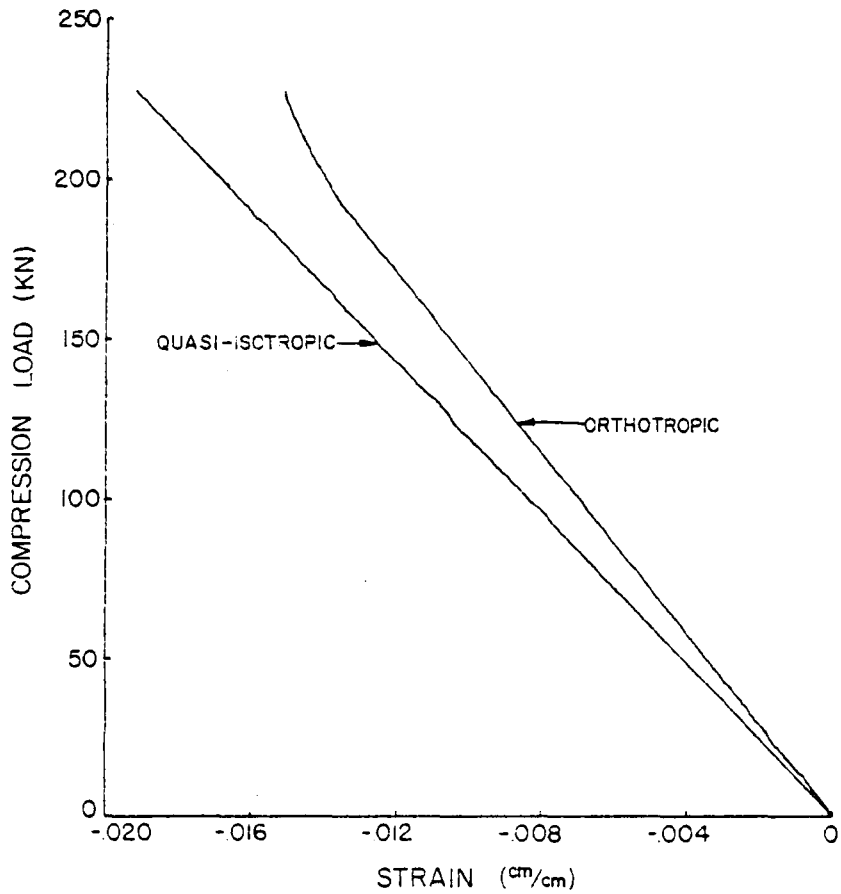

FIGURE 4-12. COMPARISON OF STRAIN LEVELS IN EACH TYPE PANEL ON THE BOUNDARY OF 3.81 cm ($1\frac{1}{2}$ in) DIAMETER HOLE.

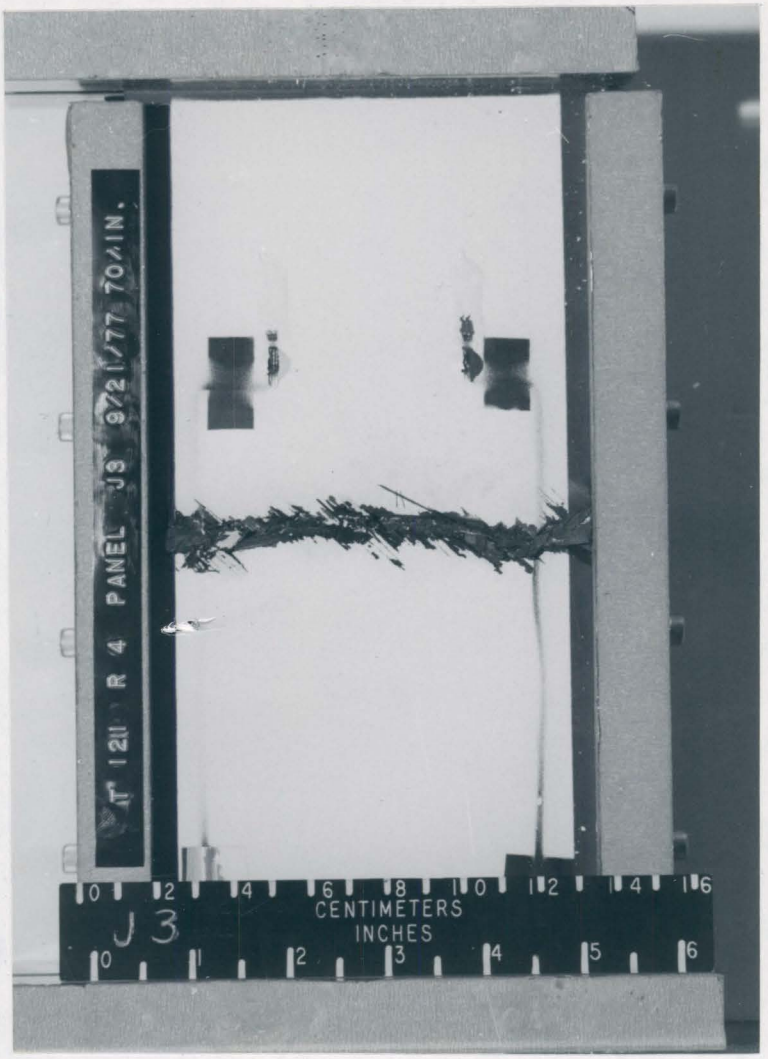

FIGURE 4-13. TYPICAL FAILED 48 PLY QUASI-ISOTROPIC PANEL.

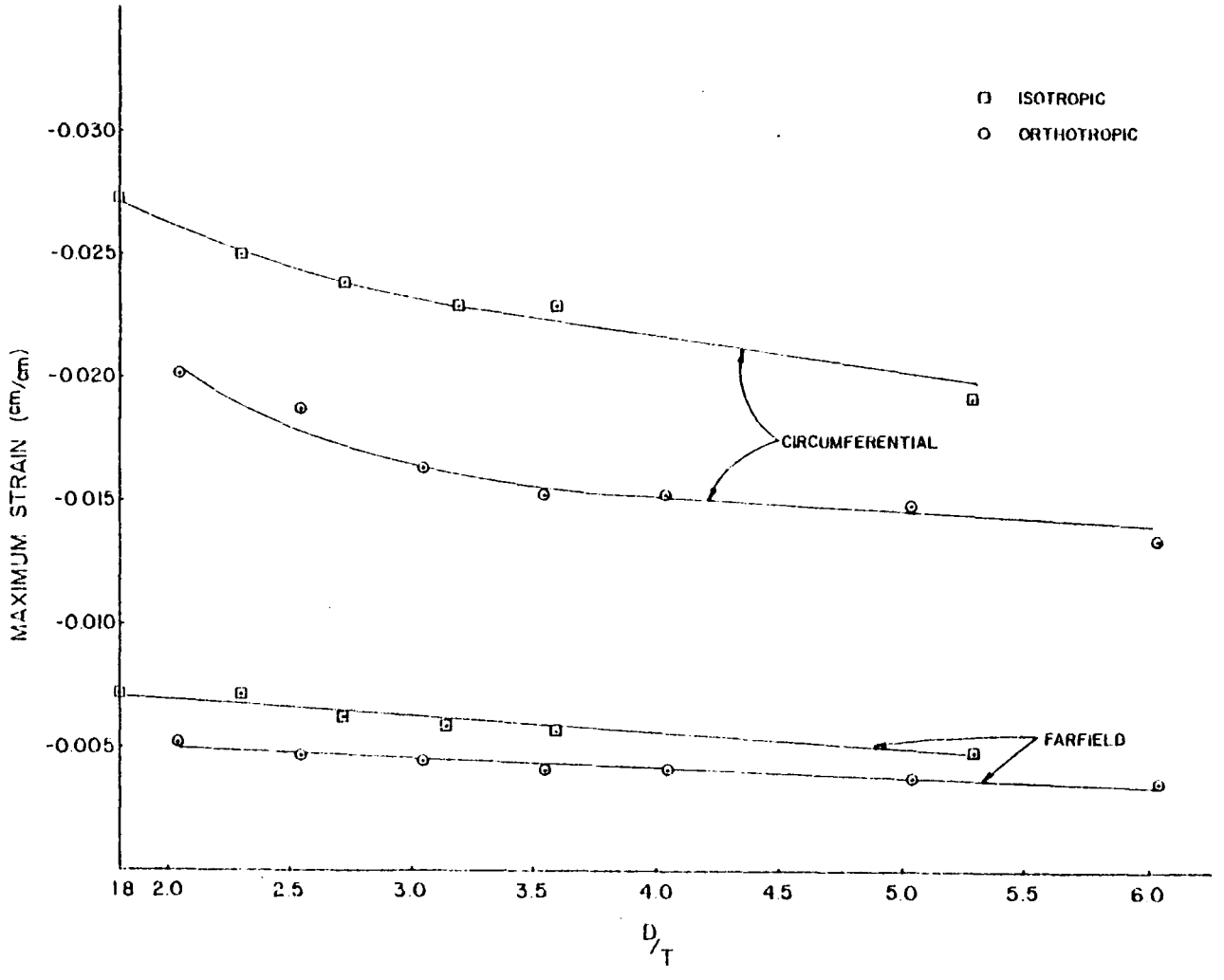

FIGURE 4-14. STRAIN TREND WITH INCREASING HOLE SIZE. 48 PLY.

holding length and width approximately constant. The strain level is larger in the quasi-isotropic case. The experimental data are reported in terms of diameter-to-thickness ratio, $\frac{D}{T}$ in order to alleviate the dependence on thickness which was 0.625 cm (0.246 in.) for orthotropic and 0.702 cm (0.276 in.) for quasi-isotropic plates. The difference in thickness was due to the fact that the orthotropic and quasi-isotropic laminates were fabricated by different suppliers.

The variation with diameter of normal strain, ε_z, on the lateral centerline of the cutout is reported in Figure 4-15. From the erratic behavior of normal strain, ε_z, for the quasi-isotropic series it is concluded that ε_z is highly influenced by micromechanical imperfections such as voids and poor fiber-matrix interface integrity. This is further accentuated by the higher strain levels in the quasi-isotropic panels.

Both analytical and experimental results exist for the effects of varying $\frac{D}{T}$. Rybicki and Schmueser [10] take a finite element approach to cutouts, modeling one-eighth of a laminate by assuming quarter point symmetry in a symmetric laminate. They report decreasing σ_θ for a 2.54 cm (1.0 in.) diameter hole and decreasing ply thicknesses in a family of nine ply laminates which are analytically defined by material properties of the laminae. The applied load is taken to be tension, and the material response, linear elastic.

Whiteside et al [22] present experimental results for the reduction of tensile strength with increasing $\frac{D}{T}$. Both hole diameter and laminate thickness are varied. The hole diameter to thickness ratio is seen to

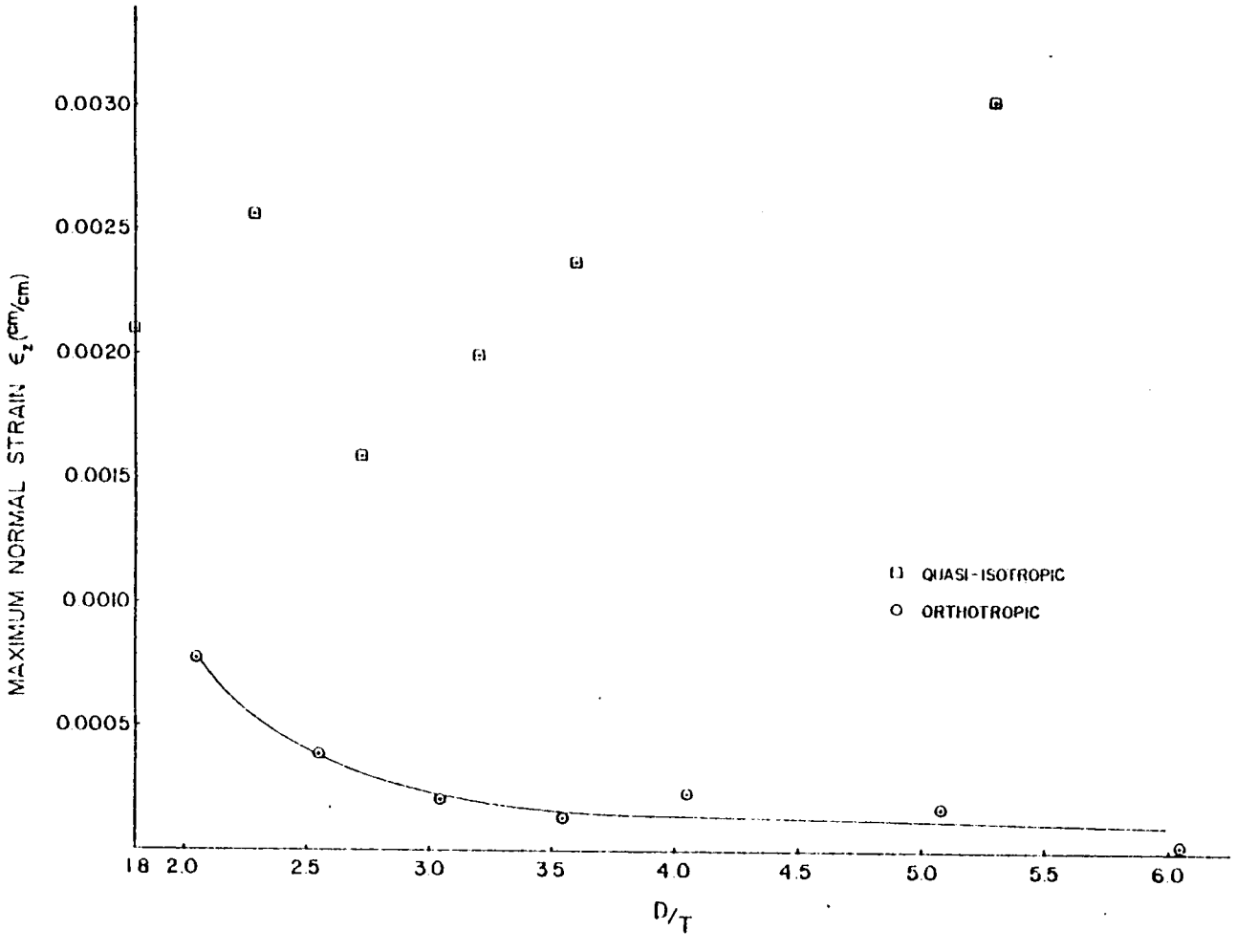

FIGURE 4-15. THE VARIATION OF NORMAL STRAIN WITH HOLE DIAMETER. 48 PLY.

have a pronounced influence on tensile strength, especially for small holes. Data is presented in the form of strength reduction factor which varies from 1.5 to 2.3 for $\frac{D}{T}$ ratios of 1.2 to 21.8.

The 48 ply laminates of the present investigation exhibited a combination of buckling and strength failure. For $\frac{D}{T} \leq 0.504$ bifurcation is evidenced by the reversal of back-to-back longitudinal gages with no post-buckling strength, Figures 4-1a,b. Greater $\frac{D}{T}$ ratios yielded explicit compression strength failures with no gage reversal and no moire fringe patterns developed. Figures 4-16 and 4-17 are the normalized failure load plots with increasing hole size for the orthotropic and quasi-isotropic laminates, respectively.

The bending gradients in the orthotropic specimens of $\frac{D}{T} = 0.0$ and 0.253 were severe enough to cause material failure at the end of the side supports as previously discussed. For $\frac{D}{T} = 0.504$ the degree of buckling was reduced, though still present, and material failure propagated laterally from the hole. All other panels failed around the hole before the buckling load was reached. Therefore, a threshold exists at $0.504 < \frac{D}{T} < 1.01$ in which the mode of failure of orthotropic plates has a transition from buckling to material dominated. The ultimate load for plates with cutouts in Figure 4-16 reduced to approximately 50 percent of the control specimen ultimate load.

In contrast, there is no stability threshold in Figure 4-17 for the quasi-isotropic specimens. The only panels to fail in buckling were the control specimens which failed at the quarter plate points, the location

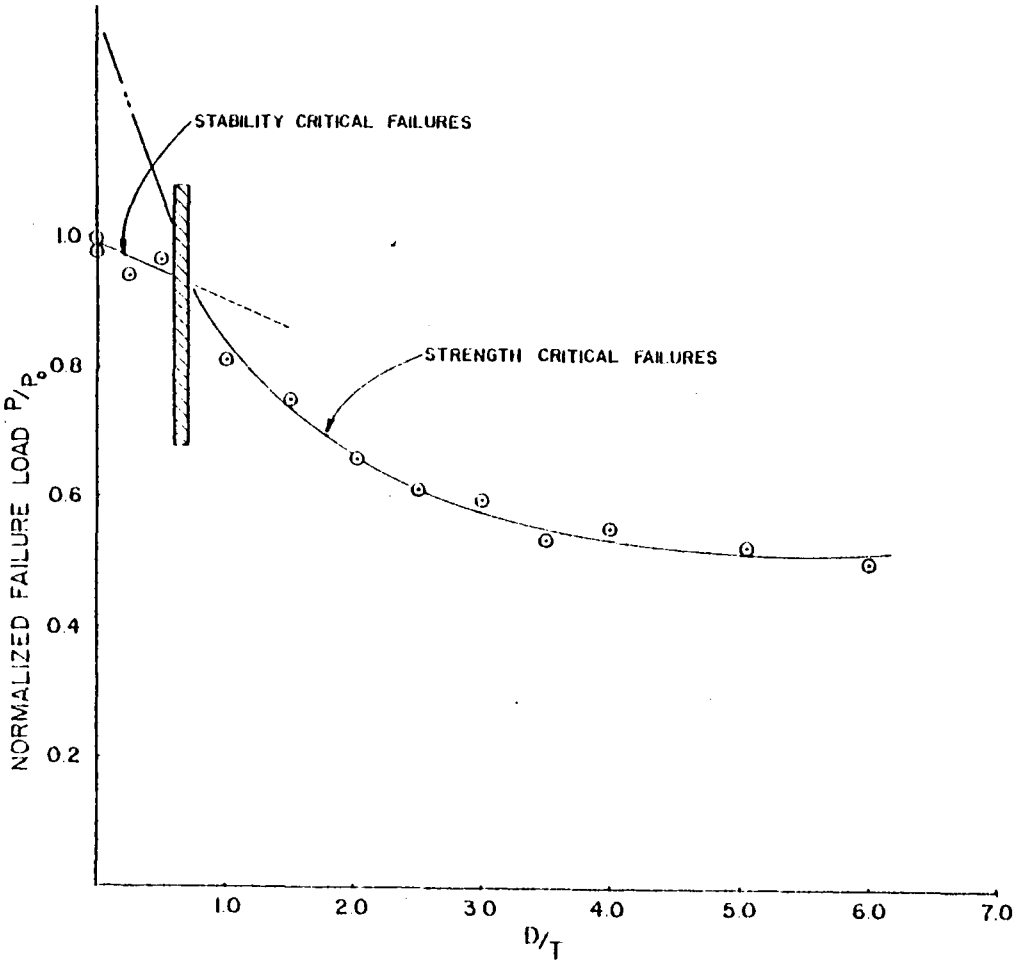

FIGURE 4-16. FAILURE LOAD VERSUS $\frac{D}{T}$ FOR 48 PLY ORTHOTROPIC. P_o IS FAILURE LOAD OF PANEL WITHOUT A CUTOUT.

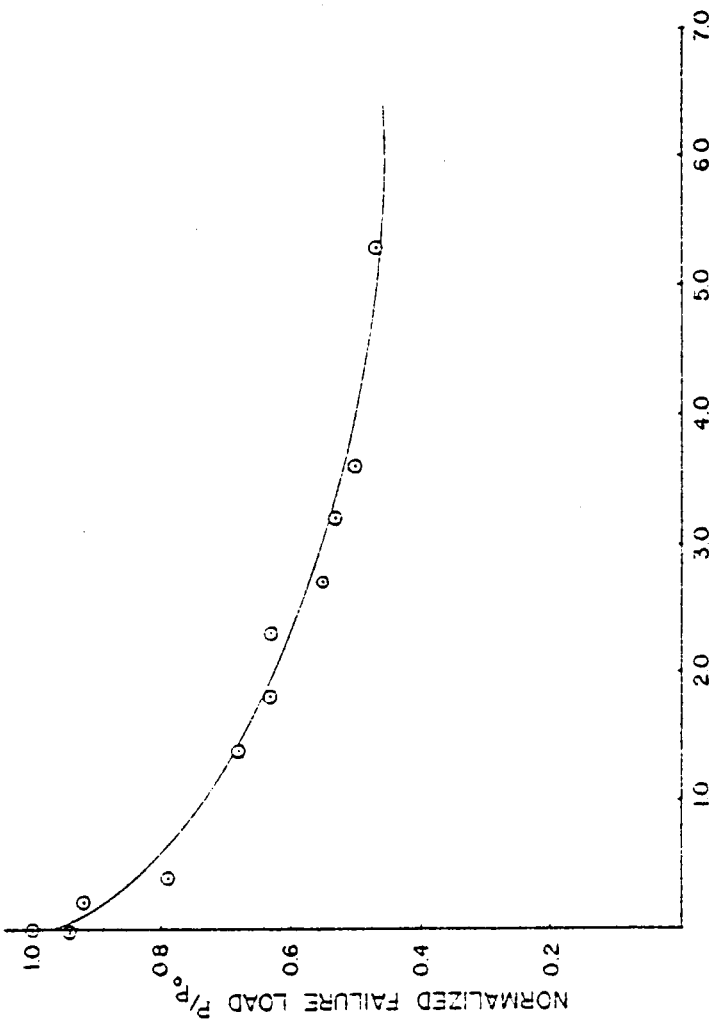

FIGURE 4-17. FAILURE LOAD VERSUS $\frac{D}{T}$ FOR 48 PLY QUASI-ISOTROPIC.

of maximum transverse deflection in the m-2, n=1 mode. The quasi-isotropic control specimens failed at an average of 5.6 percnet higher load than the orthotropic panels. For diameter to thickness ratios of $0.253 \leq \frac{D}{T} \leq 1.530$, the orthotropic specimens exhibited greater strength but failed in buckling, whereas all quasi-isotropic plates with cutouts failed in strength due to the presence of the hole. In every case of $\frac{D}{T} > 1.530$ the failure mechanisms for both laminate configurations were due to the presence of the cutout with failure loads differing by no more than 6.5 percent. Considering that the orthotropic control specimen failure was due to the side support anomaly, and, assuming its strength would exceed that of the quasi-isotropic control with improved boundary conditions, then, in general, for $\frac{D}{T} < 1.5$ the orthotropic layup is superior while for $\frac{D}{T} > 1.5$ either configuration would perform equally well.

4.1.3 Strain Concentration and Width Effect

The removal of potential load carrying material from the center of a panel causes internal load transferral and strain concentrations which not only depend on the shape of the cutout, but on the amount of material removed. For circular holes in infinite isotropic plates the stress concentration factor on the hole centerline normal to load application is 3.0 [1]. The orthotropic extension of this theory, developed by Savin [23], expresses the stress concentration factor of an infinite, homogeneous orthotropic plate as a function of laminate material properties,

$$SCF_{\sigma} = \sqrt{2\left(\frac{E_x}{E_y} - \nu_{xy}\right) + \frac{E_x}{G_{xy}}}$$

where E_x, E_y, ν_{xy} and G_{xy} are the material stiffnesses for a balanced laminate. This relationship yields a value of 3.56 for the orthotropic and 3.00 for the quasi-isotropic materials in this investigation. Any deviation from these values for changing hole diameter must be due to the finiteness of the specimen since hole size does not appear in the SCF_{σ} expression and the only deviation of experiment from theory is the proximity of the plate edge.

Figures 4-18 and 4-19 show the variation of the experimentally determined elastic strain gradient along the lateral centerline as a function of hole diameter for the orthotropic and quasi-isotropic cases, respectively; hole sizes vary from 0.635 cm ($\frac{1}{4}$ in.) to 3.810 cm ($1\frac{1}{2}$ in.) and all plates are 12.70 cm (5.0 in.) wide. The 0.635 cm ($\frac{1}{4}$ in.) holes were too small to accomodate a hole boundary circumferential gage. The reduction of the strain gradient was more pronounced in the orthotropic case which, in general, had a higher SCF_{ε} and a lower far field strain level.

Specimens wider than 12.70 cm (5.0 in.) were fabricated in order to determine what effect the proximity of the plate edge had on both the SCF_{ε} and the lateral strain gradient. These additional panels had widths of 15.24, 19.04 and 22.86 cm (6.0, 7.5 and 9.0 in.). Hole sizes were chosen to preserve a diameter-to-plate width, $\frac{D}{W}$, ratio of 0.1667. Due to problems in machining, no 19.05 cm wide quasi-isotropic panel was tested.

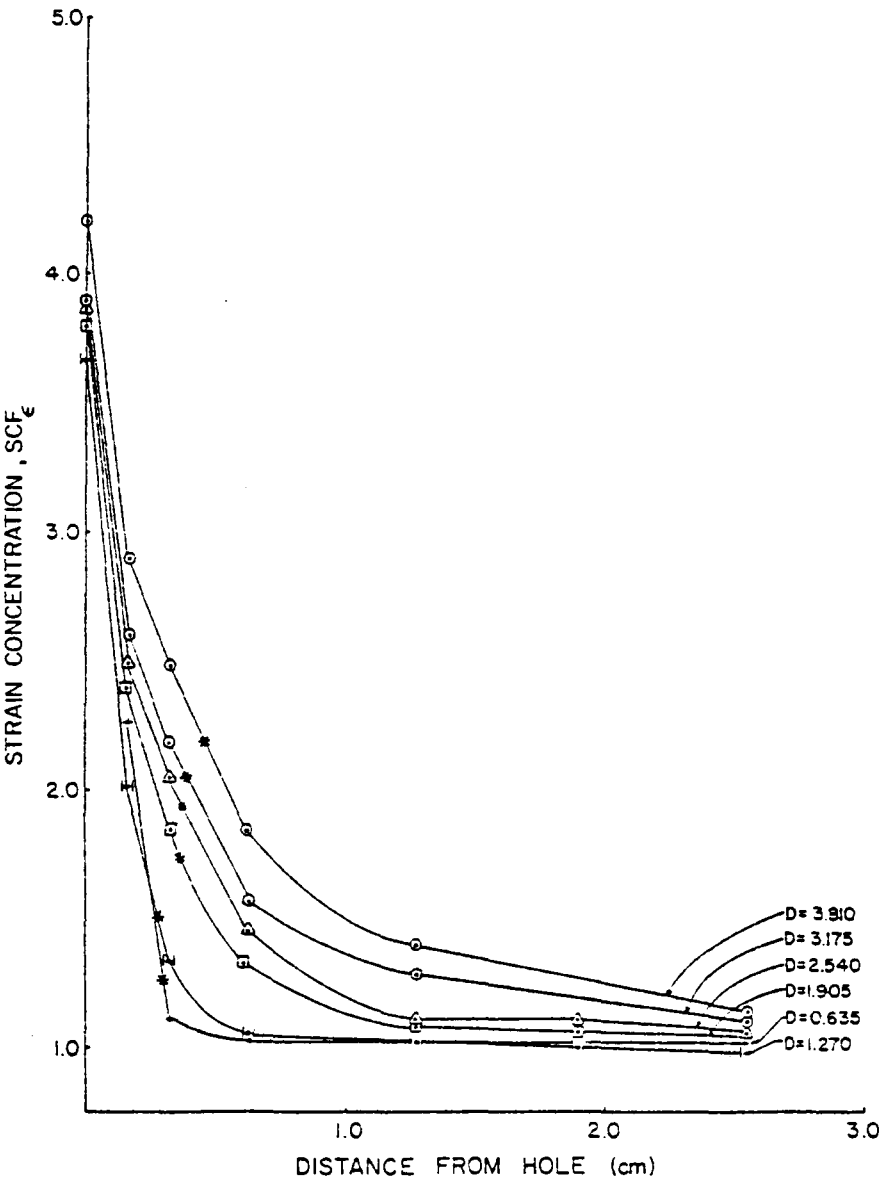

FIGURE 4-18. EXPERIMENTAL STRAIN GRADIENT AWAY FROM HOLE FOR INCREASING HOLE DIAMETER, D. 48 PLY ORTHOTROPIC.

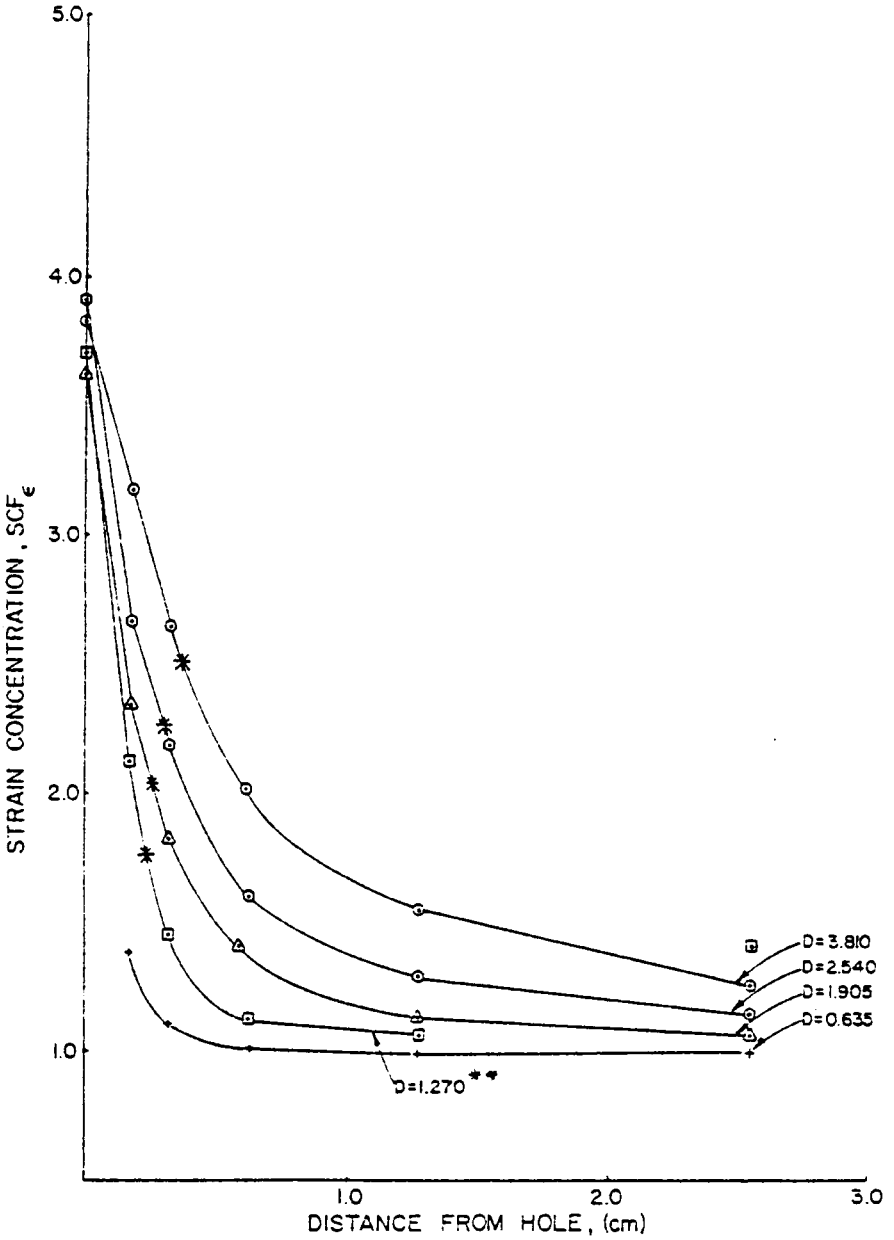

FIGURE 4-19. EXPERIMENTAL STRAIN GRADIENT AWAY FROM HOLE FOR INCREASING HOLE DIAMETER, D. 48 PLY QUASI-ISOTROPIC. 3.175 cm HOLE NOT TESTED. **EXTREME DATA POINT QUESTIONABLE.

The 19.05 and 22.86 cm (7.5 and 9.0 in) wide panels buckled in the m=n=1 mode with failure occurring so rapidly after bifurcation that no post-buckling strength developed, Figures 4-20 and 4-21. The pre-failure buckling is not due to the $\frac{D}{W}$ ratio or hole size but is caused by the reduction in critical load which accompanies an increase in width as seen in the following expression for an isotropic material [25],

$$N_{x_{cr}} = \frac{K\pi^2 Et^3}{12(1-\nu^2)w^2},$$

where K is the end fixity constant, E the Young's modulus, t the thickness, w the width and ν the Poisson's ratio of the plate.

The SCF_ε and strain gradient are compared to 12.70 cm (5.0 in) wide panels with corresponding cutout diameter in Figure 4-22 through 4-24. Since each of the curves represents only one specimen, no general trend can be deduced from these plots. Intuitively, one would expect the increased width to result in a closer approximation to the theoretical infinite plate orthotropic SCF_ε. As the $\frac{D}{W}$ ratio decreases, the strain level in the lateral gradient increases in all cases except the quasi-isotropic response in Figure 4-23. To further examine the width effect, the strain concentration data for these figures has been tabulated in Table 4-2.

To understand how the amount of material affected by the strain concentration varies with hole size, the ratio of the far field failure strain of the control specimen to the failure strain for each hole size was determined,

FIGURE 4-20. MOIRE FRINGE PATTERN SHOWING BUCKLED SHAPE OF WIDE PANEL m=n=1. PANEL IS 22.86 cm (9.0 in) WIDE WITH 3.81 cm ($1\frac{1}{2}$ in) DIAMETER HOLE, 48 PLY QUASI-ISOTROPIC.

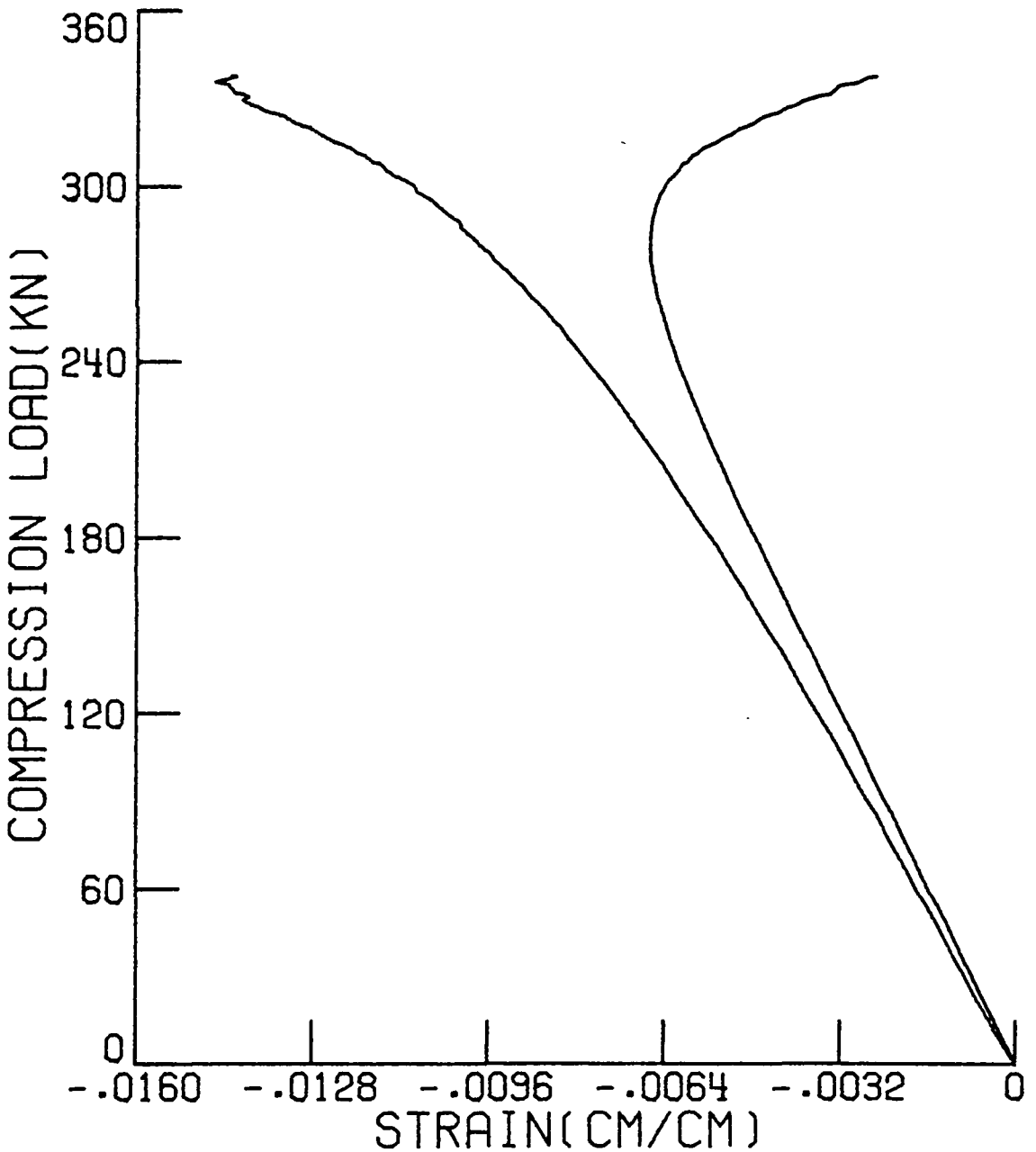

FIGURE 4-21. STRAIN REVERSAL OF TWO BACK-TO-BACK GAGES SHOWING EVIDENCE OF BUCKLING. THIS IS THE STRAIN PLOT FOR FIGURE 4-20.

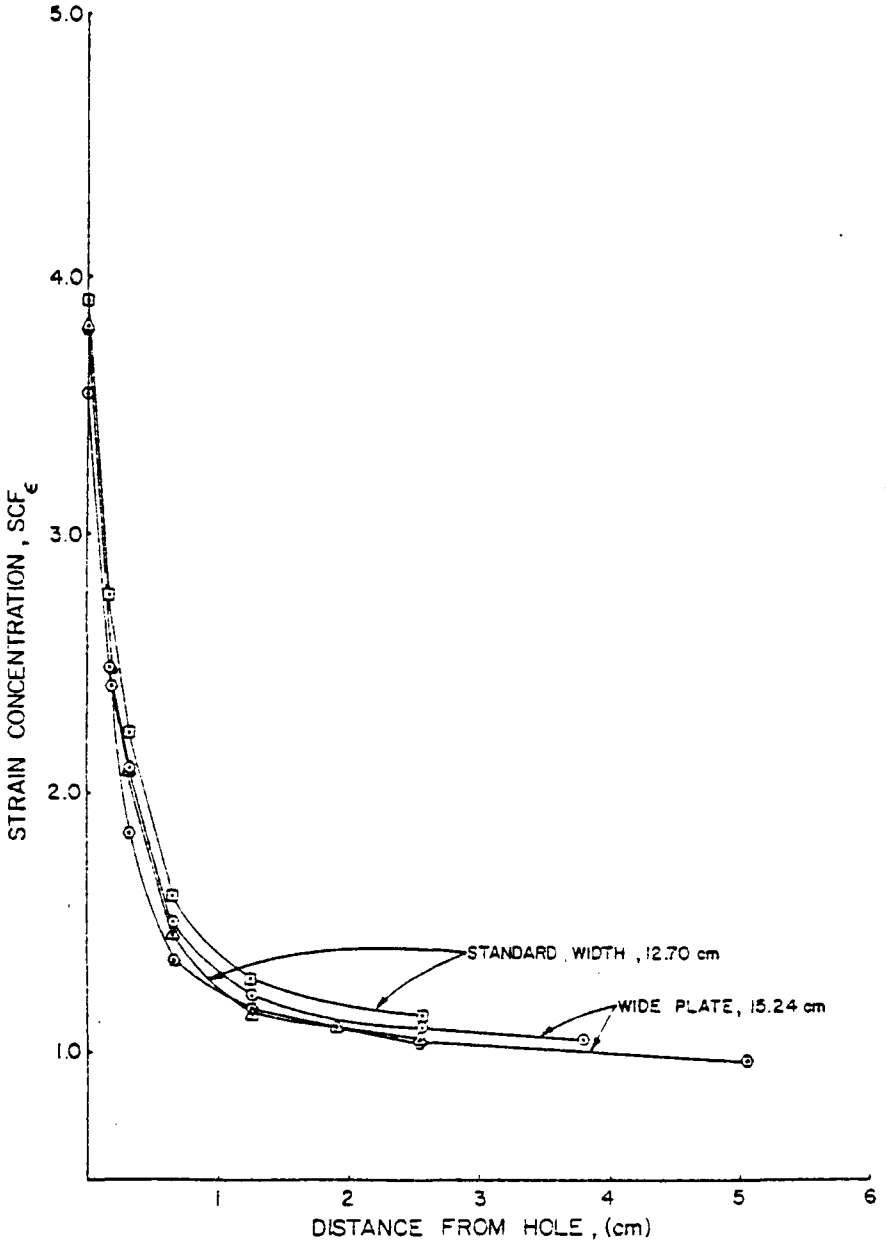

FIGURE 4-22. EFFECT OF WIDTH ON SCF_ε AND STRAIN GRADIENT. 2.54 cm (1.0 in) HOLE FOR BOTH LAMINATES.

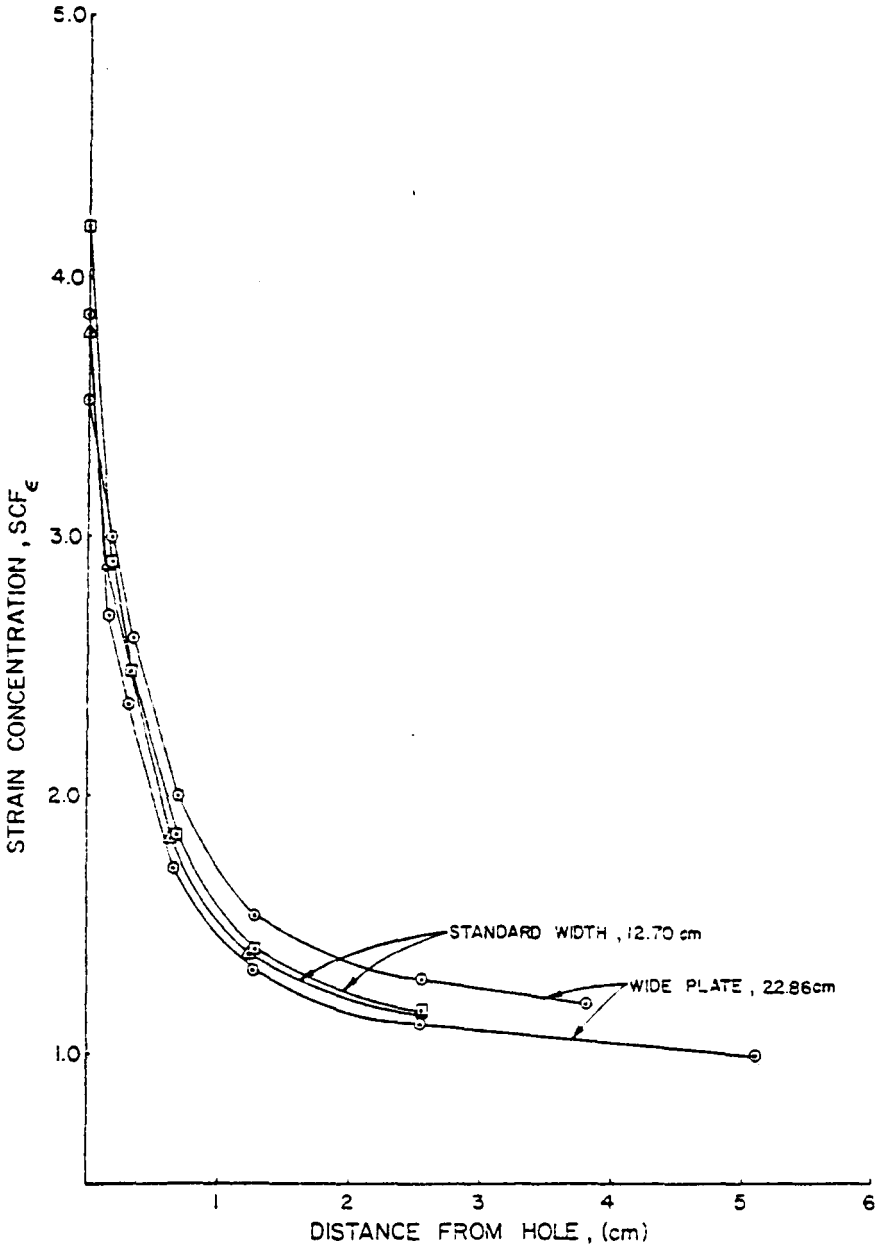

FIGURE 4-23. EFFECT OF WIDTH ON SCF_ε AND STRAIN GRADIENT. 3.81 cm (1.5 in) HOLE FOR EACH LAMINATE.

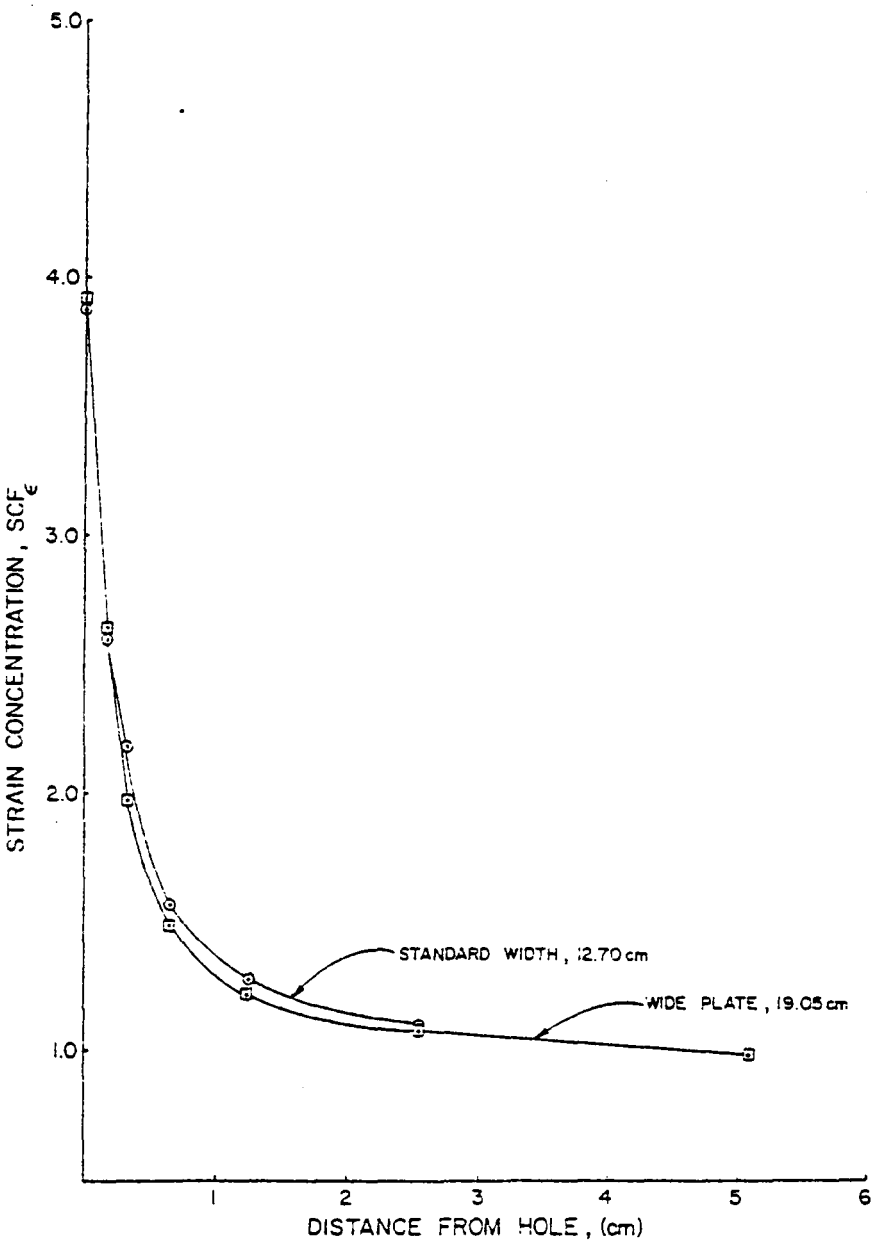

FIGURE 4-24. EFFECT OF WIDTH ON SCF$_\varepsilon$ AND STRAIN GRADIENT. 3.81 cm HOLE. 48 PLY ORTHOTROPIC.

Table 4-2

Strain Concentration in 48 Ply Laminates

Hole Dia., cm	Panel Width, cm	Distance From Cutout, cm 0.0	.1588	.3175	.6350	1.270	1.905	2.540	3.810	5.080
						SCF_ε				
		Orthotropic Panels								
0.635	12.70	-	2.26	1.11	1.04	1.02	-	1.02	-	-
1.270	12.70	3.66	2.01	1.35	1.06	1.01	1.00	0.98	-	-
1.905	12.70	3.80	2.39	1.85	1.31	1.09	1.06	1.05	-	-
2.540	12.70	3.85	2.48	2.06	1.46	1.11	1.10	1.05	-	-
	15.24	3.80	2.40	1.84	1.35	1.16	-	1.04	0.96	-
3.175	12.70	3.87	2.58	2.17	1.57	1.28	-	1.11	-	-
	19.05	3.91	2.64	1.96	1.49	1.22	-	1.07	-	0.98
3.810	12.70	3.84	2.90	2.48	1.85	1.41	-	1.18	-	-
	22.86	3.87	2.70	2.37	1.73	1.34	-	1.15	-	1.06
		Isotropic Panels								
0.635	12.70	-	1.39	1.11	1.01	0.99	-	0.98	-	-
1.270	12.70	3.72	2.11	1.45	1.13	1.06	-	1.43*	-	-
1.905	12.70	3.63	2.36	1.82	1.36	1.14	-	1.05	-	-
2.540	12.70	3.90	2.66	2.18	1.60	1.27	-	1.13	-	-
	15.24	3.55	2.49	2.10	1.50	1.23	-	1.10	1.05	-
3.810	12.70	3.84	3.17	2.65	2.05	1.55	-	1.26	-	-
	22.86	3.52	3.00	2.61	2.02	1.54	-	1.29	1.20	-

*Questionable Data Point

$$\frac{\varepsilon_{f\ control}}{\varepsilon_{f\ cutout}} = \text{Strain Concentration Ratio.}$$

By plotting this value on the ordinate of the SCF_{ε} plots for each diameter, the amount of material at or above the failure strain of the panel without a cutout may be read on the abscissa and are indicated by the asterisks on Figures 4-18 and 4-19. Although the far field failure strain of a panel with a cutout decreases as the diameter increases, the amount of material around the cutout at high strain magnitudes increases. As the width of the panel increases, the amount of material beyond the ultimate strain level decreases and the panel carries higher load. Attempts to characterize this length from a fracture mechanics point of view, however, were unsuccessful.

4.2 Twenty-Four Ply Specimens

The importance of the series of 24 ply specimens in this investigation is to characterize the effect of a cutout on the behavior of a panel which is buckling critical. The laminate response is defined in terms of failure strain, buckling and post-buckling stiffness and the effect of hole diameter. Also, comparisons to recent results in the literature are discussed.

4.2.1 Buckling and Post-Buckling Behavior

For the present study, buckling was defined experimentally as a reversal in strain experienced by the far field back-to-back strain gages coincident with a change in the slope of the load-displacement

curve. Where material imperfections influenced the onset of bifurcation and where only initial bifurcation took place, the critical load was selected as the intersection of the extended slopes of the elastic and tangent moduli as shown in Figure 4-25 for a 0.3175 cm ($\frac{1}{8}$ in) cutout. For the quasi-isotropic panels smooth transition was made from the flat plate to the buckled shape of two halfwaves in the longitudinal direction, m=2, for hole diameters of 2.54 cm (1.0 in) or less. The moire´ fringe pattern in the post-buckled state is shown in Figure 4-26 for a 1.588 cm ($\frac{5}{8}$ in) diameter hole under a load of 100.0 kPa (22.5 kip).

The far field gages were positioned equi-distant from the loaded plate edge and lateral centerline of the hole. The response of these gages is shown in Figure 4-27 for the same panel as Figure 4-25. The gages located along the lateral centerline showed significant strain relief after buckling with the exception of the gage 2.54 cm (1.0 in) from the hole, Figure 4-28a. The strain at this location was influenced by the proximity of the side support which prevented bending from occuring. A similar trend is seen in the strain concentration factor which reduces as buckling proceeds, Fgiure 4-28b. In this case, the SCF_ε was defined as the strain near the hole divided by the average strain in the far field gages which were on opposite sides of the panel. Thus, a local gage which was on the convex (tensile) side of the deformed shape and experienced compressive strain relief with respect to the average far field strain would show a SCF_ε below 1.0. Bifurcation caused relief also in the hole boundary circumferential

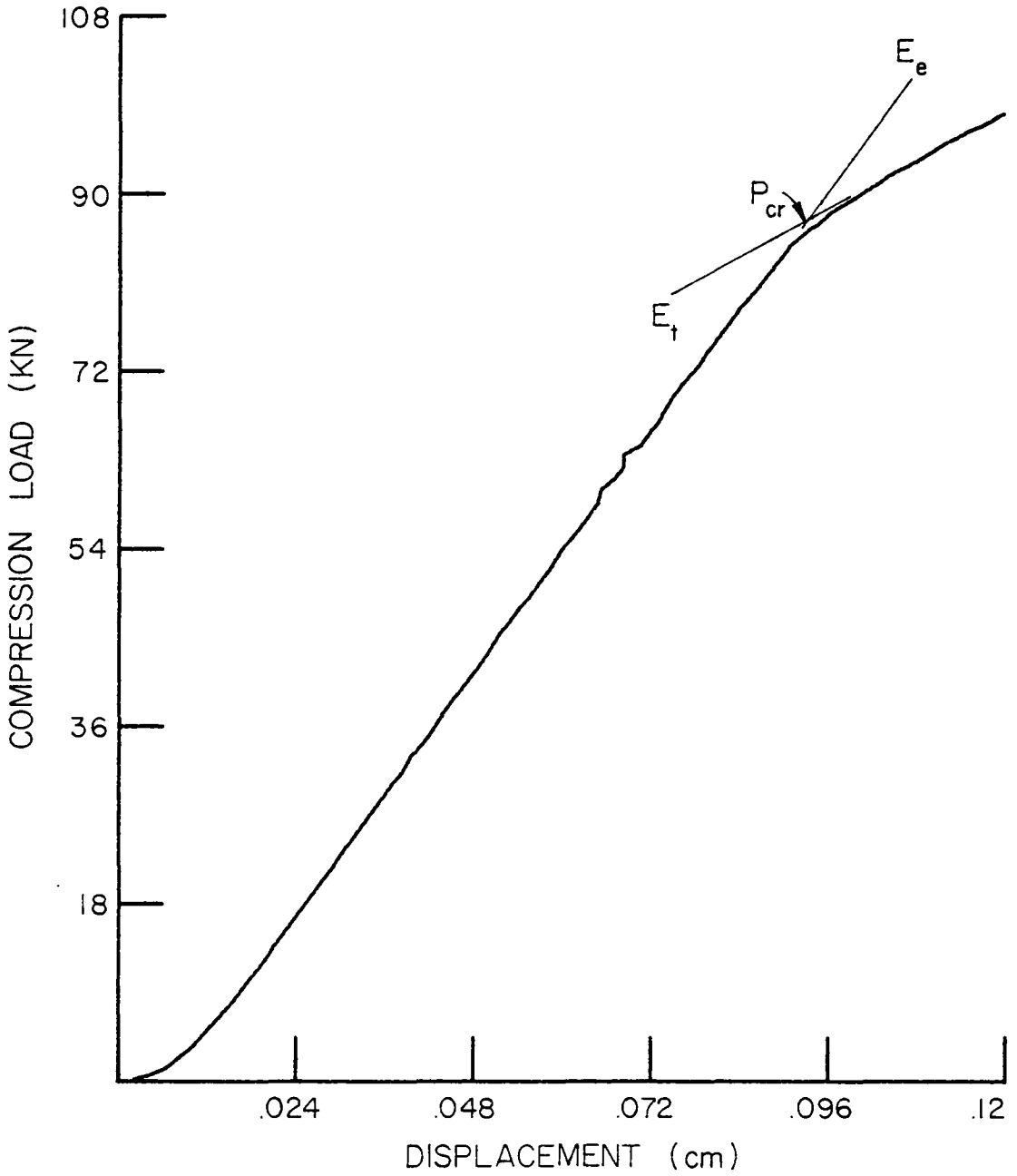

FIGURE 4-25. LOAD-DISPLACEMENT CURVE OF QUASI-ISOTROPIC PANEL WITH A 0.3175 cm ($\frac{1}{8}$ in) DIAMETER HOLE. CRITICAL LOAD IS SHOWN TO BE 87.85 kN (19.5 kips).

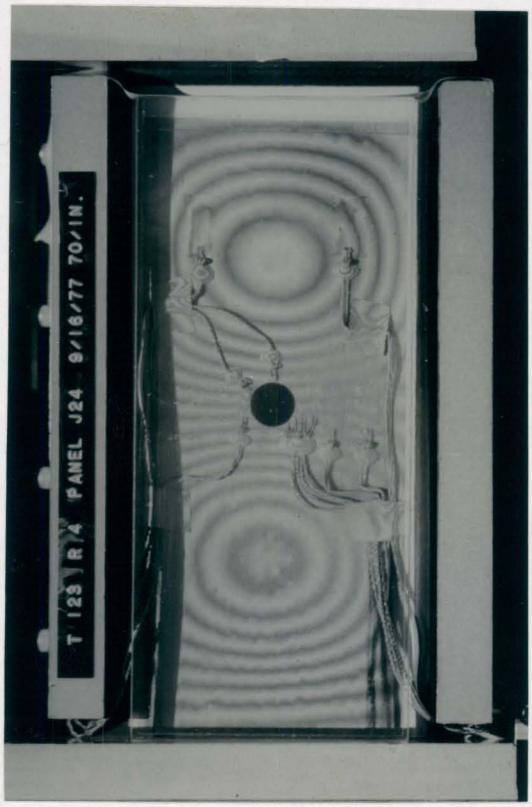

FIGURE 4-26. THE MOIRÉ FRINGE PATTERN FOR A 24 PLY QUASI-ISOTROPIC PANEL IN THE POST-BUCKLED STATE. THE SHAPE CORRESPONDS TO m=2, n=1 AT A LOAD OF 100.1 kN (22.5 kip).

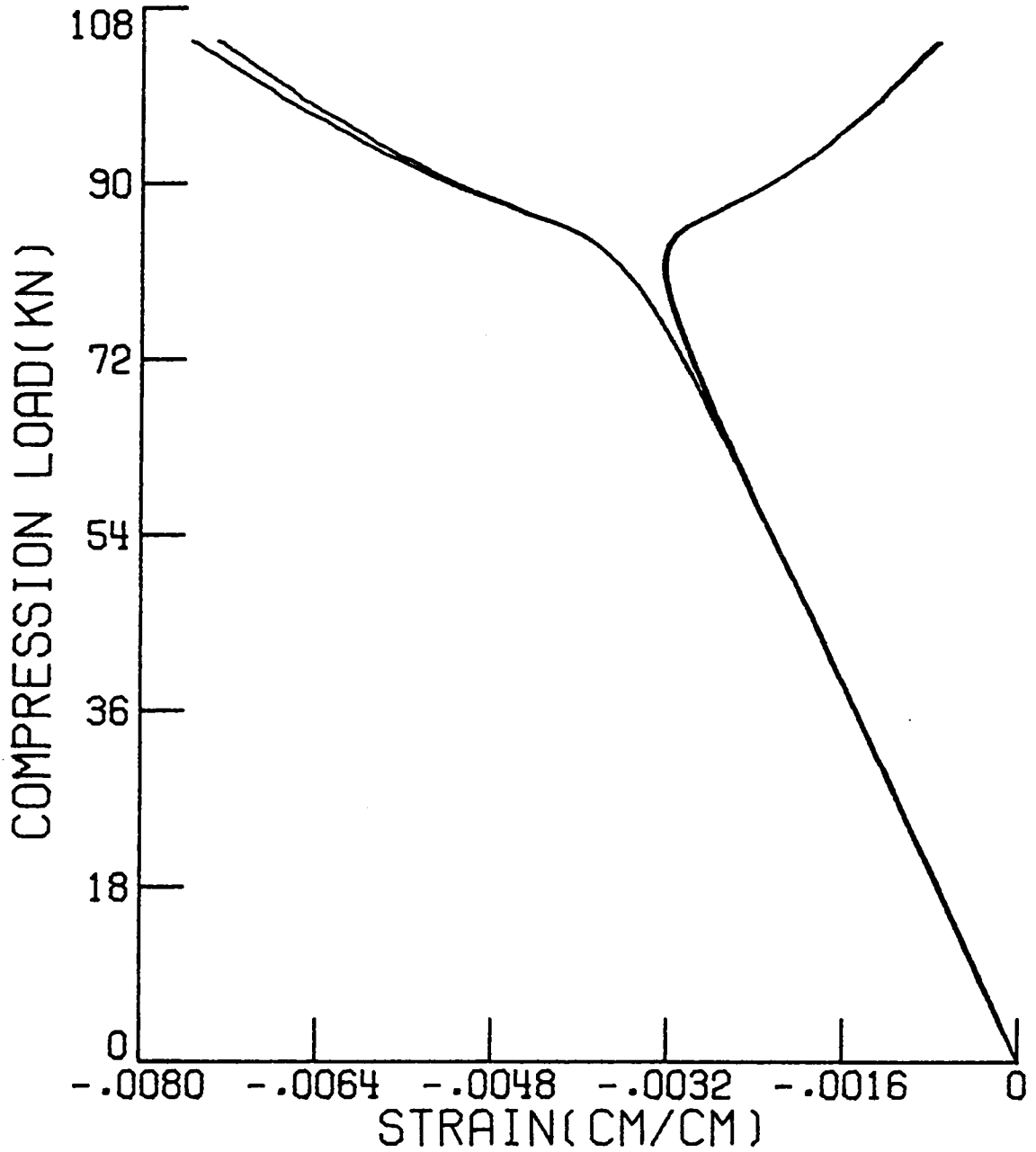

FIGURE 4-27. TYPICAL RESPONSE OF BACK-TO-BACK FAR FIELD GAGES IN PLATE BUCKLING (m=2, n=1).

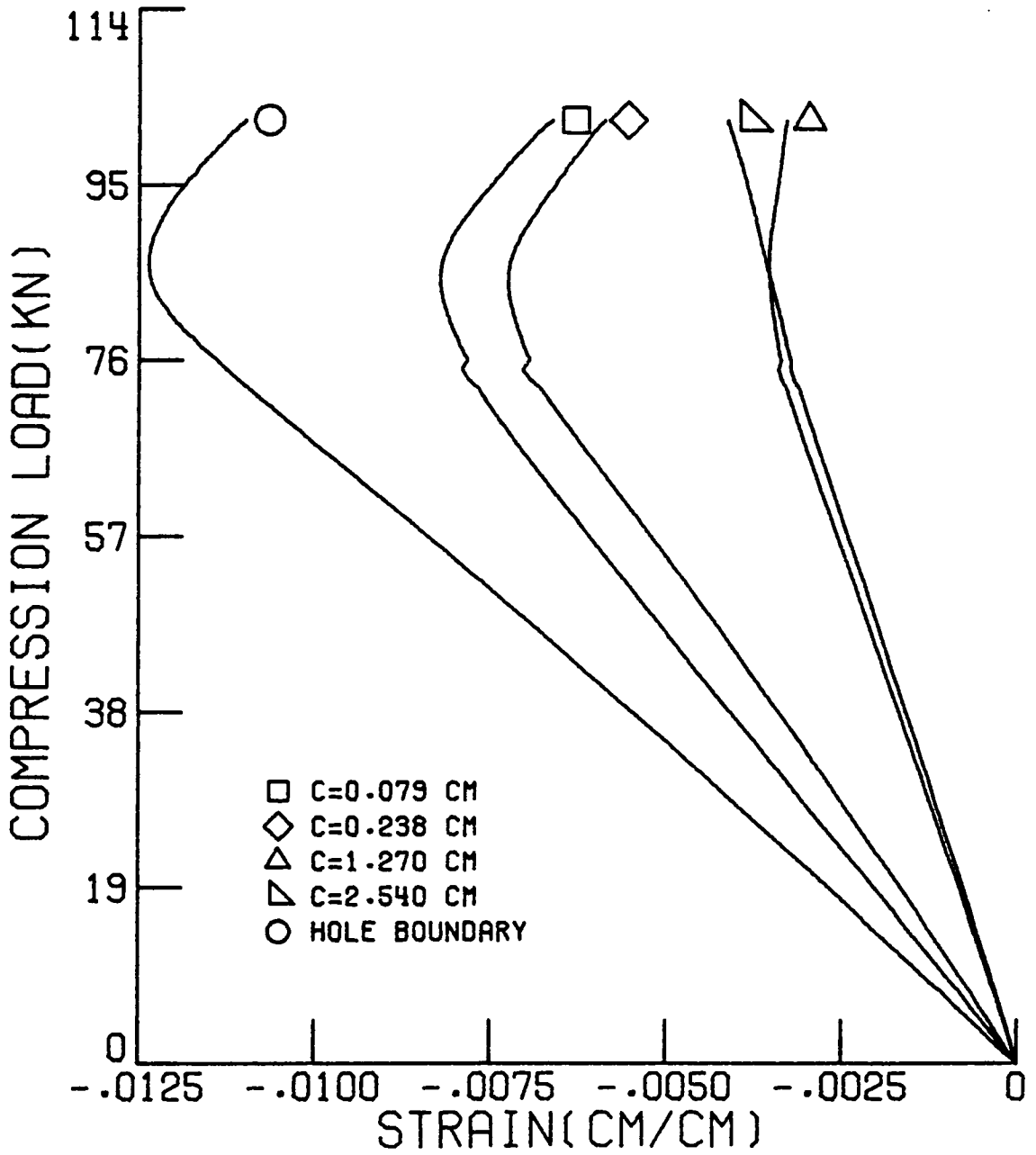

FIGURE 4-28a. RESPONSE OF STRAIN GAGES ALONG THE LATERAL CENTERLINE AT VARYING DISTANCES FROM HOLE. QUASI-ISOTROPIC PANEL, 1.59 cm ($\frac{5}{8}$ in) DIAMETER HOLE. C IS THE DISTANCE FROM THE HOLE BOUNDARY.

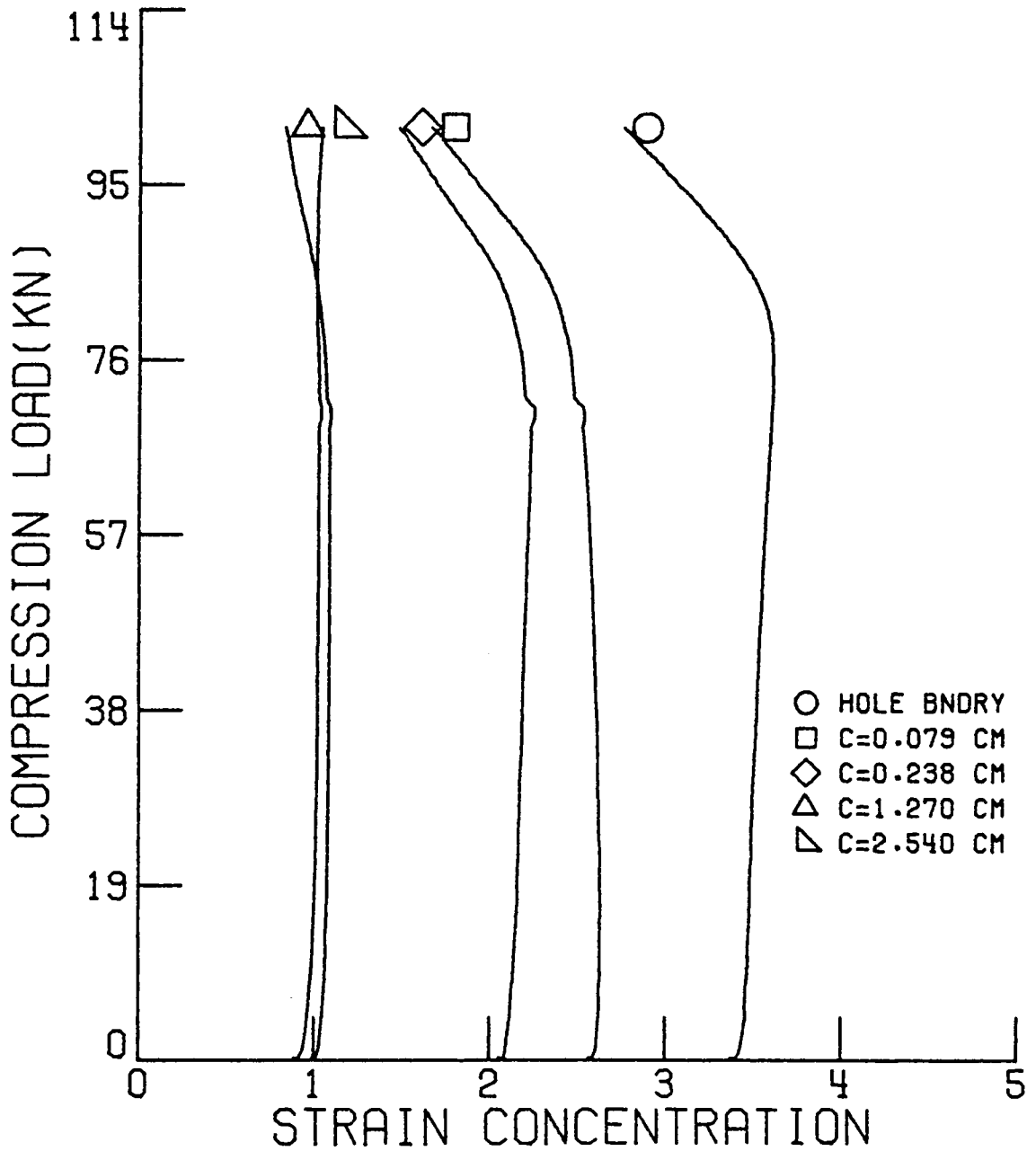

FIGURE 4-28b. VARIATION OF STRAIN CONCENTRATION WITH LOAD. FOR A QUASI-ISOTROPIC PANEL WITH A 1.59 cm ($\frac{5}{8}$ in) CUTOUT C IS THE DISTANCE FROM THE HOLE BOUNDARY.

strain measured on the longitudinal centerline but had little effect on the through-the-thickness strain at 90 degrees from the load axis, Figure 4-29.

Material behavior of the 24 ply specimens, including the change of stiffness with buckling, is tabulated in Table 4-3. As shown in this table, for these laminates, the size of the hole has little or no effect on results.

The largest diameter hole tested in this series of quasi-isotropic laminates was 3.81 cm ($1\frac{1}{2}$ in). This was the only specimen to buckle into one halfwave, m=n=1, Figure 4-30. The strain magnification on the concave side of the post-buckled shape near the hole caused failure to occur at a load level well below that of the orthotropic panels. Figure 4-31 shows the effect of buckling on the local strain. The hole boundary circumferential strain experienced relief with the onset of buckling while the strain recorded by the surface gages was significantly intensified.

The orthotropic speicmens, however, displayed initial buckling in the form of one halfwave, m=n=1, which progressed to the two halfwave shape, m=2, n=1, with increased load. For hole sizes up to 1.27 cm ($\frac{1}{2}$ in) the corresponding average changes in stiffness were -32 percent for m=1 and -61 percent for m=2 from the initial flat plate stiffness. This response is shown in Figure 4-32 for a 1.588 cm ($\frac{5}{8}$ in) hole where E_e, E_{t_1} and E_{t_2} are the moduli in the prebuckling, m=1 and m=2 ranges, respectively. Indistinct laminate response throughout the mode transition load range due to localized delamination made it dif-

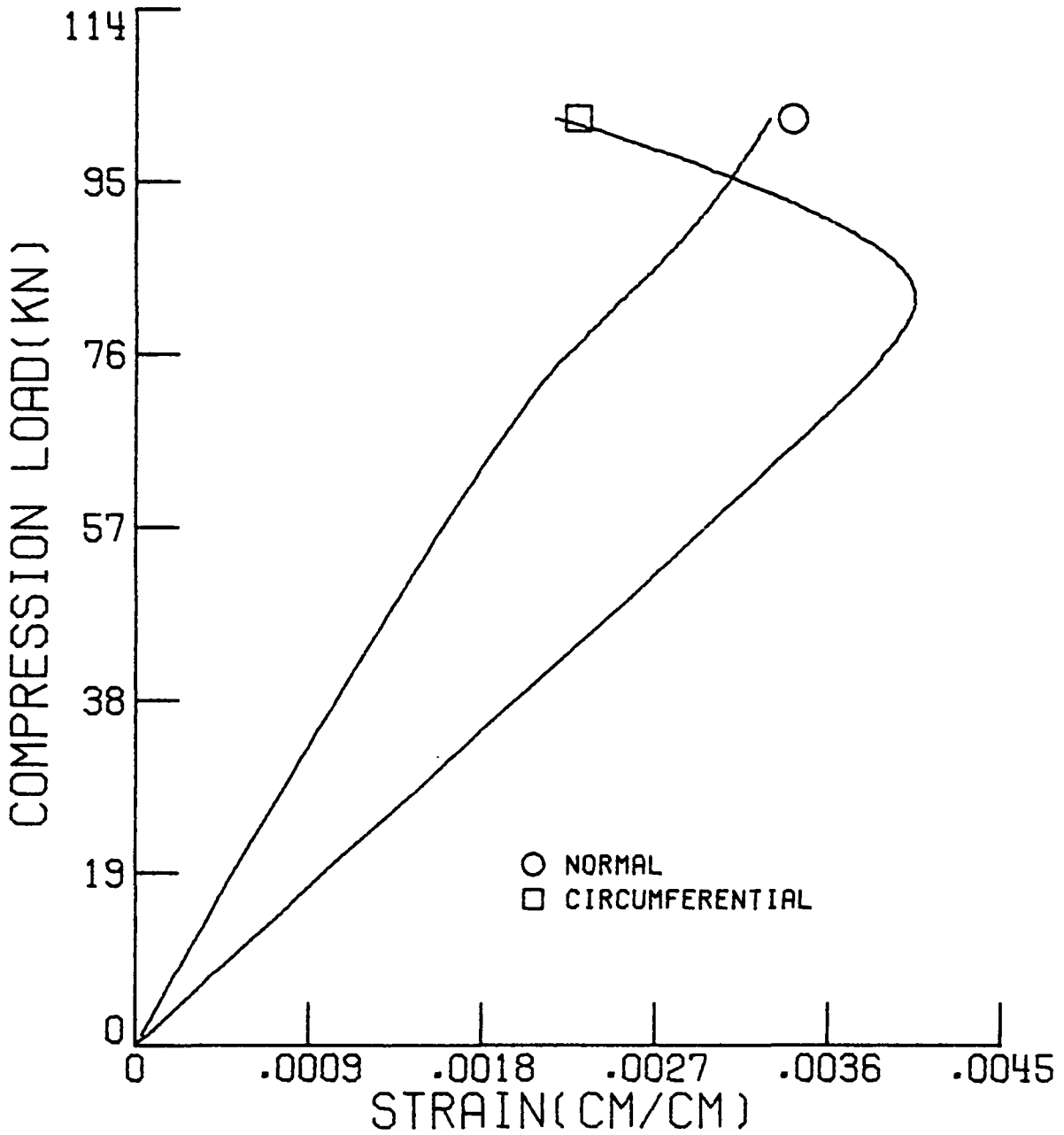

FIGURE 4-29. HOLE BOUNDARY GAGE RESPONSE FOR CIRCUMFERENTIAL STRAIN ON THE LONGITUDINAL CENTERLINE AND NORMAL STRAIN ON THE LATERAL CENTERLINE. PANEL J24.

Table 4-3

Buckling Behavior of 24 Ply Quasi-Isotropic Panels

Panel Number	Hole Diameter cm	Elastic Modulus MPa x 10^4	Tangent Modulus MPa x 10^4	Modulus Change %	Buckling Load, kN	Failure Load, kN (kips)
J28	0.1588	5.808	2.218	-61.8	78.3	104.5 (23.50)
J29	0.3175	5.750	2.010	-51.1	81.6	103.2 (23.20)
J27	0.4763	5.819	2.350	-59.6	74.9	107.9 (24.25)
J31	0.6350	4.026	2.079	-48.4	64.6	94.1 (21.15)
J25	0.7938	5.313	2.397	-54.9	83.6	108.1 (24.30)
J26	0.9525	5.616	2.236	-60.1	81.0	105.0 (23.60)
J32	1.1113	4.542	2.051	-54.8	71.3	96.3 (21.65)
J21	1.2700	5.670	2.190	-61.4	78.6	97.1 (21.82)
J24	1.5875	5.434	2.405	-55.7	75.1	100.5 (22.60)
J35	1.9050	5.310	2.369	-55.4	70.8	91.7 (20.68)
J22	2.5400	5.464	2.263	-58.6	89.6	103.6 (23.30)
J30	3.8100	4.831	3.147	-34.8*	75.5	83.7 (18.83)
J37	-	4.268	1.707	-60.0	82.7	100.3 (22.55)

* m=1

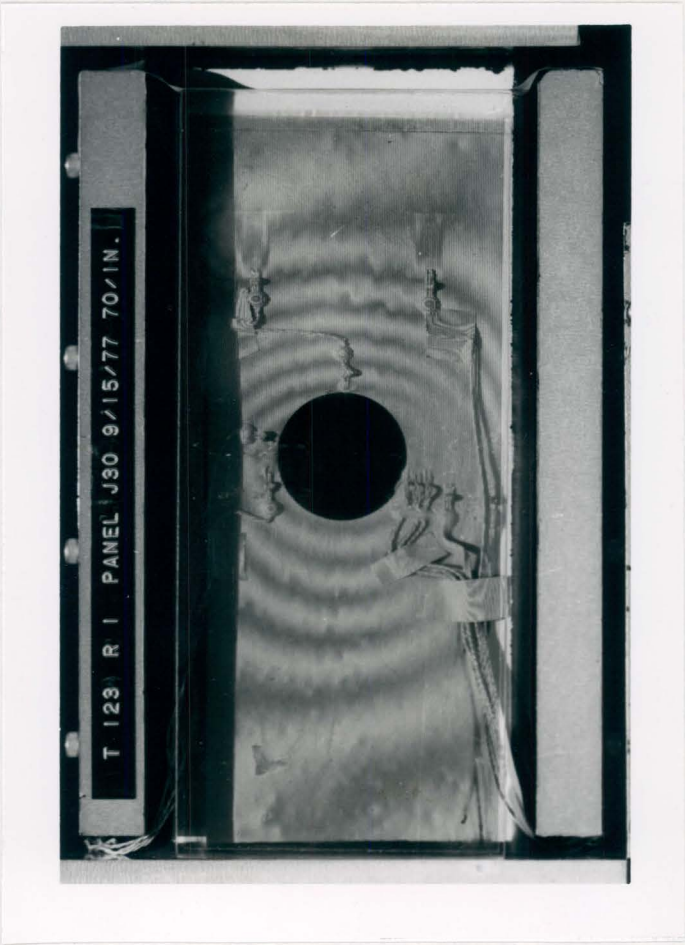

FIGURE 4-30. THE QUASI-ISOTROPIC PANEL WITH A 3.81 cm ($1\frac{1}{2}$ in) CUTOUT BUCKLED IN THE ONE HALFWAVE MODE m=n=1.

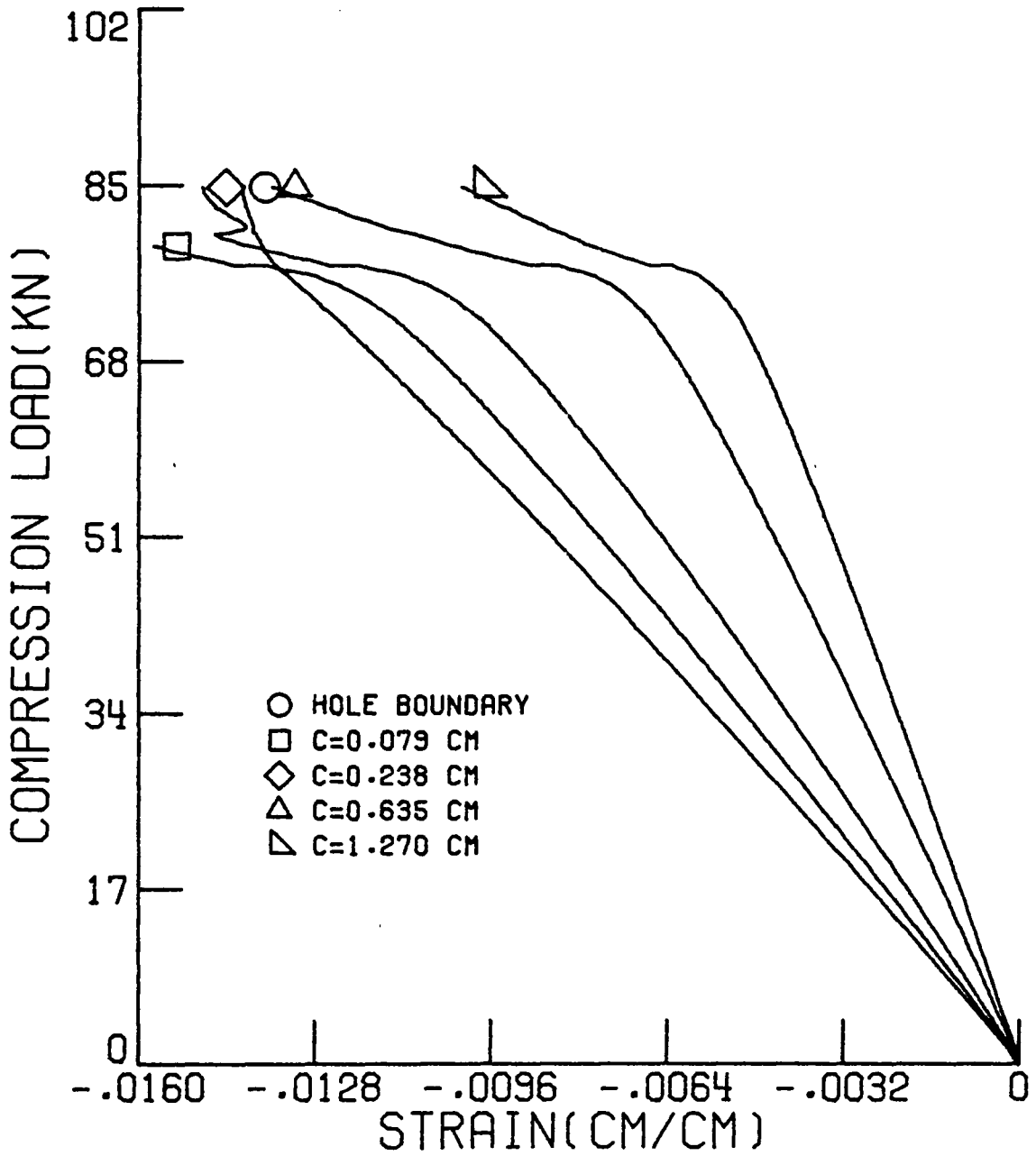

FIGURE 4-31. THE RESPONSE OF THE STRAIN GAGES ON THE LATERIAL CENTER-LINE OF THE PANEL BUCKLING IN AN m=1 MODE. QUASI-ISOTROPIC 3.81 cm ($1\frac{1}{2}$ in) DIAMETER HOLE. C IS DISTANCE FROM CUTOUT.

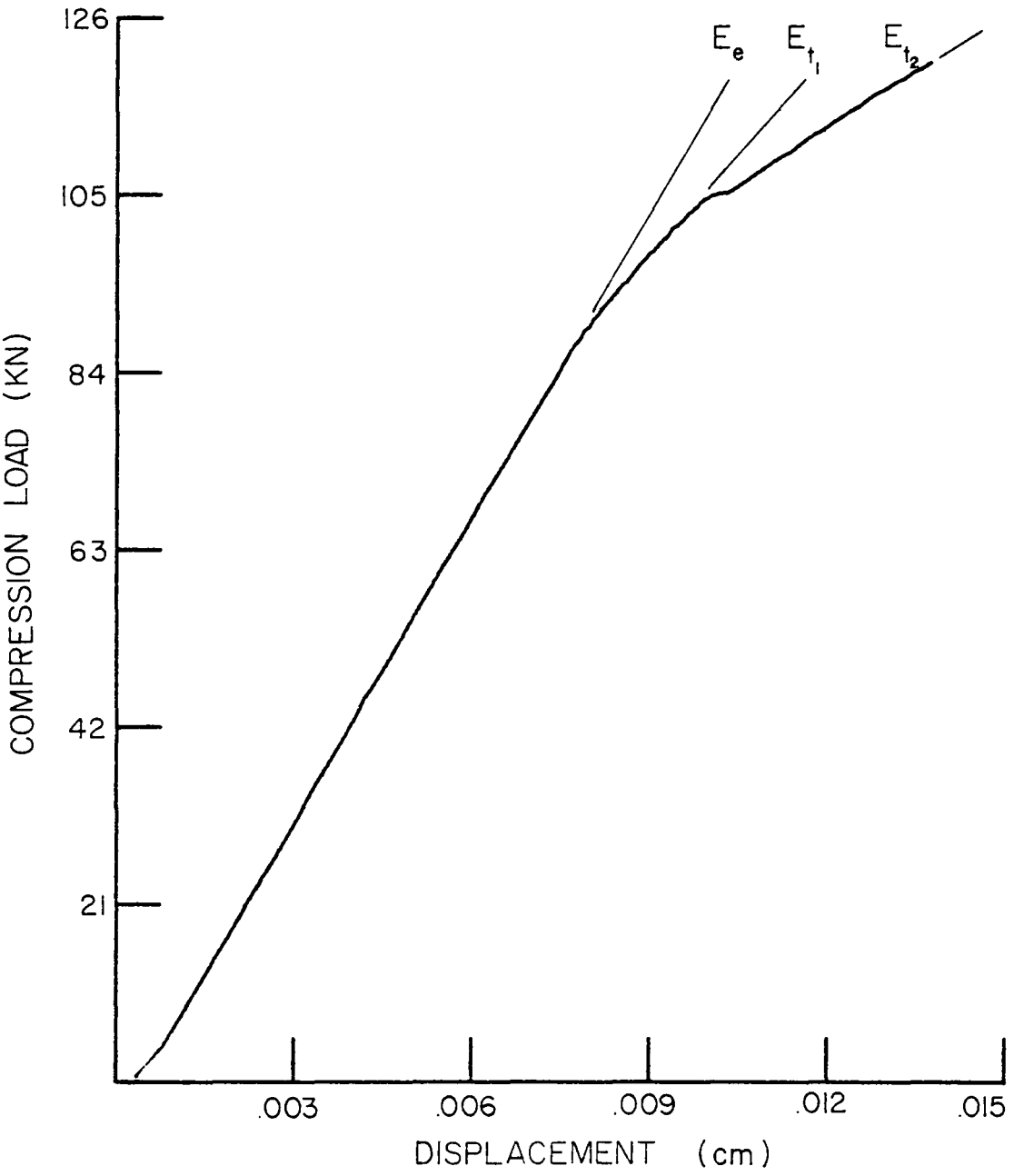

FIGURE 4-32. LOAD-DISPLACEMENT RELATIONS SHOWING REDUCTION IN STIFFNESS WITH APPLIED LOAD. HOLE DIAMETER IS 1.588 cm ($\frac{5}{8}$ in).

ficult to determine the intermediate stiffness in many cases. Except where noted, initial and final moduli are tabulated, Table 4-4, with the buckling load reported as the load at which strain reversal first occurred.

The moiré fringe patterns which developed during load application were beneficial in determining when out-of-plane displacement occurred. The patterns developed throughout the load range are shown in Figures 4-33a-d for the panel in Figure 4-32.

The effect on the strain level at the lateral centerline through each mode change was important to understand the local laminate response around the cutout. In general, the strain magnification resulting from bifurcation into the single halfwave shape, Figure 4-31, was relieved with the onset of the second halfwave, Figure 4-34. Therefore, the strain concentration due to the presence of the hole did not significantly influence panel failure in the double halfwave mode. Failure occurred as a result of strain concentration at the end of the side supports due to high out of plane deflection gradients caused by buckling as in the 48 ply control specimens.

In the 1.91 cm ($\frac{3}{4}$ in) and 2.54 cm (1.0 in) diameter panels, the strain magnification around the hole in the single halfwave shape was sufficient to cause local material failure. This reponse was similar to that of Figure 4-31 for the quasi-isotropic laminates. A series of fringe patterns, Figure 4-35a-d, show the material failure occurring as the second halfwave begins to form. The moiré fringe surface was the compression side of the deformed shape. The load-displacement curve

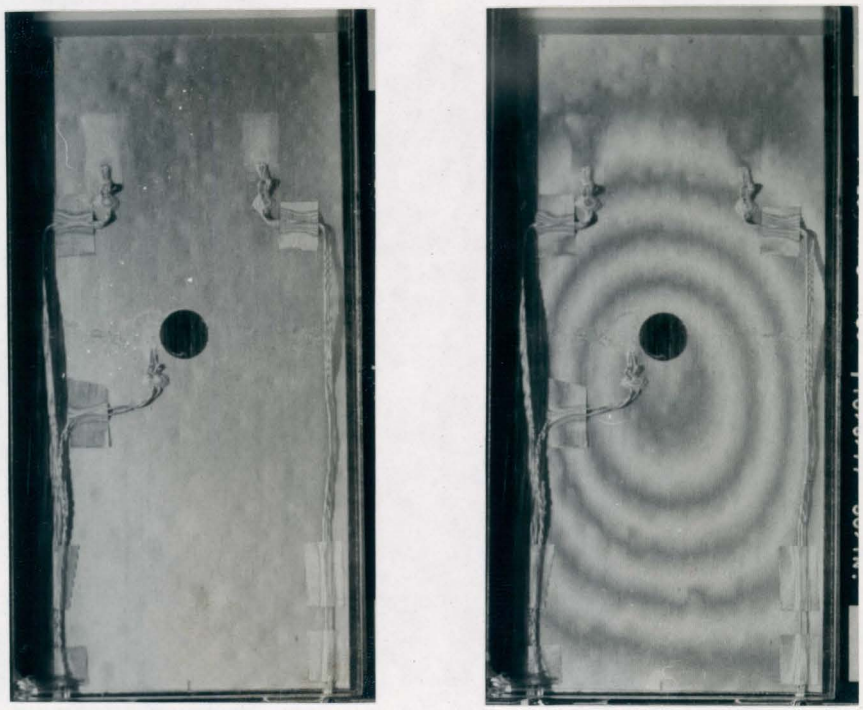

(a) (b)

FIGURE 4-33. THE MOIRE FRINGE RESPONSE a) FOR A FLAT PLATE UNDER NO LOAD AND b) AFTER INITIAL BIFURCATION INTO A ONE-HALFWAVE SHAPE. 24 PLY ORTHOTROPIC, HOLE DIAMETER 1.588 ($\frac{5}{8}$ in).

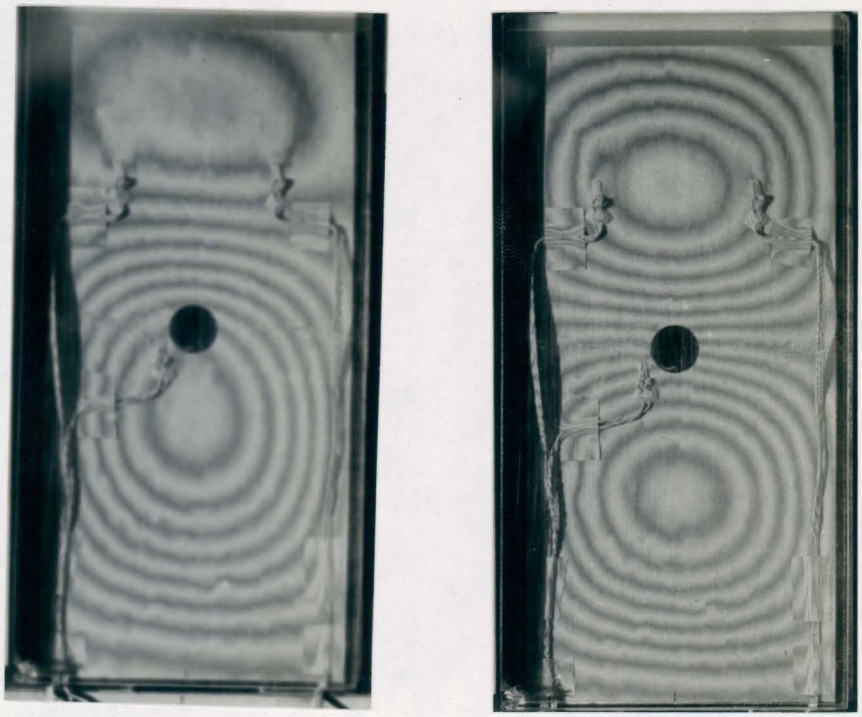

(c) (d)

FIGURE 4-33. WITH CONTINUED LOAD APPLICATION A SECOND HALFWAVE IS SEEN TO c) MOVE DOWN FROM THE TOP OF THE PANEL AND d) RESULT IN A FINAL BIFURCATED STATE OF m=2, n=1.

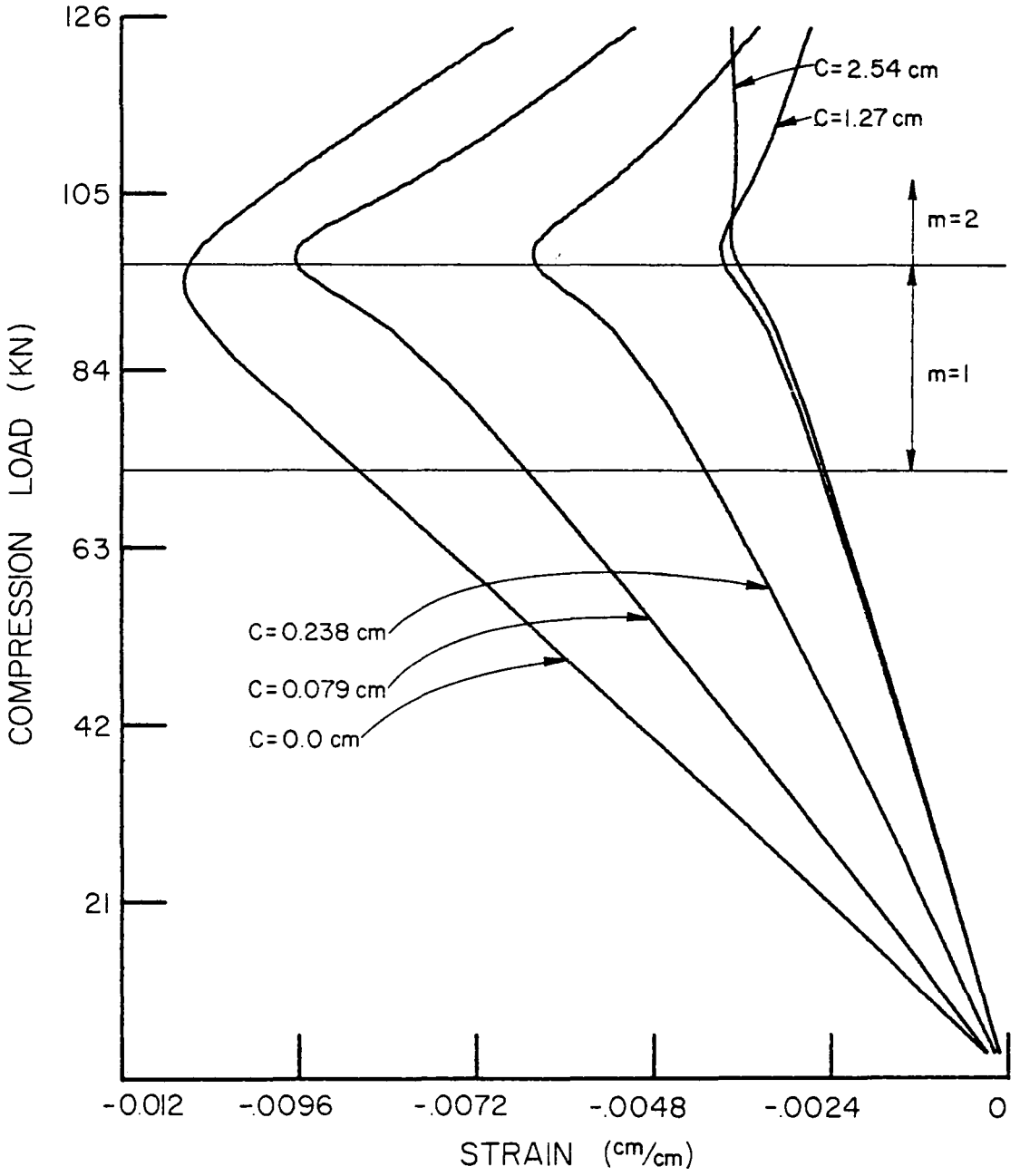

FIGURE 4-34. THE RESPONSE OF GAGES NEAR THE HOLE IN DIFFERENT BIFURCATED CONFIGURATIONS. C IS DEFINED AS THE DISTANCE FROM THE HOLE BOUNDARY. DIAMETER IS 1.27 cm ($\frac{1}{2}$ in).

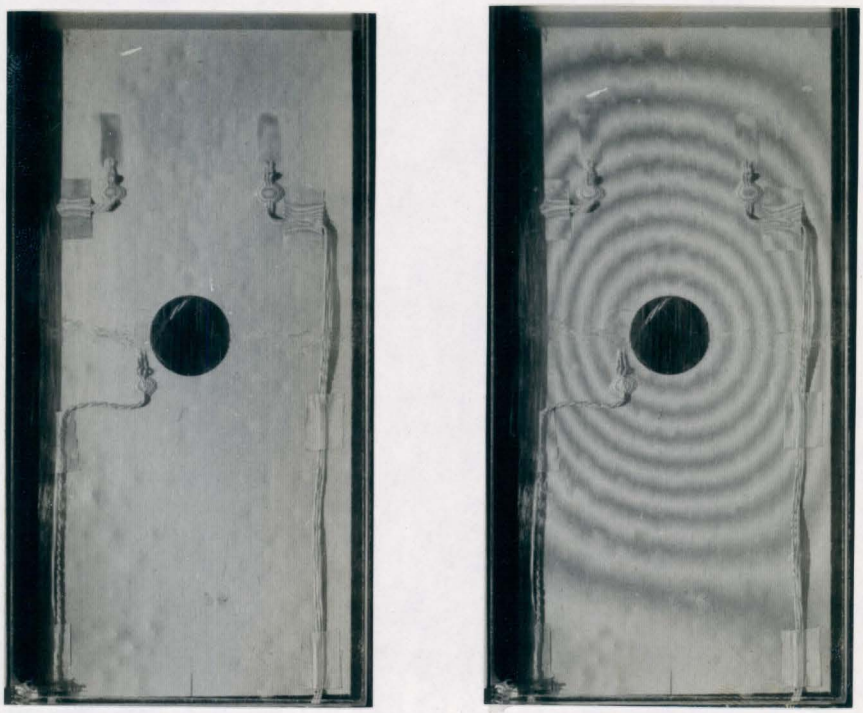

(a) (b)

FIGURE 4-35. THE MOIRÉ FRINGE PATTERN RESPONSE a) FOR A FLAT PLATE UNDER NO LOAD AND b) AFTER INITIAL BIFURCATION INTO THE m=n=1 SHAPE. 24 PLY ORTHOTROPIC HOLE DIAMETER 2.54 (1.0 in).

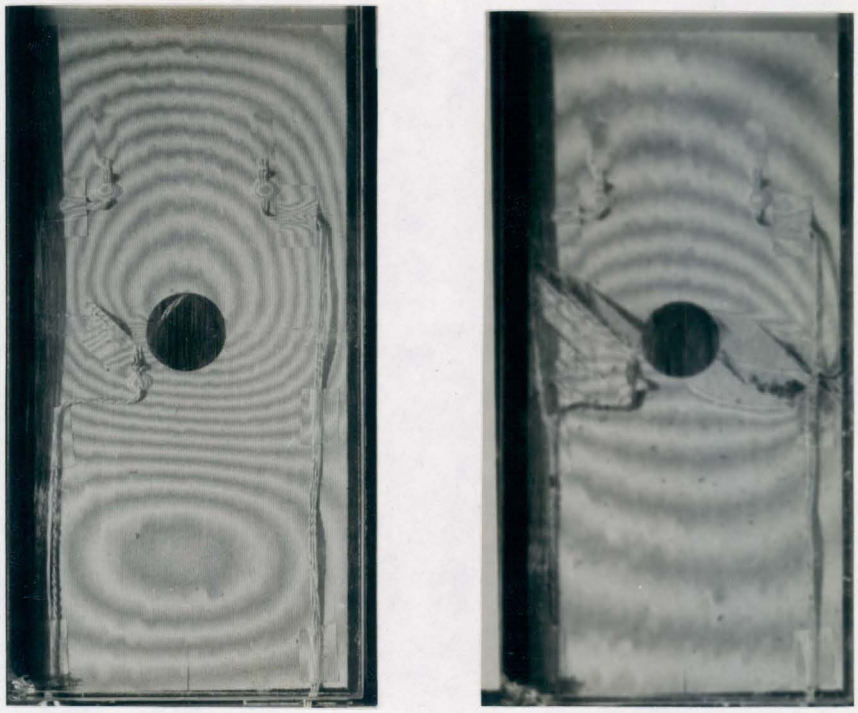

(c) (d)

FIGURE 4-35. AS THE SECOND LONGITUDINAL HALFWAVE BEGINS TO FORM, THE COMPRESSIVE STRAINS AROUND THE HOLE CAUSE c) LOCAL MATERIAL FAILURE AT A LOAD OF 109.1 kN (24.53 kip) AND d) PANEL FAILURE AT 111.9 kN (25.15 kip).

depicting the single mode change is shown in Figure 4-36.

4.2.2 Failure Strain

Ritchie and Rhodes [24] and Kumai [4] present analytical solutions for the buckling load and, in the former case, post-buckling behavior of perforated isotropic plates. Their results, presented along with those of other investigators, show a decrease in critical load with increasing hole size in quasi-isotropic materials for aspect ratios of 1 and 2. For the present work, there was no dependence of ultimate load on hole diameter, as evidenced by Tables 4-3 and 4-4. Neither was there a critical load trend apparent with increasing cutout size. Figure 4-37 shows critical strain regions of both laminates versus diameter-to-width ratio, $\frac{D}{W}$, for 12.70 cm (5.0 in) wide panels. The average critical strains were 0.0033 cm/cm and 0.0030 cm/cm for the quasi-isotropic and orthotropic plates, respectively.

The variation of ultimate strain with hole size is shown in Figure 4-38. Failure occurred as a result of strain concentrations due to the end of the side support and not as a result of high deflection gradients in the troughs of the deformed mode shape which is the case for a true post-buckling failure. Therefore, the far field strain levels at failure were more dependent on the effect of the applied boundary conditions in the deformed shape than the transverse deflection gradients of the panel. This could explain why there is not more separation in the ultimate strain levels of the two laminates.

The decrease in ultimate strain for higher $\frac{D}{W}$ was caused by the absence of strain relief which accompanied a mode change from m=1 to

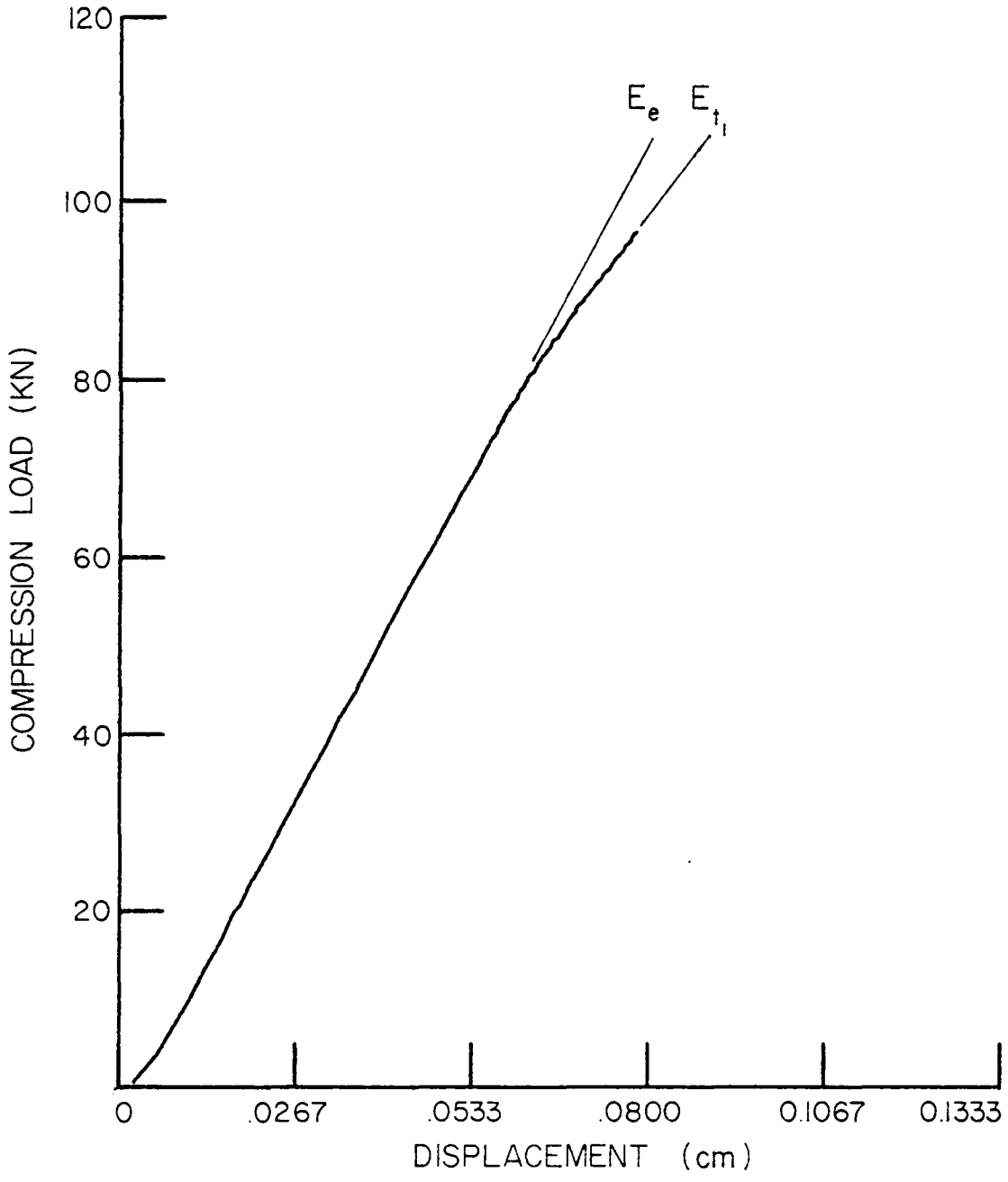

FIGURE 4-36. SINGLE MODE CHANGE OF 3.81 cm ($1\frac{1}{2}$ in) DIAMETER HOLE IN A 24 PLY ORTHOTROPIC LAMINATE.

Table 4-4

Buckling Behavior of 24 Ply Orthotropic Panels

Panel Number	Hole Diameter cm	Elastic Modulus MPa x 10^4	Tangent Modulus MPa x 10^4	Modulus Change %	Buckling Load, kN	Failure Load, kN (kips)
K21	0.1588	6.620	2.611	-60.6	105.6	111.8 (25.14)
K22	0.3175	6.442	2.799	-56.5	86.5	128.6 (28.90)
K23	0.4763	6.702	2.643	-60.6	90.8	129.9 (29.20)
K24	0.6350	6.682	2.614	-60.9	97.2	128.6 (28.90)
K25	0.7938	6.697	2.459	-63.2	85.6	121.7 (27.35)
K26	0.9525	6.921	2.572	-62.8	89.3	127.2 (28.60)
K27	1.1113	6.788	2.290	-66.3	88.8	124.3 (27.95)
K28	1.270	6.902	2.654	-61.8	85.4	123.2 (27.70)
K29	1.5875	6.702	2.626	-60.8	86.5	121.7 (26.90)
K30	1.9050	6.993	4.608	-34.8*	81.0	105.4 (23.70)
K31	2.5400	6.681	4.661	-30.4*	77.5	111.9 (25.15)
K32	-	7.158	2.783	-61.1	84.8	115.2 (25.90)
K33	-	6.982	2.926	-58.1	81.8	114.3 (25.70)

* m=1

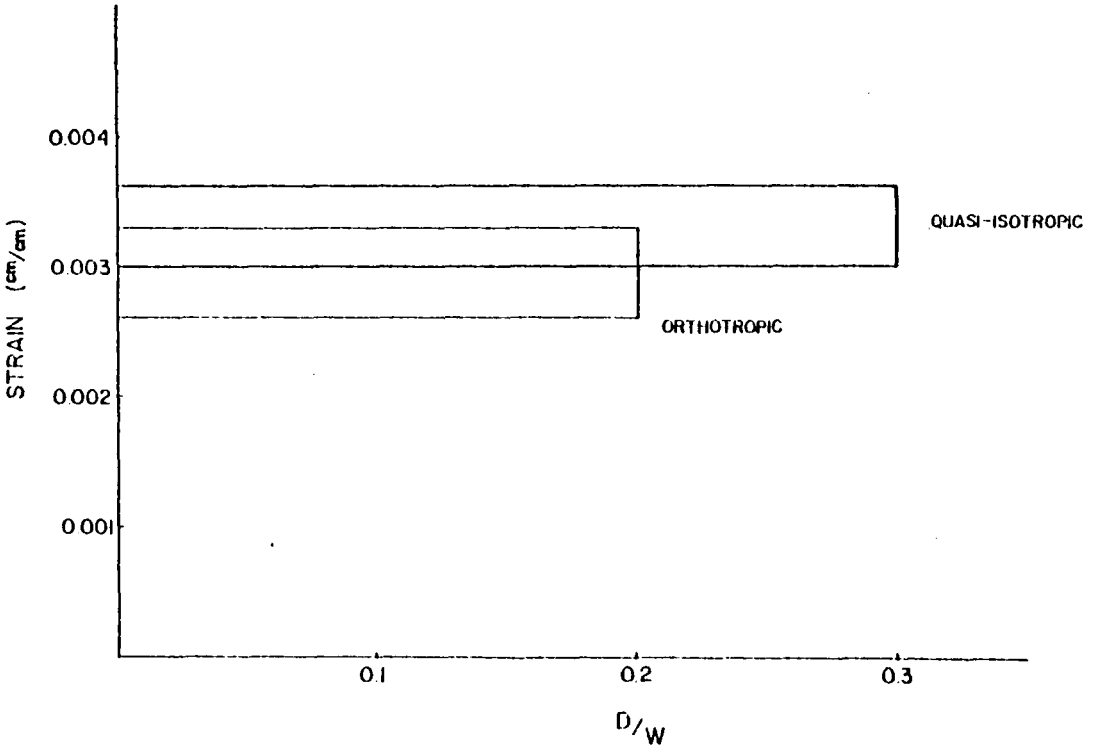

FIGURE 4-37. CRITICAL STRAIN REGIONS FOR 24 PLY SPECIMEN INDEPENDENT OF HOLE SIZE PRESENT.

m=2. The larger cutout diameters delayed the mode change in these specimens until local material failure around the hole occurred, causing panel failure in the m=1 shape. These data points are specified by an asterisk on Figure 4-38.

4.3 Data Correlation

The experimental results for both the 24 ply and the 48 ply laminates have been presented. The purpose of this section is to correlate the behavior of each series in order to draw general conclusions about the compressive behavior of composite plates with circular cutouts.

4.3.1 Correlation of Failure Mode

The failure of the 48 ply specimens was primarily strength dominated due to the strain concentration around the hole causing initial local material failure in the orthotropic panels and sudden catastrophic failure in the quasi-isotropic laminates. The 24 ply behavior, in constrast, was dominated by buckling with substantial transverse displacement occurring before failure. The hypothesis for the difference in failure mode is that the buckling strain in the thin plates is low enough that the SCF_{ε} due to the hole does not cause local material failure around the hole before buckling of the panel, and subsequent strain relief, occurs. By increasing the thickness approximately 100 percent the buckling strain, which is proportional to the square of the thickness, is increased to the extent that the SCF_{ε} around the cutout becomes important. The relationship, given by Timoshenko for an isotropic, homogeneous, simply supported plate is [25]

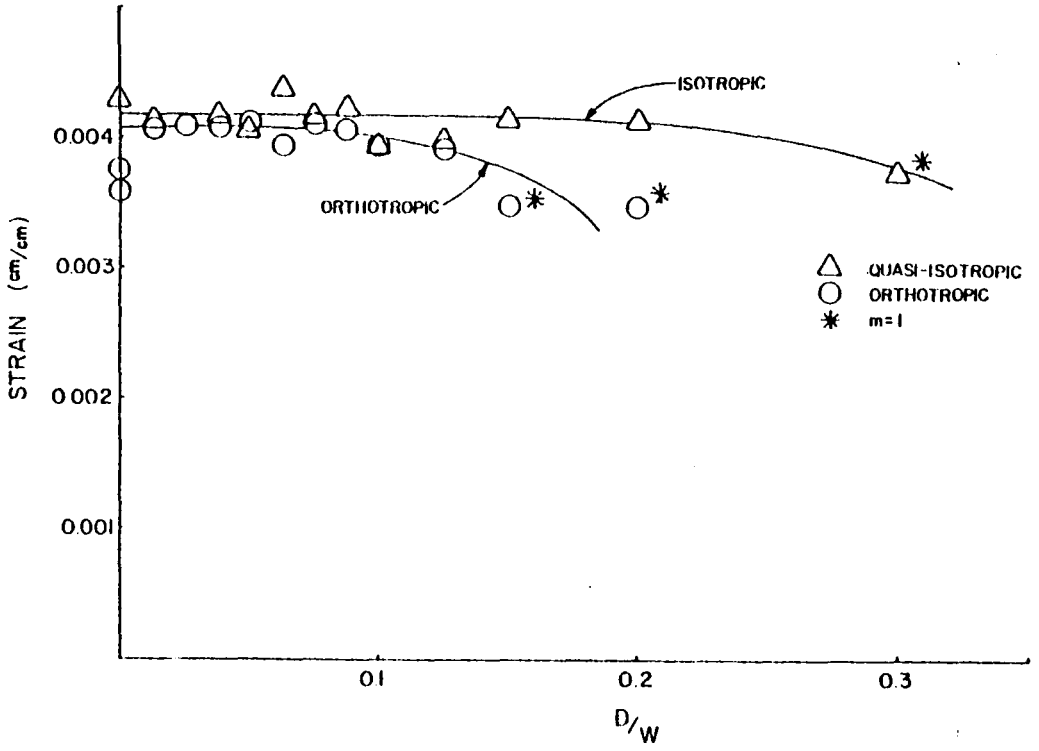

FIGURE 4-38. ULTIMATE STRAIN LEVELS FOR 24 PLY PANELS.

$$\sigma_{cr} = \frac{k\pi^2 Et^2}{12(1\nu^2)w^2}$$

where k is the end fixity constant, E is the Young's modulus of the material, ν, Poisson's ratio, and t and w the thickness and width of the plate, respectively. By the isotropic linear elastic constitutive relation this becomes

$$\varepsilon_{cr} = \frac{k\pi^2 t^2}{12(1-\nu^2)w^2} . \qquad (4\text{-}1)$$

To examine this theory, a 24 ply quasi-isotropic specimen was sized to increase the buckling strain in order to determine whether or not the hole would dominate the compressive behavior. The average critical strain of the quasi-isotropic plates was 0.0035 cm/cm. This, in addition to the fact that the 48 ply specimens showed hole effects at an average global strain of 0.007 cm/cm led to the use of 0.007 cm/cm as a design strain level. From Equ. (4-1), holding all other values constant, the strain dependence on width is found to be

$$\frac{\varepsilon_{cr1}}{w_2^2} = \frac{\varepsilon_{cr2}}{w_1^2} .$$

Using 0.0035 cm/cm as ε_{cr1}, and 0.007 cm/cm as ε_{cr2}, and 12.70 cm (5.0 in) as w_1, leads to a value of w_2 of 8.89 cm ($3\frac{1}{2}$ in) is obtained. Therefore, a 24 ply specimen which is 8.89 cm ($3\frac{1}{2}$ in) wide should yield a buckling strain of 0.007 cm/cm. To size the cutout, SCF_ε data

from the quasi-isotropic series indicated that a $\frac{D}{W}$ ratio of 0.125 < $\frac{D}{W}$ < 0.150 would result in a SCF_{ε} of 3.57. A 1.27 cm ($\frac{1}{2}$ in) cutout size, $\frac{D}{W}$ = 0.1428 was selected.

Figures 4-39a,b show the results of this test. Failure occurred due to local buckling in the m=1 mode with neither bifurcation nor post-buckling strength exhibited by the load-displacement curve. The failure surface propagated radially to either side of the plate from the hole as was characteristic of the 48 ply strength critical panels. The average far field strain was 0.0065 cm/cm which was between the failure strain of the wider quasi-isotropic panels of $\frac{D}{W}$ of 0.125 and 0.150. In general, the mode of failure changed from that of a buckling critical 24 ply specimen to that typical of a strength dominated 48 ply panel

4.3.2 Correlation of Failure and Buckling Loads

The failure and buckling loads for all specimens are reported in Figure 4-40 normalized with respect to the classical buckling load for simply supported orthotropic plates of the same stiffnesses [19]. These are plotted versus the square of the hole radius divided by the product of the thickness and the width in order to account for variations in geometry. The four distinct regions of the plot are: the 24 ply side support failures; the buckling loads which include all 24 ply and selected 48 ply panels; the 48 ply strength failures; and the strength/stability transition region. These are each discussed in detail below.

As previously mentioned, all 12.70 cm wide 24 ply specimens failed

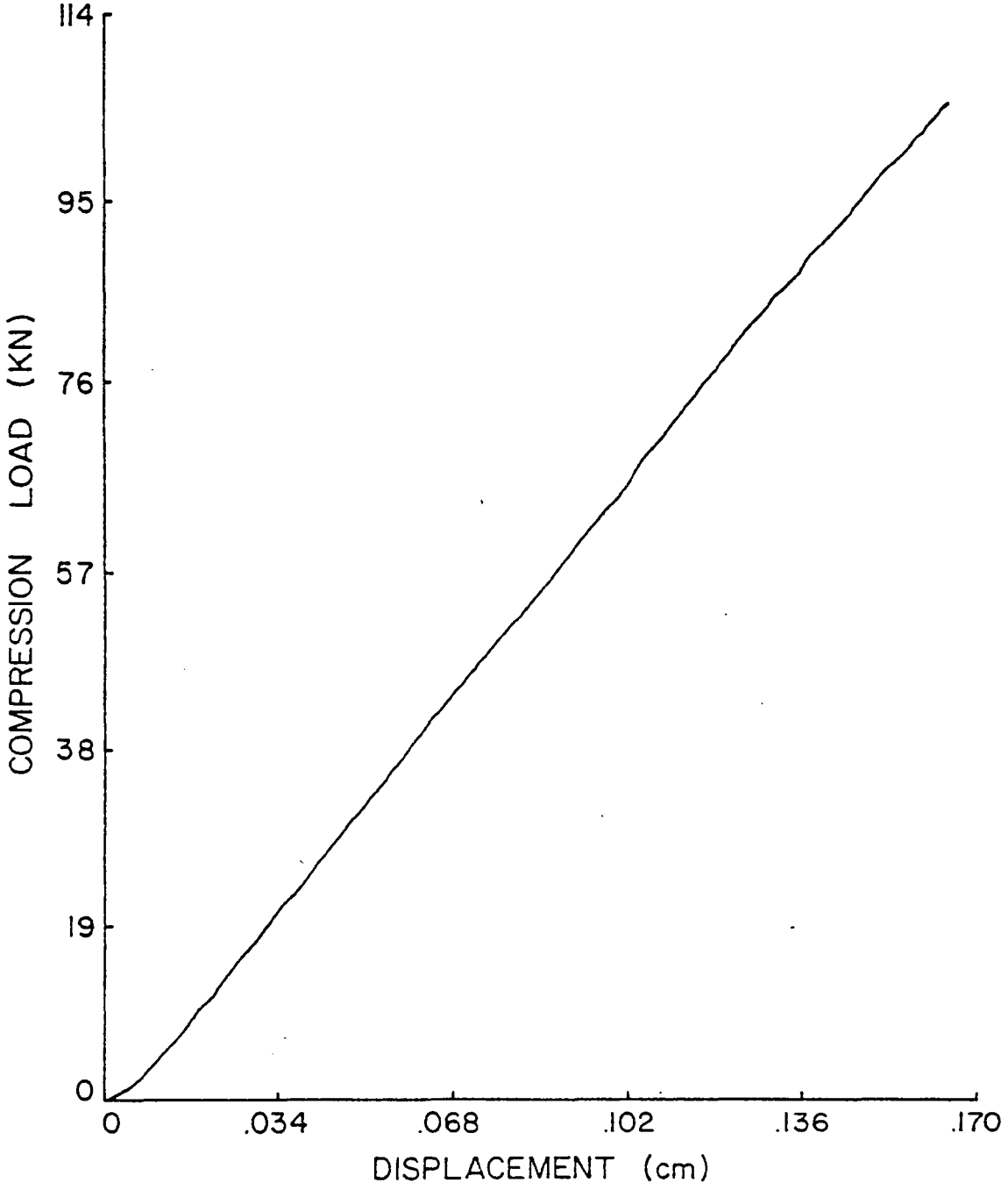

FIGURE 4-39a. LOAD-DISPLACEMENT CURVE FOR THE QUASI-ISOTROPIC 24 PLY STRENGTH FAILURE SPECIMEN 8.89 cm ($3\frac{1}{2}$ in) WIDE WITH 1.27 cm ($\frac{1}{2}$ in) DIAMETER CUTOUT.

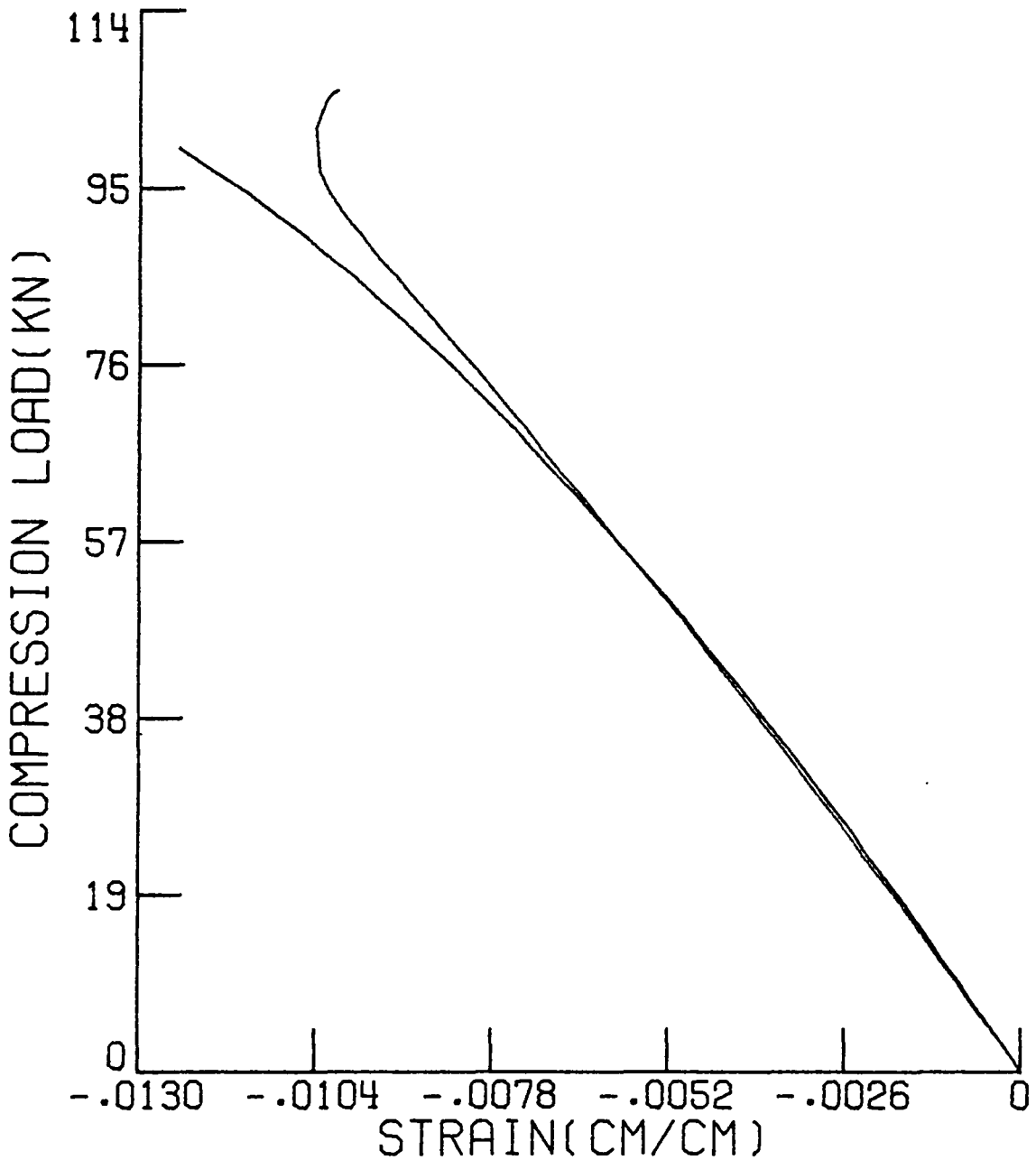

FIGURE 4-39b. LOCAL BUCKLING AROUND HOLE SHOWN BY STRAIN RESPONSE OF BACK-TO-BACK GAGES 0.3175 cm ($\frac{1}{8}$ in) FROM HOLE BOUNDARY.

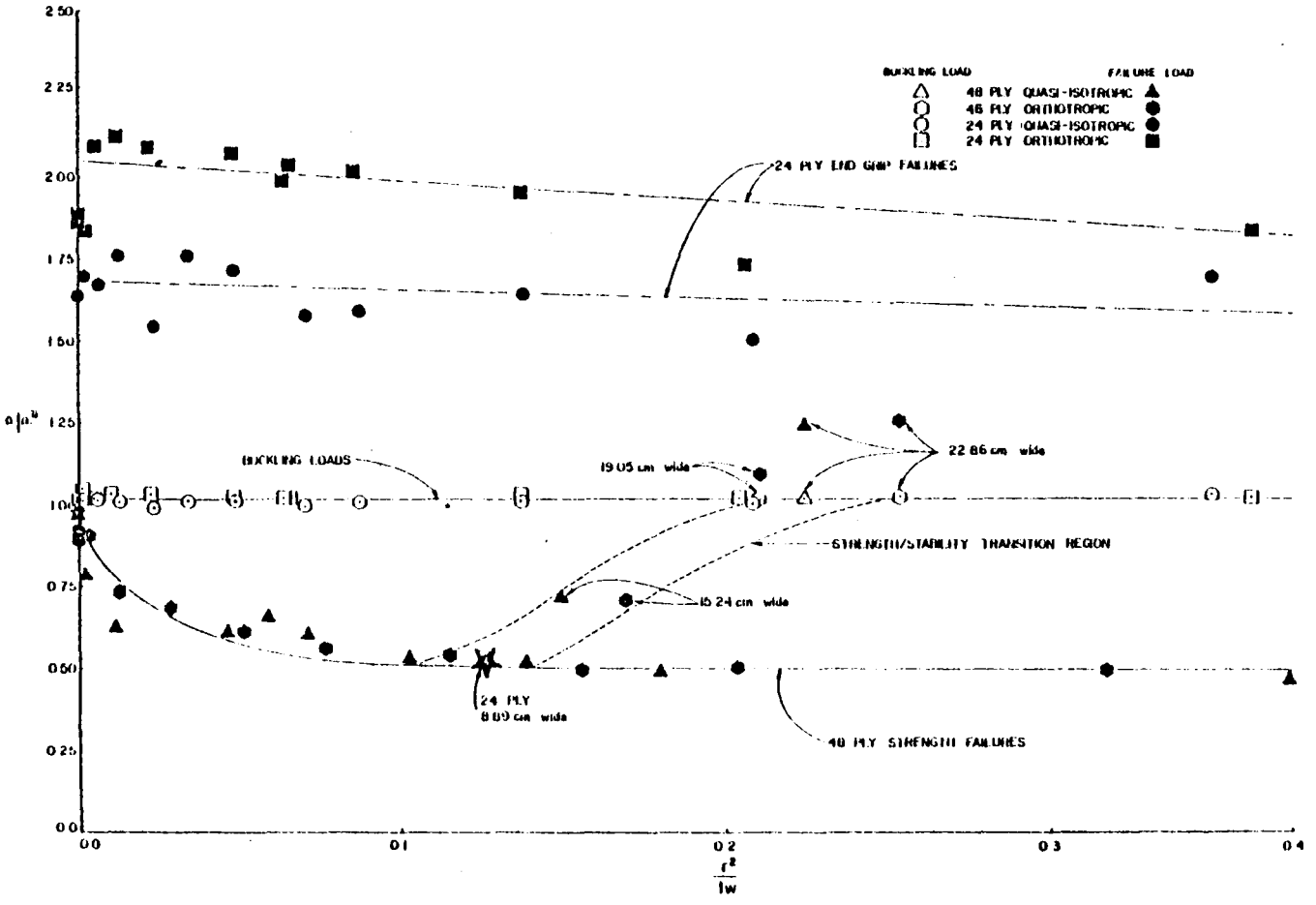

FIGURE 4-40. NORMALIZED FAILURE AND BUCKLING LOADS, ALL SPECIMENS.

at the end of the side supports. If the assumption is made that the strain concentration due to the end of the support became significant at the same magnitude of transverse deflection, then the linearly decreasing trend of the curve suggests that the influence of the hole was to increase the amount of out-of-plane displacement for a given load. The hole had more effect in the orthotropic than in the quasi-isotropic configuration. For every filled symbol in this region there is a corresponding open symbol on the buckling loads curve which represents the normalized critical load of that panel. The difference in ordinate values between the open and filled symbols represents the amount of post-buckling strength present in the panel in terms of multiples of the classical buckling load. The post-buckling strength of the orthotropic series exceeds that of the quasi-isotropic panels.

The buckling loads curve is composed of all of the 24 ply panels tested as well as the 19.05 cm and 22.86 cm ($7\frac{1}{2}$ and 9.0 in) wide 48 ply panels. The importance of this plot is the absence of any effect of hole size up to $\frac{r^2}{tw} = 0.4$ which corresponds to a $\frac{D}{W}$ of 0.2. In addition, the shape of the initial bifurcation, m=1 or m=2, did not influence the curve. The orthotropic panels characteristically buckled at a slightly higher load than the quasi-isotropic panels.

The size of the cutout had the greatest effect on the strength failure of the 48 ply specimens. In general, the presence of a hole served to rapidly reduce the strength of a panel with increasing cutout diameter approximately 50 percent of that of a panel without a hole.

As the diameter of the hole approaches the width of the plate, an additional reduction should take place, but this was not experienced for the $\frac{D}{W}$ ratios of this investigation.

Failure of the 15.24 cm (6.0 in) wide panels fall in a region between those dictated by buckling and those controlled by strength. The bending which accompanied the onset of bifurcation magnified the compressive strain around the hole enough to cause local material failure before strain reversal and a tangent modulus could develop. The exact shape of the strength/stability transition region is not, at this point, clearly defined, but its existence is evident from these panels. The aspect ratio of the 19.05 cm and 22.86 cm ($7\frac{1}{2}$ and 9.0 in) panels was small enough to allow buckling to occur before failure. Again the difference in ordinate values between the filled and open symbols is a measure of post-buckling strength. The failure of these three panels resulted from material failure around the hole as in the 15.24 cm (6.0 in) specimens.

Finally, the failure load of the 8.89 cm ($3\frac{1}{2}$ in) wide 24 ply quasi-isotropic panel which was sized to increase the global strain level and induce material failure was plotted on Figure 4-40 and is seen to fall on the curve of the 48 ply strength failures. This indicates that failure due to the presence of the hole is due to the high material strain and SCF_{ε} which are caused by the cutout. Thus, the transition from stability to strength dominated failure can be accurately characterized by consideration of global strain levels within the laminate.

Chapter 5

SUMMARY AND CONCLUSIONS

An experimental investigation was conducted to determine the behavior of graphite epoxy plates with circular cutouts under uniaxial compressive load. Laminates having 24 and 48 plies were examined with hole sizes ranging up to 3.81 cm ($1\frac{1}{2}$ in) in plates which measure 25.40 cm (10.0 in) by 12.70 cm (5.0 in). Wider plates were constructed preserving a diameter-to-width ratio of 0.1667 in order to examine any effect of width. Two different stacking sequences were tested, orthotropic (E_x/E_y = 2.016) and quasi-isotropic (E_x/E_y = 1.0), to ascertain the effect of differing material properties. The conclusions which can be drawn from the results of these tests are reported in this chapter.

In general, the effect of including a cutout in the 48 ply fiber-reinforced plate is to decrease the load carrying capability of the plate. The amount of reduction depends on the plate geometry and more specifically, the cutout diameter. Primary factors in determining whether or not a panel buckled before failing were the far field strain level and the strain concentration factor (SCF_ε) around the hole. The orthotropic lay-up exhibited a higher SCF_ε and a lower far field strain level than the quasi-isotropic orientation.

The sequence of events leading to failure in the orthotropic laminates was local delamination, local buckling and panel collapse. The failed region consisted of areas of delamination, buckling and fiber

breakage. The quasi-isotropic panels, in contrast, failed suddenly and catastrophically leaving a powdery failure surface extending from the cutout to the panel sides. The average far field failure strains were 0.0030 cm/cm and 0.0033 cm/cm for the orthotropic and quasi-isotropic panels, respectively.

The orthotropic orientation appeared to carry higher load for small holes because degradation of strength with hole size was not as severe for orthotropic panels as it was for quasiisotropic specimens. For the orthotropic panels a threshold existed between $0.504 \leq \frac{D}{T} \leq 1.01$ at which the mode of failure changes from buckling to material strength domination. No such threshold existed for the quasi-isotropic series. For this reason, below a $\frac{D}{T}$ of 1.01 the orthotropic laminate is superior while for $\frac{D}{T} \geq 1.01$ either configuration would perform equally well.

Buckling occurred readily in the 24 ply specimens in two halfwaves in the longitudinal direction, m=2. The effect of bifurcation was to create strain relief in the vicinity of the hole and to allow post-buckling strength to develop. The hole dimension had no effect on the buckling load for thin laminates. The 24 ply orthotropic laminates first bifurcated into the one halfwave shape, m=n=1 and then changed to m=2, n=1 with increased load. The corresponding reductions in stiffness were 32 percent and 61 percent, respectively. Strain relief around the hole was experienced with the formation of the second halfwave. Bifurcation in the 24 ply quasi-isotropic specimens was only in the m=2 mode up to a cutout diameter of 1.91 cm ($\frac{3}{4}$ in). For the largest hole sizes

in the 24 ply series, 2.54 cm (1.0 in) in the quasi-isotropic and 1.91 cm ($\frac{3}{4}$ in) and 2.54 cm (1.0 in) in the orthotropic laminates, the mode shape at failure was m=1 with the strain magnification on the compressive side of the deformed panel causing local material failure around the hole for both lay-ups.

In an attempt to affect the change in failure mode from buckling to strength dominated, a 24 ply quasi-isotropic panel was sized to increase the buckling strain level. By decreasing the panel width the buckling strain was raised above the strain level at which local material failure occurs around the hole. No buckling was present; the failure was typical of that observed in a 48 ply hole-dominated plate. This implies that the behavior of a composite plate in compression can be characterized by understanding the strain levels to be experienced throughout the load profile.

REFERENCES

1. Kirsch, R., "Die Theorie der Elastizitat und Die Bedurfnisse Der Festigkeitslehre," Zeitschrift Verein Deutscher Ingenieure, July 16, 1898.

2. Howland, R. C. J., "On the Stresses in the Neighbourhood of a Circular Hole in a Strip under Tension," Philosophical Transactions of the Royal Society (London), Series A, Vol. 229 (1929), p. 49.

3. Levy, S., Woolley, R. M., Kroll, W. D., "Instability of Simply Supported Square Plate with Reinforced Circular Hole in Edge Compression," Journal of Research of the National Bureau of Standards, Report Paper 1849, Vol. 39, December 1947, p. 571.

4. Kumai, T., "Elastic Stability of the Square Plate with a Central Circular Hole under Edge Thrust," Proceedings of 1st Japan National Congress for Applied Mechanics, 1951.

5. Schlack, A. L., "Elastic Stability of Pierced Square Plates," Experimental Mechanics, Volume 4, June 1964, p. 167.

6. Greszczuk, L. B., "Stress Concentrations and Failure Criteria for Orthotropic and Anisotropic Plates with Circular Openings," Composite Materials Testing and Design (2nd Conference) ASTM STP 497, 1972, pp. 363-381.

7. Green, A. E. and Zerna, W., Theoretical Elasticity, Oxford at the Claredon Press, 1954.

8. Tang, S., "Interlaminar Stresses Around Circular Cutout of Composite Plates Under Tension," Presented at 18th Structural Dynamics and Materials Conference, San Diego, March 21-23, 1977, pp. 251-259.

9. Rybicki, E. F., and Hopper, A. T., "Analytical Investigation of Stress Concentrations Due to Holes in Fiber Reinforced Plastic Laminated Plates, Three Dimensional Models," AFML-TR-73-100, Battelle Columbus Laboratories, June 1973.

10. Rybicki, E. F., and Schmueser, D. W., "Three Dimensional Finite Element Stress Analysis of Laminated Plates Containing a Circular Hole," AFML-TR-76-92, Battelle Columbus Laboratories, August 1976.

11. Nuismer, R. J. and Whitney, J. M., "Uniaxial Failure of Composite Laminates Containing Stress Concentrations," Fracture Mechanics of Composites, ASTM STP 593, 1975, pp. 117-142.

12. Whitney, J. M. and Nuismer, R. J., "Stress Fracture Criteria for Laminated Composites Containing Stress Concentrations," Journal of Composite Materials, Volume 8, July 1974, p. 253.

13. Whitney, J. M. and Kim, R. Y., "Effect of Stacking Sequence on the Notched Strength of Laminated Composites," Composite Materials: Testing and Design (4th Conference), ASTM STP 617, 1977, pp. 229-242.

14. Whitney, J. M., "The Effect of Stress Concentrations on the Fracture Behavior of Fiber Reinforced Composite Materials," Twelfth Annual Meeting of the Society of Engineering Science, University of Texas at Austin, October 20-22, 1975, p. 173.

15. Levy, A., Armen, H., Whiteside, J., "Elastic and Plastic Interlaminar Shear Deformation in Laminated Composites under Generalized Plane Stress," Proceedings of the Third Conference on Matrix Methods in Structural Mechanics, AFFDL-TR-71-160, 18-21 October 1971, pp. 959-990.

16. Daniel, I. M., Rowlands, R. E., Whiteside, J. B., "Deformation and Failure of Boron-Epoxy Plate with Circular Hole," Analysis of the Test Methods for High Modulus Fibers and Composites, ASTM STP 521, 1973, pp. 143-164.

17. Rowlands, R. E., Daniel, I. M., Whiteside, J. B., "Geometric and Loading Effects on Strength of Composite Plates with Cutouts," Composite Materials: Testing and Design (3rd Conference), ASTM STP 546, 1974, pp. 361-375.

18. Daniel, I. M., Rowlands, R. E., and Whiteside, J. B., "Effects of Material and Stacking Sequence on Behavior of Composite Plates with Holes," Experimental Mechanics, Volume 14, Number 1, January 1974.

19. Ashton, J. E., Whitney, J. M., Theory of Laminated Plates, Technomic Publishing Company, 1970.

20. "Standard Method of Test for Fiber Content of Reinforced Resin Composites," Designation D-3171-73, 1976 Annual Book of ASTM Standards Part 36.

21. Dana, J. R., Barker, R. M., "Three-Dimensional Finite-Element Computer Program - User's Guide," VPI-E-74-19, Virginia Polytechnic Institute and State University, August 1974.

22. Whiteside, J. B., Daniel, I. M., and Rowlands, R. E., "The Behavior of Advanced Filamentary Composite Plates with Cutouts," AFFDL-TR-73-48, June 1973.

23. Savin, G. N., Stress Concentration Around Holes, Pergamon Press, Ltd., 1961.

24. Ritchie, D., Rhodes, J., "Buckling and Post-Buckling Behavior of Plates with Holes," Aeronautical Quarterly, Volume 26, November 1975.

25. Timoshenko, S., Theory of Elastic Stability, McGraw Hill Book Company, 1936.

26. Prabhakara, M. K., and Chia, C. Y., "Post-Buckling of Angle-Ply and Anisotropic Plates," Ingenieur Archiv, Volume 45, 1976.

27. Harris, G. Z., "Buckling and Post-Buckling of Orthotropic Laminated Plates," Presented at 16th Structures, Structural Dynamics and Materials Conference, Denver, Colorado, May 27-29, 1975.

28. Grimes, G. C., Greimann, L. F., "Analysis of Discontinuities, Edge Effects, and Joints," Composite Materials, Structural Design and Analysis, Volume 8, Academic Press, 1974.

29. Belie, R. G., and Appl, F. J., "Stress Concentrations in Tensile Strips with Large Holes," Experimental Mechanics, April 1972.

30. Ueng, C. E. S., "Stress Concentration Factors Around a Circular Hole in Laminated Composites," Advances in Engineering Sciences, Volume II, 13th Annual Meeting of the Society of Engineering Science, Hampton, Virginia, November 1-3, 1976.

The vita has been removed from the scanned document

THE COMPRESSIVE FAILURE OF GRAPHITE/EPOXY PLATES WITH CIRCULAR HOLES

by

James F. Knauss

(ABSTRACT)

The results of an experimental investigation into the compressive behavior of T300-5208 graphite/epoxy plates measuring 12.70 cm by 25.40 cm and containing circular cutouts ranging to 3.81 cm are reported. Two thicknesses, 24 ply and 48 ply were chosen to differentiate between stability failures due to buckling and strength failures due to the presence of the cutout.

The critical load of the 24 ply panels was found to be independent of hole size with bifurcation occurring in the two halfwave mode longitudinally and one halfwave laterally in the quasi-isotropic panels. For the orthotropic 24 ply panels, bifurcation began in the one halfwave shape in each direction but changed to the two halfwave shape before failure. Consistent post-buckling strength was exhibited by both laminate configurations.

The 48 ply specimens displayed decreasing ultimate load with increasing hole diameter to approximately 50% of the no-hole panel ultimate for a diameter-to-width ratio of 0.30. The 48 ply orthotropic panels displayed a strength/stability threshold between cutout diameters of 0.3175 cm and 0.635 cm. Panels with cutout diameters below 0.3175 cm displayed buckling before failure and those with cutouts larger

than 0.635 cm experienced material failure around the hole before panel collapse. The 48 ply quasi-isotropic panels showed no sign of such a threshold with failure due to the hole occurring for all hole sizes.